Norwegian University
of Life Sciences

Master's Thesis 2021 60 ECTS

Faculty of Chemistry, Biotechnology and Food Science

Lysophosphatidic acid (LPA) regulation of collective cell migration

Sofie Persdatter Sangnæs

Master of Science, Biotechnology

Lysophosphatidic acid (LPA) regulation of collective cell migration

Oslo University Hospital,
Department of Microbiology

and

Norwegian University of Life Science (NMBU),
Faculty of Chemistry, Biotechnology and Food Science

Acknowledgements

This master project was carried out between August 2020 and May 2021 at Oslo University Hospital, Department of Microbiology and Norwegian University of Life Science (NMBU), Faculty of Chemistry, Biotechnology and Food Science.

First, I would like to thank my main supervisor at Department of Microbiology, Emma Lång. Your exceptional guidance and support during this period have been crucial for me both during the laboratory work, with data analysis and while writing the thesis. This year would never been the same without your enthusiasm and work spirit, and this thesis would not have been the same without all the good feedback you have given on the way.

Next, I wish to express my gratitude to the research group I have been lucky to be a part of. You have all been so helpful and supportive, and always available for my many questions. I would like to thank the group leader, and my co-supervisor, Stig Ove Bøe, for the many useful discussions and your enthusiasm about Python-based scripts and microscopy techniques. Thank you, Anna Lång, for teaching me how to use the microscopes and for all help with analysis and image processing, and thanks to Pernille Blicher for guidance at the laboratory.

Furthermore, I would like to thank Sherif Khooder for performing the shRNA knockdown process, telling me all the details about it and being available for my questions about Western blot. Thank you to Mari Kaarbø for all expert help and guidance with performing qPCR analysis. In addition, thank you to Huda Al-Baldawi and Natalia Berges Jimenez for advises at the laboratory and to the other members of the staff for tips and tricks.

I also wish to thank my supervisor at Faculty of Chemistry, Biotechnology and Food Science, Dzung Diep, for being available for questions and support throughout this project.

Thank you to all the students in the student office at Department of Microbiology, and to my fellow students sharing both problems and good results during the period.

Finally, a thank you to my friends and family for encouragement and support throughout my whole study time. A big extra thank you to my boyfriend who has shared both good and less enthusiastic moments, and quality breaks with ice cream, with me at the home office while writing his own master thesis.

Ås, May 2021

Sofie Persdatter Sangnæs

Abstract

The human body is covered by a protective barrier, the skin. The skin is daily subjected to cuts and bruises, wounds that are normally healed without scars. However, sometimes the wound healing process of the skin fails, and chronic wounds is formed. In order to develop new and non-invasive strategies to improve the healing process in chronic wounds, it is necessary to fully understand the mechanisms of wound healing. Collective cell migration is an essential process of wound healing. Cell migration requires filament structures in the cytoskeleton, in particular, formation of actomyosin networks.

Lysophosphatidic acid (LPA) is involved in many biological functions. LPA has the ability to promote migration of keratinocytes and fibroblasts, and thereby participate in wound repair. The mechanisms for LPAs regulatory role in wound healing are not fully established. The aim of this master project is therefore to contribute to a better understanding of how LPA activates and regulates collective cell migration in human skin. The research is based on an established *in vitro* experimental system including the human keratinocyte cell line HaCaT.

Cell movements in quiescent epithelial sheets were monitored by live cell imaging to study migration patterns formed after different stimuli. The mRNA expression levels of the six LPA receptors (LPARs) in HaCaT cells were estimated. Furthermore, visualization of actomyosin networks was performed using immunofluorescence (IF) staining and live cell imaging of a HaCaT cell line expressing fluorescent labelled actin. The effect of the LPAR1 inhibitor Ki16425 was examined based on cell migration patterns and actomyosin expression. Finally, a LPAR1 knockdown cell line was established using the shRNA technique. Western blot analysis was used to evaluate the knockdown efficiency and changes in cell morphology and migration behaviour were examined.

The results showed that LPA was able to activate and regulate collective cell migration of keratinocyte cell sheets and it was observed a correlation between actomyosin networks and cell sheet coordination. It was also estimated expression of all six LPARs in HaCaT cells, but LPAR4 was expressed in lower amount. LPAR1 was observed to be important for LPAs regulatory role of collective cell migration, but it was not alone involved in these responses.

Sammendrag

Menneskekroppen er dekket av en beskyttende barriere, huden. Huden blir daglig utsatt for kutt og merker, sår som normalt heler uten å etterlate arr. Likevel kan det forekomme feil i sårhelingsprosessen som medfører kroniske sår. For å kunne utvikle nye non-invasive strategier for å forbedre helingsprosessen i kroniske sår, er det nødvendig å forstå mekanismene for sårhelingsprosessen fullt ut. Kollektiv cellemigrering er en essensiell prosess for sårheling. Cellemigrering avhenger av filamentstrukturer i cytoskjelettet, spesielt actomyosin.

Lysofosfatidsyre (LPA) er involvert i mange biologiske funksjoner. LPA har evnen til å fremme migrering av keratinocytter og fibroblaster, og dermed inngå i sårhelingsprosessen. Mekanismene for LPAs regulatoriske rolle i sårheling er ikke fullstendig etablert. Målet med dette masterprosjektet er derfor å bidra til en bedre forståelse for hvordan LPA aktiverer og regulerer kollektiv cellemigrering i menneskehud. Forskningen er basert på et etablert *in vitro* eksperimentelt system som inkluderer den humane keratinocytt-cellelinjen HaCaT.

Cellemigrering i et hvilende epitelcellelag ble studert ved levende cellemikroskopi for å undersøke migreringsmønstre som dannes av ulike stimuli. Uttrykksnivået av mRNA for de seks LPA-reseptorene (LPAR) i HaCaT-celler ble estimert. Videre ble actomyosin-nettverk visualisert ved bruk av immunofluorescens (IF) og mikroskopi av en HaCaT-cellelinje som uttrykker fluorescerende aktin. Effekten av LPAR1 inhibitoren Ki16425 ble undersøkt basert på cellemigreringsmønstre og uttrykk av actomyosin. Til slutt ble det laget en cellelinje med nedregulert LPAR1 ved bruk av shRNA-teknikk. Analyser med Western blot ble utført for å evaluere effekten av nedregulering i cellelinjen, og endringer i cellemorfologi og migreringsegenskaper ble undersøkt.

Resultatene viste at LPA hadde evnen til å aktivere og regulere kollektiv cellemigrering i keratinocytt-cellelag, og det ble observert en korrelasjon mellom actomyosin-nettverk og koordinering av celler i cellelag. Det ble også estimert uttrykk av alle seks LPAR i HaCaT-celler, men LPAR4 var uttrykt i mindre mengder. Observasjoner viste at LPAR1 var viktig for den regulatoriske rollen til LPA i kollektiv cellemigrering, men LPA var ikke involvert i disse responsene alene.

Abbreviations

ATX	Autotaxin
BSA	Bovine serum albumin
cDNA	Complementary DNA
C_T	Threshold cycle
ddPCR	Droplet Digital PCR
DNA	Deoxyribonucleic acid
dsDNA	Double stranded DNA
EGF	Epidermal growth factor
EGFR	EGF receptor
FBS	Fetal bovine serum
FRET	Fluorescence resonance energy transfer
gDNA	Genomic DNA
GFP	Green fluorescent protein
HRP	Horseradish peroxidase
IDE	Integrated development environment
IF	Immunofluorescence
IMDM	Iscove's Modified Dulbecco's Medium
LPA	Lysophosphatidic acid
LPAR	LPA receptor
LTR	Long terminal repeats
mRNA	Messenger RNA
PBS	Phosphate-buffered Saline
PCR	Polymerase chain reaction
PenStrep	Penicillin-Streptomycin
PFA	Paraformaldehyde
PIC	Pre-integration complex
PIV	Particle image velocimetry
qPCR	Quantitative PCR
RFP	Red fluorescent protein
RIN^e	RNA integrity number equivalent
RISC	RNA-induced silencing complex
RNA	Ribonucleic acid
RNAi	RNA interference
ROCK	Rho-associated kinase
ROI	Region of interest
rRNA	Ribosomal RNA
RT	Reverse transcription
SCR	Scrambled control
shRNA	Short hairpin RNA
siRNA	Small interfering RNA
STED	Stimulated Emission Depletion
TAE	Tris-acetate-EDTA (EDTA: Ethylenediamine-tetraacetic acid)
Tm	Melting temperature
WT	Wildtype cells

Table of Contents

1 Introduction

1.1 The human skin

The human body is covered by skin protecting underlying cells and tissue from mechanical, thermal, and chemical injury, and intrusion of microorganisms. Being the largest sensory organ of the body, the skin provides information about the 'outside world'. In general, the skin has a remarkable ability to heal when it is injured and to fight infections in open wounds (Sjaastad et al., 2016). However, some wounds fail to heal properly and become chronic. The wound healing process of human skin is described below (section 1.2).

The skin is composed of the epidermis, a multi-layered superficial epithelium, and the dermis, an underlying layer of dense, fibrous connective tissue. The basal cell layer is the innermost layer of epidermis, and the place where stem cells divide and further differentiate into keratinocytes or melanocytes before they migrate to replace lost cells from the upper skin layers. Most epidermal cells are keratinocytes. Keratinocytes synthesize fibrous keratin proteins, which among other things are an important filamentous part of the cytoskeleton of epithelial cells (Sjaastad et al., 2016).

The basal lamina is a specialized form of extracellular matrix keeping the epidermis attached to the dermis by forming a mechanical connection between them. The basal lamina has in general a critical role in the body, lying beneath all epithelial cells and surrounding individual muscle cells, fat cells and Schwann cells in addition to separate the cells from connective tissue and form mechanical connection. The basal lamina serves as highways for cell migration, is important in tissue renewal, and it is able to determine cell polarity (Alberts et al., 2015e).

Collagen is the most abundant protein in the body constituting 25 % of the total protein mass (Alberts et al., 2015e). Collagen is an important component of the skin expressed in the superficial layers of the dermis and in the basal lamina. The collagen fibres in the dermis are arranged as bundles running parallel to the skin surface and connected into a network forming structures that support the epidermis and give it its contours (Sjaastad et al., 2016). Type IV Collagen is one of the two major components in basal lamina (Alberts et al., 2015e).

1.2 The wound healing process

One of the most complex processes in the human body is wound healing. The process is timely regulated and includes a variety of cell types and biological pathways. The wound healing process is divided into several stages including haemostasis, inflammation, growth, re-epithelialization and remodelling (Rodrigues et al., 2019). An overview of the different stages in the wound healing process is given in the following text.

The first stage is haemostasis that activates cellular responses leading to limit blood loss. These responses include constriction of the blood vessels by contraction of the vascular smooth muscle cells, activation of platelets and the blood coagulation cascade forming a protective blood clot. The last step of haemostasis is fibrinolysis that leads to degradation of the blood clot, an important step to disable the clot to completely stop the blood flow (Murphy, 2017; Rodrigues et al., 2019).

Inflammation, or the inflammatory response, is defined as the local accumulation of fluid, plasma proteins and white blood cells initiated by physical injury, infection or a local immune response. There are five symptoms caused by inflammation; heat, pain, redness and swelling (Parham, 2015). A variety of different molecules is involved in this step of wound healing. Chemokines, a specific form of cytokines, is secreted by mast cells and have an important role of guiding neighbouring cells, often white blood cells to the wounded site (Rodrigues et al., 2019). Cytokines induce local dilation of blood capillaries, which increases the blood flow and causes heat and redness in the skin. The dilation introduces gaps in the blood vessel endothelium making it permeable for blood plasma that leak into the connective tissue. The increased local fluid volume causes swelling and pain (Parham, 2015). The most abundant white blood cells in the wound are neutrophils. Neutrophils secrete microbial agents as proteases, growth factors, integrins and cytokine receptors. The proteases are enzymes that both degrade antimicrobial activity and the wounded area to prepare formation of new skin layers. Neutrophils produce extracellular traps to capture pathogens, and can, as macrophages and dendritic cells, perform phagocytosis by response to different growth factors (Rodrigues et al., 2019).

The next stage of wound healing is growth of new connective tissue, also called granulation tissue. This provides stability and prepare the wounded area for regeneration of new skin layers (Rodrigues et al., 2019). Cytokines released from inflammatory cells establish gradients attracting keratinocytes, fibroblasts, and endothelial cells. Fibroblasts are stimulated by growth factors to proliferate and synthesize collagen restoring the extracellular matrix and the

mechanical properties of healed skin (Guerra et al., 2018). Angiogenesis, formation of new blood vessels from pre-existing ones, is essential for reestablishment of normal blood flow and to provide nutrients and maintain the oxygen homeostasis in the new tissue (Guerra et al., 2018).

Re-epithelialization is the next stage of wound healing, induced by several growth factors stimulating keratinocytes to migrate and proliferate in the basal cell layer of epidermis. When stimulated, the keratinocytes are responsive to factors from the epidermal and fibroblast growth factor family that upregulates keratin and is important for migration. Keratinocytes in the wound can integrate with fibroblasts, endothelial cells and immune cells, which is important for complete cell closure (Rodrigues et al., 2019).

The last stage of wound healing is remodelling. Remodelling occurs after the wound closure is completed, and includes reorganization and contraction of the extracellular matrix leading to a reduced scar. Collagen fibres synthesized in the growth stage are replaced with a stronger type increasing the ultimate tensile strength of the skin (Guerra et al., 2018). The healed area of epithelial cells shifts from a state of hypoxia to cell quiescence. This is the end point of wound healing, in most cases, but some wounds continue to undergo remodelling for several months or years (Rodrigues et al., 2019).

Wounds can be classified as acute or chronic based on the healing time. A wound is classified as acute if it heals within three weeks after injury through the processes mentioned above (Dreifke et al., 2015). Failures to complete the specific steps in the wound healing process will activate pathological processes that lead to formation of hypertrophic scars, fibrosis, or non-healing wounds (Guerra et al., 2018). If the wound persists for three months or longer, it is classified as chronic (Dreifke et al., 2015). Chronic wounds frequently present a delay in the inflammatory or proliferative stages of the healing process. Diabetes and obesity are usually associated with chronic wounds. Chronic non-healing wounds constitute a very high economic and social impact to the society. There is no efficient wound heling therapy available today, and as the general population grows older the prevalence of chronic wounds is expected to increase. Therefore, it is essential to fully understand the mechanisms of wound healing in order to develop new and non-invasive strategies to improve the healing process in chronic wounds (Guerra et al., 2018).

1.3 HaCaT

When studying cellular processes *in vitro*, experiments are commonly designed using established and commercial available cell cultures, so-called cell lines. One of these is the HaCaT cell line established by Boukamp et al. (1988). HaCaT is an immortalized, but not transformed, keratinocyte cell line derived from human epidermis. The criterion to be immortalized is to survive more than 140 cell passages. This cell line is not differentiated and will always stay as keratinocytes, with a normal cell cycle, like the progenitor epithelial cells in the basal cell layer of epidermis. The cell line was named based on its human origin and its propagation abilities under growth condition with low calcium (Ca^{2+}) levels and elevated temperature (Boukamp et al., 1988).

HaCaT cells have been shown to be able to differentiate and form specific epithelial cell layers in *in vitro* 3D cultures (Mao et al., 2018). The HaCaT cells can be regarded as a substitute to progenitor cells in the basal layer of epidermis, where cells can become activated and participate in cell migration and proliferation during the re-epithelialization stage of wound healing. Thus, this cell line is a good choice when studying molecular mechanisms of cell migration in relation to wound healing in human skin.

1.4 Cell migration

Cell migration is an important process during development, wound healing and immune responses. Cells can migrate either as single cells or as a unit in a collective, known as collective cell migration. During embryogenesis, single cells migrate to specific target locations, and coordinated cell migration in the form of epithelial cell sheets creates the structures of a body. Cell migration requires the three basic filament structures in the cytoskeleton; actin filaments, microtubules and intermediate filaments, and a variety of cytoskeletal accessory proteins like motor proteins (Alberts et al., 2015f). Cell polarization is essential for single cell migration, since it helps the cell determine the direction of its movements (Pandya et al., 2017). This also occur during collective cell migration, where connected cells develop a polarized cell sheet based on leader and follower cells as described in section 1.4.4.

Collective cell migration is essential in physiological processes such as formation of tissues and organs during development, and later in life for wound healing, tissue renewal and angiogenesis. Abnormal collective cell migration is associated with pathological processes such

as cancer dissemination, where tumour cells can move using multicellular streaming, tumour budding and collective invasion (Pandya et al., 2017). Collective cell migration is established by and dependent on multiple factors and signalling pathways leading to collective cell polarization, mechanocoupling and cytoskeletal rearrangements (Haeger et al., 2015).

1.4.1 Mechanisms for cell migration

Cells migrate in response to changes in the extracellular matrix and specific external signals including chemical and mechanical signals that activate motility mechanisms like chemotaxis, haptotaxis and durotaxis. Chemotaxis is defined as attracting or repelling cell guidance due to the presence of a chemical gradient caused by chemokines, altered pH and growth factors. Notably, chemotaxis can be induced by the migrating cells themselves by establishing a self-generated chemokine gradient along the migrating collective (Haeger et al., 2015).

Haptotaxis is directing cell movements along a gradient of immobilized ligands caused by different levels or distribution of extracellular matrix proteins as collagen, fibronectin, and matrix-bound cytokines among others (Haeger et al., 2015). Durotaxis describes migrating cells preference of a stiff substrate, where cells are moving in response to a stiffness gradient (Lo et al., 2000).

Collective cell migration can also be guided by electrical signals. The mechanism where migration is directed relative to an electric field is called electrotaxis (Haeger et al., 2015). This has been shown to be a mechanism of importance for wound healing. An *in vivo* study of wounds in human skin confirmed the presence of an electric current that was gradually increasing towards the centre of the wound. The same study monitored monolayers of rat corneal epithelium and observed a correlation between increased electric field strength and increased migration velocity (Zhao et al., 2006).

1.4.2 Growth factors

Blood consists of cellular content, red and white blood cells and platelets, and a liquid carrier, plasma. Plasma without clotting proteins is blood serum, which contains several essential wound healing factors as growth factors, cytokines and antimicrobial components. Abundant proteins and peptides present in plasma and serum are albumins, globulins, and lipoproteins (Psychogios et al., 2011).

Growth factors are defined as extracellular signal proteins that stimulate cell growth, survival and proliferation (Alberts et al., 2015c). As described in section 1.2, several growth factors are

involved in the process of wound healing. The epidermal growth factor family, including the epidermal growth factor (EGF), is one group of growth factors known to activate keratinocytes during re-epithelialization (Rodrigues et al., 2019).

In a paper published by Lång et al. (2018), it was shown that blood serum can activate collective cell migration of skin cells in a static quiescent cell state to begin to move. EGF receptors (EGFRs) are transmembrane proteins that are important in many biological processes. It is shown that activation of EGFRs are essential for activation of cellular movement (Koivisto et al., 2006), but that EGF signalling alone is not enough to make the cells move collectively in the same direction (Lång et al., 2018). Other growth factors also shown to contribute during the wound healing process, are transforming growth factor-β and insulin growth factor (Rodrigues et al., 2019). However, other signalling molecules present in human blood can also stimulate activation of cell migration such as the phospholipid lysophosphatidic acid (LPA) (Thorlakson et al., 2017).

1.4.3 Lysophosphatidic acid (LPA)

Lysophosphatidic acid (LPA) is one of the simplest phospholipids found in nature. LPA is most abundant in blood serum, but is also present in other body fluids as tears and saliva, and a variety of tissues (Lei et al., 2019). LPA appears in different structure species, according to variation in its fatty acid chain, which is shown to mediate varied affinity for the LPA receptors and thus contribute to different biological effects (Hernández-Araiza et al., 2018). Autotaxin (ATX) is shown to be a major metabolic regulator of LPA production and activation, and this ATX-LPA axis is considered important for many biological functions and it is involved in different cancer types (Riaz et al., 2016). The structure of LPA and common LPA species are presented in Figure 1.1. The length of the fatty acid chain and the level of saturation is what differs the LPA species.

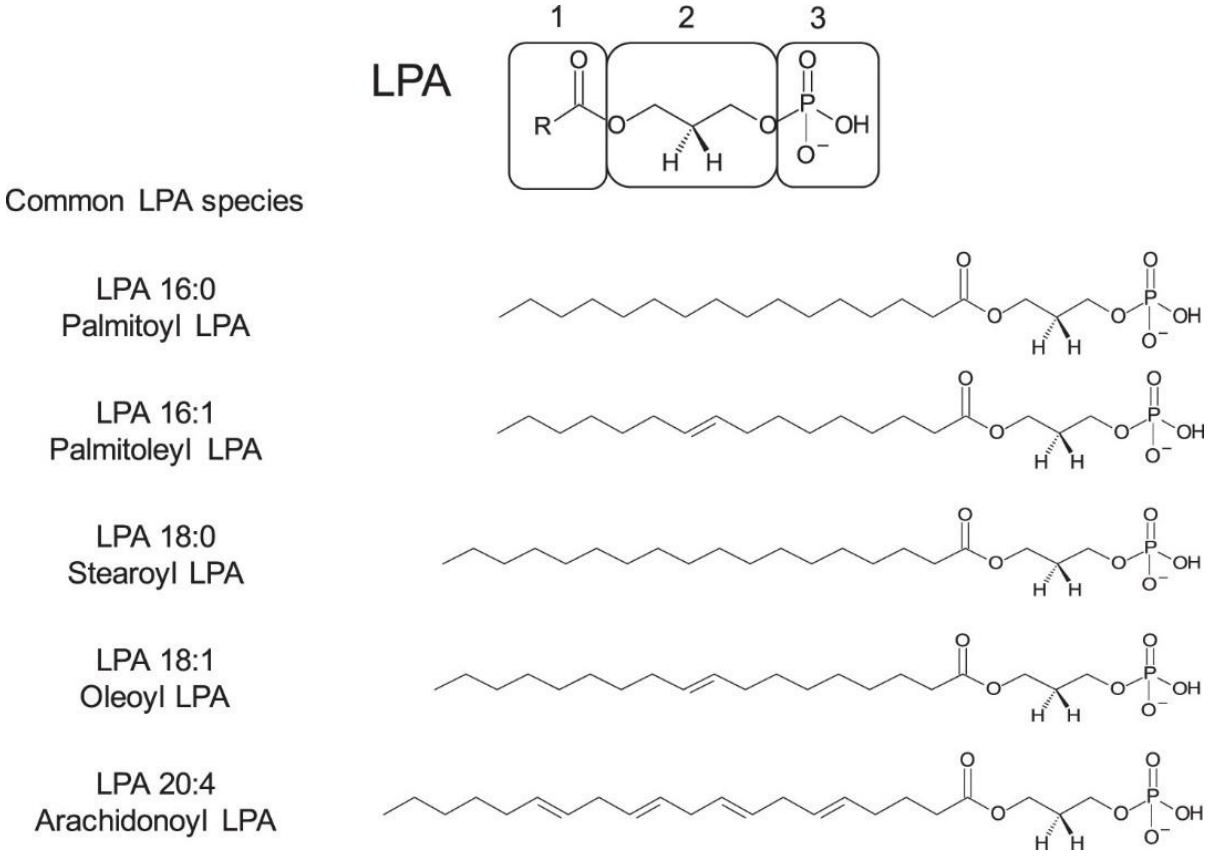

Figure 1.1: Structure of Lysophosphatidic acid (LPA) and common species. The structure of LPA consists of a fatty acid chain (1), a glycerol backbone (2) and a phosphate group (3). Here, the most abundant species in mammal serum are shown. The illustration is obtained from Hernández-Araiza et al. (2018).

LPA activates intracellular signalling pathways through G-protein-coupled receptors in the cell membrane. Studies have identified six LPA receptors (LPARs), which are divided into two families based on endothelial differentiation. The endothelial differentiation gene (*Edg*) family include the receptors LPAR1, LPAR2 and LPAR3, and the non-*Edg* family is consisting of LPAR4, LPAR5 and LPAR6 (Lei et al., 2019; Riaz et al., 2016). The receptors are able to activate cellular responses through multiple heterotrimeric G-proteins divided in four subfamilies. All receptors can signal through two or more of these subfamilies, and each subfamily is thereby, in most cases, influenced by stimulation of more than one LPAR (Riaz et al., 2016). Figure 1.2 is a schematic overview of the six LPARs and signalling pathways they are known to activate.

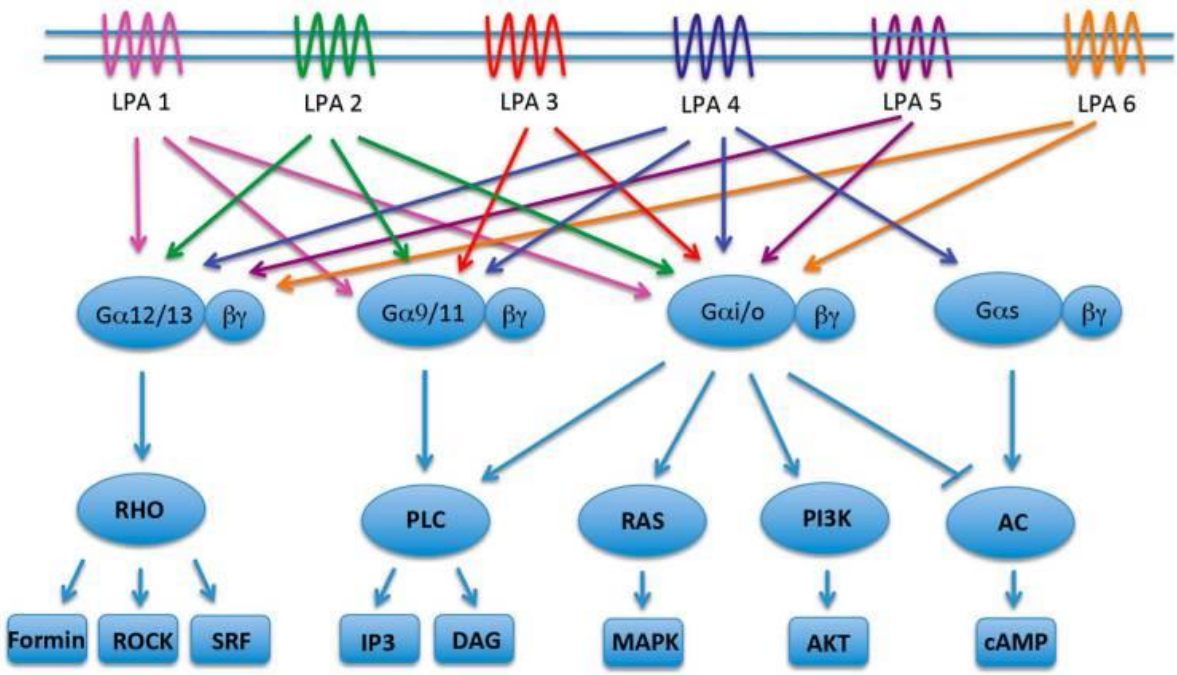

Figure 1.2: The six LPA receptors and their signalling pathways. LPA activates intracellular signalling pathways through the G-protein-coupled receptors LPAR1-6. Each receptor activates cellular responses through two or more G-protein subfamilies, which is part of different signalling pathways. The illustration is obtained from Riaz et al. (2016).

LPA has also been shown to regulate biological functions through other signalling pathways than G-protein-coupled receptors, as receptor-independent pathways and intracellular nuclear hormone receptors. LPA is involved in a broad spectrum of processes from physiological processes as promoting smooth muscle contraction, regulation of blood pressure, embryonic development and inflammation, and pathological processes as tumour progression. LPA is also involved in wound healing processes (Lei et al., 2019).

The ability of LPA to promote proliferation, differentiation, migration of keratinocytes and fibroblasts, and participate in skin repair is shown by *in vitro* experiments (Lei et al., 2019; Mazereeuw-Hautier et al., 2005). A research by Thorlakson et al., 2017 showed that LPA activates human oral keratinocytes during wound repair in the mouth. They concluded that LPA has a favourable role in wound heling of oral epithelia, due to the fact that LPA is found in saliva and is being released from activated cells after wounding (Thorlakson et al., 2017). LPA levels in the local skin tissue are also shown to increase after injury (Lei et al., 2019; Mazereeuw-Hautier et al., 2005), and evidence exists for LPAs ability to shorten the time required for wound healing in animal models of skin wounds (Rhim et al., 2010).

The molecular mechanisms for LPA's regulatory role in wound healing are not fully established, but it is proposed to be related to seven different processes that are summarized in the review by Lei et al. (2019). One of these suggestions is that LPA has the ability to activate signalling pathways or upregulate migration-related proteins to promote activation of cell migration of fibroblasts and keratinocytes.

1.4.4 Actomyosin

The actomyosin, filament assemblies of actin and myosin II proteins, is a crucial part of the cell's cytoskeleton. The cytoskeleton is located in the cell cortex and it is important for cell stability and involved in cell migration. Myosin motor proteins drive contraction by sliding actin filaments past one another in an energy consuming process. This process is driving muscle contractions during physical exercise, but it is also essential in other cells. In non-muscle cells the contractility is regulated by actomyosin in disordered networks, and gradients of actomyosin contractility is driving cell shape changes during cell division, migration, and tissue formation (Koenderink & Paluch, 2018).

The extracellular matrix is linked to the cytoskeleton through integrin-based adherence complexes. Through the junctions in the complexes, cells are able to sense the environment and respond to mechanical forces acting across the junctions (Alberts et al., 2015d). The actomyosin filaments, as a part of the cytoskeleton, can thereby be used by the cells to sense changes in their environment and thus influence cell shape dynamics, differentiation and cell migration (Koenderink & Paluch, 2018).

Dynamic assembly and disassembly of actin filaments are important for cell migration. This dynamic process is regulated by a variety of tightly coordinated proteins like the actin related proteins 2/3 complex (Arp2/3 complex) and nucleation promoting factors (Schaks et al., 2019). In single cell migration, actin polymerization plays an important role in driving the formation of protrusive membranes called lamellipodia. Actomyosin is also thought to have a central role in mechanosensing during collective cell migration (Pandya et al., 2017).

Leader cells are localized in the front of a unit of collectively migrating cells. They receive guidance signals and instruct the other distinct cell population in the collective, the follower cells, through cell-cell junctions (Haeger et al., 2015). The leader cells determine the direction and speed in the collective migrating unit of cells. To generate integrin-based forward traction, the leader cells extend actomyosin-mediated protrusions. Differential organization of actin

filaments and activity levels of actomyosin contractility are required for polarisation and maintenance of leader cells (Pandya et al., 2017).

The actomyosin machinery can be regulated and organized in different ways, which results in different migratory strategies depending on cell type, cell number and tissue structure (Pandya et al., 2017). The Rho-associated protein kinase (ROCK) 1 and 2 are activated downstream of Rho GTPase, shortened Rho-ROCK, and act through several pathways to regulate the actin cytoskeleton and subsequently cell migration (Kümper et al., 2016).

1.4.5 The experimental system used to study cell migration

Many studies have been performed to understand mechanisms that regulate cell migration. The studies are performed using different experimental systems like scratch or barrier assays to examine how cells move collectively into an open area. Experiments performed during the course of this project are based on an *in vitro* experimental system previously published by Lång et al. (2018).

The main hallmarks of this assay are use of confluent keratinocyte cell sheets, and synchronization of the cells by serum deprivation resulting in a quiescent cell state in the cell sheet. Serum deprivation is maintained for a time period of 48 to 72 hours and subsequently serum re-stimulation of the confluent quiescent cell sheet result in activation of a highly coordinated collective cell migration response followed by cell division. The collective cell migration patterns were tracked using live cell imaging and the acquired data was analysed using the technique particle image velocimetry (PIV) described in the following section (Lång et al., 2018). The difference between this experimental system and other assays on collective cell migration is that it does not include a free space or an open area. Also, there is no apparent chemical gradient present, since the stimulating factors in serum are available to the entire cell sheet.

1.4.6 Particle image velocimetry (PIV) analysis

The method of particle image velocimetry (PIV) was first mentioned in 1984. The more modern form of the method is described by Adrian (2005) as ‘an accurate and quantitative measurement of fluid velocity vectors at a very large number of points simultaneously’. The method has evolved a lot and gone through a digitalisation over the years, starting as a system consisting of a pulsed laser with a light sheet illuminating particles at µm size in gases and liquids recorded photographically (Adrian, 2005).

For use in research and image analysis today, PIV analysis is typically performed on acquired data by use of automated tools as Python-based scripts. Live cell imaging provides a time lapse of images, one frame for each time point. PIV divides each image into small squares and changes in each square are registered between each frame. Used in this project, cell nuclei and changes in the position of the cells between the frames are detected and measured using PIV. Changes between two sequential frames are illustrated by a vector field that describe the observed changes in cell position. The size of the vector indicates the level of difference in nuclei position and thus how far the cell nucleus has moved between two time points. The direction of the vector indicates the direction of the movement. This vector field is further updated with a new image frame generating velocity fields that change over the time of image acquisition.

The final vector field generated as a two-dimensional velocity field will summarize total changes in position and the direction of the total changes in position and the direction of the positional change over time. This vector field can further be analysed by other Python-based scripts and can thereby provide information of cell sheet velocities, the direction of cell migration and the level of coordination of cell movements over time.

1.5 Fluorescence in biological research

When studying cells or tissues, cell components or the cells behaviour, it is useful to be able to visualize the interesting parts and outline them from other disturbance, or to track the cells and their movements. This can be done using fluorescent molecules, fluorophores, or by staining part of the cells with direct or indirect immunofluorescent dyes. Fluorophores are visualized by light excitation in a fluorescent microscope. Light energy with a wavelength in a specific spectrum is absorbed by the fluorophore, which then reach an excited state of higher energy before returning to its ground energy state and emit light energy with a longer wavelength. The emitted light is the coloured light that is detected by a detector and subsequently visualized in the microscope. Fluorescence has been used in biological research in the last century, and technological discoveries and development in chemistry have led to development of different kinds of fluorophores (Thermo Fisher Scientific, s.a.-a).

1.5.1 Fluorescent protein tags

One way of visualizing cellular components or proteins is with fluorescence with the use of biological fluorophores to tag cells or tissue, or to fuse it with a protein of interest. The first one ever used in research was GFP (green fluorescent protein) cloned from a jellyfish (Thermo Fisher Scientific, s.a.-a). Some of the other commercial fluorescent proteins available are RFP (red fluorescent protein) and mCherry. A fluorescent protein tag can be introduced into the cells by lentiviral infection, making the cell line transgenic (Kita-Matsuo et al., 2009; Lång et al., 2012). The transgenic cells will express the incorporated fluorescent protein and thereby be fluorescently tagged. An advantage of this method of fluorescence is that it can be applied in living cells, the cells stay alive and can be used in live cell imaging experiments.

1.5.2 Immunofluorescence (IF) staining

Fluorescent labelling, or staining, describe the process where a reactive derivative of a fluorophore is covalently attached to another molecule. Often, the derivate is attached to amino acids or proteins, but it can be directed to most molecules. A wide variety of systems for detection and quantitative measurements in biological research are applied with fluorescent staining (Thermo Fisher Scientific, s.a.-a).

Immunofluorescence (IF) staining of cells is commonly performed with the fluorophore derivative attached to antibodies. To visualize the part of the cell of interest the IF procedure utilizes the specific binding between the antibody and the antigen. A primary antibody binds to the specific protein, while the secondary antibody binds to the primary antibody. Detection of the protein of interest is then performed by detection of a fluorescent label, the fluorophore derivative, attached to the secondary antibody (Im et al., 2019).

E-cadherin and Aurora B are two proteins that can be detected by antibodies. E-cadherin is an adhesion protein important for formation of cell-to-cell interactions (Van Roy & Berx, 2008). Aurora B is a kinase that re-localizes from centromeres to midbodies during cell division. A midbody is formed between two daughter cells near the end of cytokinesis, and is thus a good marker for studies on related cells (Afonso et al., 2017). The use of antibodies in fluorescent staining is called indirect IF, however, another method, direct IF, is also available for visualizing of cellular proteins (Im et al., 2019).

Direct IF is based on other fluorescent molecules than antibodies. These dyes bind directly to its target in the cell, and additional steps in the staining protocol are therefore not required.

Phalloidin binding to actin filaments and DAPI colouring cell nuclei, are examples of direct staining of cellular components. Cell fixation is an essential step performed prior to IF staining, immobilizing antigens, or other target proteins, by preserving morphology and not disturbing cellular architecture (Im et al., 2019).

1.6 Estimating gene expression

Polymerase chain reaction (PCR) is a widely used method in molecular biological research, medical diagnostics, and forensics. The principle of PCR is to amplify specific regions of DNA by using sequence-specific primers, heat treatment and multiple cycles of DNA synthesis. Either DNA or cDNA can be used as template for PCR (Alberts et al., 2015a). There are mainly two types of PCR, qualitative and quantitative. The qualitative PCR can be used to detect absence or presence of a specific DNA sequence, while quantitative PCR (qPCR) is detecting the amount of a target sequence in a sample relative to the initial amount of the gene of interest. Quantitative PCR (qPCR) is thereby a common application used for estimating gene expression (Vandesompele, 2019).

1.6.1 RNA and cDNAs

RNA is an essential part of the protein synthesis and gene regulation. When estimating gene expression, RNA is isolated from the cells. RNA is a quite stable molecule due to thermodynamics but can rapidly be digested by ubiquitous RNase enzymes. Therefore, an RNA sample can contain large amount of RNA, but have poor quality and integrity with shorter RNA fragments present. Gene expression analysis performed based on RNA with poor quality may cause incorrect product detection due to reduced sensitivity for detecting transcripts expressed in low levels. An automated approach, the Agilent bioanalyzer system, to analyse the quality of the RNA has been developed (Schroeder et al., 2006).

Isolated RNA with good quality is converted to complementary DNA (cDNA) through the process of reverse transcription (RT) prior to quantitative PCR analysis. The RT reaction can be included as part of the PCR analysis or performed in a separate reaction. cDNA synthesis is based on messenger RNA (mRNA) in the sample being transcribed to DNA complementary to the RNA. By performing the procedure in two steps, a generated cDNA pool can be stored and used for multiple reactions. cDNA is more stable and more resistant to degradation than RNA (Vandesompele, 2019).

When using cDNA as template for RNA, it is important to avoid contamination and disturbance by other molecules, as genomic DNA (gDNA). Including an additional step to remove gDNA during RNA isolation is therefore recommended. Primers can also be designed in order to avoid amplification of remaining gDNA, since gDNA contains both introns and exons while cDNA only contains exons. Intron spanning primers is designed to hybridize the 3'-end of one exon and the 5'-end of the other exon and will thereby only amplify cDNA (Vandesompele, 2019).

1.6.2 Real-time quantitative PCR

There are two well established qPCR-techniques, real-time qPCR and Droplet Digital PCR (ddPCR). The ddPCR is the most recently developed technique of the two, where the PCR sample is split into many fractions performing thousands of PCR reaction, and the amount of amplified DNA-sequence is measured at the reaction end-point (Taylor et al., 2017). To perform real-time qPCR, a fluorescent reagent is used to detect the amount of target sequence in the sample after each cycle of DNA synthesis. Then it is possible to follow the amount amplified product at any time, in real time. Different fluorescent reagents are designed, and two of the most commonly used commercial chemistry techniques available for this purpose are SYBR® Green and TaqMan® (Thermo Fisher Scientific, s.a.-b; Vandesompele, 2019).

TaqMan® is a fluorogenic-labelled oligonucleotide probe designed specifically to the target sequence. The probe contains a fluorescent reporter dye, a fluorophore, on the 5'-end and a quencher dye on the 3'-end. As long as the probe is intact, the fluorescence from the reporter is quenched by transfer of energy to the quencher dye by fluorescence resonance energy transfer (FRET). The fluorescence is emitted from the reporter dye and reports fluorescent signals as a new DNA amplicon is produced. This occurs when the quencher and the reporter are split by cleavage of the probe, which occurs during polymerization when DNA polymerase extends the primer. The fluorescence signal is permanently increasing proportionally with product. The TaqMan chemistry and other probes has the advantage of specific hybridization between the designed probe and the target sequence (Thermo Fisher Scientific, s.a.-b; Vandesompele, 2019).

SYBR® Green is a double stranded DNA (dsDNA) binding dye. The DNA synthesis during a qPCR reaction is composed of cycles with denaturation and polymerization to amplify the target sequence and gradually generate more PCR product. During the denaturation process, SYBR® Green is released from the DNA, and during polymerization it binds again to each new copy of dsDNA. When bind to dsDNA, SYBR® Green emits fluorescent light. More PCR

product, dsDNA complementary to the target sequence, is produced as the PCR reaction progress, resulting in an increased fluorescence intensity proportioned to the amount of PCR product generated (Thermo Fisher Scientific, s.a.-b; Vandesompele, 2019).

A disadvantage with the SYBR® Green binding dye is that it binds to all dsDNA present in a sample. The fluorescence can thereby be caused by binding to nonspecific dsDNA and create false-positive signals. Due to this, qPCR analysis using the SYBR® Green dye requires specific and well-designed primers (Thermo Fisher Scientific, s.a.-b). A useful program to design and check the quality of primer sequences is BLAST®, the Basic Local Alignment Search Tool provided by the National Center for Biotechnology Information, NCBI. BLAST® provides a sequence database that can be used to compare and estimate statistical significances for regions of similarity in nucleotide or protein sequences. In addition, the database provides a specialized Primer-BLAST search tool (NCBI, n.a.; Ye et al., 2012). When designing, performing and publishing results based on real-time qPCR experiments, the MIQE guidelines defining Minimum Information for Publication of Quantitative Real-Time PCR Experiments (Bustin et al., 2009) is a useful tool for generating reliable and unequivocal result interpretation.

1.7 Knockdown of a gene

Protein function can be studied by use of experiments performing loss-of-function mutations in individual genes encoding a particular protein. This can be done by specific inhibition or by gene expression knockdown of the protein of interest. A widely used method for gene-specific degradation or silencing is RNA interference (RNAi) technology. RNAi is also a naturally occurring mechanism in animals, plants, and fungi, which is used for protection against viruses and transposable elements (Alberts et al., 2015b; Han, 2018; Moore et al., 2010).

The technique of RNAi introduces a double stranded RNA molecule into a cell or organism. This RNA molecule is complementary to the target mRNA or noncoding RNA and hybridized with it (Alberts et al., 2015b), leading to degradation of the mRNA transcript. The degradation is achieved through an enzymatic pathway involving the endogenous RNA-induced silencing complex (RISC). The molecule introduced is often a small interfering RNA (siRNA) or short hairpin RNA (shRNA) (Han, 2018; Moore et al., 2010).

A siRNA is typically 21-23 nucleotides long generated exogenous by chemical synthesis or *in vitro* transcription. Transfection by a lipid carrier to facilitate cellular uptake or by

electroporation with electric pulses generating pores in the cell membrane is both methods for delivery of siRNA into cells (Han, 2018). A shRNA consists of two complementary RNA sequences of 19-22 base pairs linked together with a loop of 4-11 nucleotides. Delivery into cells can be done endogenously by use of plasmid vectors or virally produced vectors as adeno-, retro-, and lentiviral vectors (Moore et al., 2010).

The decision to use siRNA or shRNA may depend on factors like the cell type, the need of transient or stable integration and available time. Advantages with siRNAs are a variety of commercially available transfection reagents, rapidly determined knockdown efficiency and low risk of cellular toxicity. However, off-target effects due to high concentrations of cytoplasmic siRNA have been reported, and the siRNA concentration is diluted by cell division leading to impossible generation of a long-time knockdown cell line. Creation of stable knockdown cell lines is possible using shRNA, and shRNAs can infect most cell types. However, this technique is very time-consuming including both an extensive preparation of vectors cloned with a shRNA and selection of positive knockdown cells (Moore et al., 2010).

Furthermore, other established approaches for gene knockdown are also available. One approach is the use of CRISPR-Cas systems. Clustered regulatory interspaced short palindromic repeats, better known as CRISPR, together with the CRISPR-associated proteins, Cas, is originally a prokaryotic adaptive antivirus immune system. There is an enormous diversity of CRISPR-Cas systems, which has been organized in a classification hierarchy (Makarova & Koonin, 2015). These systems have been implemented to biological research and gene editing. Orthologs of the system CRISPR-Cas13a is shown to be capable to target RNA by high specificity and provide high levels of gene knockdown (Abudayyeh et al., 2017).

1.8 Detection of proteins

There are different methods to detect and quantify proteins. The methods are either spectrometric or antibody dependent. Spectrometry methods commonly used are high performance liquid chromatography and liquid chromatography-mass spectrometry (Mann et al., 2001). Antibody methods are methods as protein immunoprecipitation (Selbach & Mann, 2006), enzyme-linked immunosorbent assay (Huang, 2001), protein immunostaining (Im et al., 2019) and Western blot analysis (Mahmood & Yang, 2012). For this project, the last protein detection method mentioned is of relevance.

1.8.1 Western blot

Western blot is a commonly used method to separate and identify proteins extracted from cells or tissues, and to investigate if a protein is expressed or not. This technique can be divided into three main elements; separation of proteins by size on an agarose gel, transfer of the separated proteins to a membrane, and marking target proteins and visualize it by use of antibodies labelled with a fluorescent protein (Mahmood & Yang, 2012). During the last decades, new methods and features have evolved to improve the technique making it more sensitive and automated, and to increase the reproducibility of the results (Mishra et al., 2017).

Today there are different materials commercially available to optimize the multiple steps in the protocol in relation to the sample preparation and specific protein detection. For instance, there is two different membranes available, nitrocellulose membrane and polyvinylidene fluoride (PVDF) membrane (Mahmood & Yang, 2012; Mishra et al., 2017). The membrane is a part of a bigger system, often called a sandwich, with filter papers soaked in buffer to perform a electrophoretic transfer of the proteins from the gel to a solid support, the membrane (Mahmood & Yang, 2012). These membrane systems is today available as a pre-assembled package (Mishra et al., 2017).

The multistep protocol provides important steps to achieve a good result. One of the steps are blocking, which prevents nonspecific binding of the antibodies to the membrane (Mahmood & Yang, 2012). The antibody used for specific detection of protein is also of big relevance, and so is the signalling protein attached to the secondary antibody facilitating visualization of protein bands. There is different digital detection systems available, as colorimetric and chemiluminescence, and these systems are frequently evolved facilitating better detection methods (Mishra et al., 2017).

1.9 Aim of the thesis

Lysophosphatidic acid (LPA) has been shown to be involved in and regulate many biological functions. However, the connection between LPA cell signalling and activation of collective cell migration is not yet fully established. The aim of the thesis is therefore to contribute to a better understanding of how LPA activates and regulates collective cell migration in human skin. This project and additional research in this field will at the same time, in the bigger picture, be a step towards answering which molecules and molecular mechanisms that are involved in skin wound healing, and why some wounds become chronic and never heal.

This research is performed mainly by *in vitro* cell culture work using a keratinocyte cell line, HaCaT, derived from human skin. One of the LPA receptors, LPAR1, is selected for a more comprehensive study on its functional role in migration activation in this project. Experimental approaches as live cell imaging, immunofluorescence staining, real-time qPCR, and gene knockdown evaluated by Western blot analysis have been central in this work. The methods are used in order to examine the following aspects of LPA and its influence on the HaCaT keratinocytes:

- Study and characterize LPA mediated cell migration responses in quiescent epithelial cell sheets.
- Examine how inhibition of LPA receptor 1 affects cell migration patterns and expression of actin networks.
- Study the expression of actin networks in LPA stimulated keratinocytes, and examine the correlation between actomyosin and collective cell migration.
- Estimate the mRNA expression levels of the six LPA receptors in HaCaT cells, and investigate if one of the receptors is directly involved in LPA mediated collective cell migration.
- Establish HaCaT cell lines with knockdown of LPAR1, and study potential changes in cell morphology and migration behaviour when expression of this receptor is reduced.

2 Materials and methods

2.1 Cell culture work

In this project, experiments were performed using the immortalized human keratinocyte cell line HaCaT (Boukamp et al., 1988). Both wildtype (wt) cells and cells modified with different fluorescently labelled proteins, as specified below, were utilized. In addition, HaCaT cell lines stably expressing shRNAs for specific gene knockdown were constructed during the course of the study (section 2.6).

2.1.1 Cell lines and growth conditions

The wt cell line used in the project was HaCaT provided from Cell line service (300493; CLS). Modified HaCaT cell lines expressing fluorescently labelled proteins were also included in some experiments. These were the HaCaT mCherry-Histone H2B cell line that stably expresses fluorescently labelled Histone H2B protein in the cell nuclei (Lång et al., 2012), and the HaCaT LifeAct cell line that stably express actin filaments labelled with a fluorescent dye called RFP (red fluorescent protein). These two modified HaCaT cell lines were previously constructed by the Bøe research group.

The optimal growth conditions for these cells are 37 °C with 5 % CO_2. The growth medium used was Iscove's Modified Dulbecco's medium (IMDM; Merck Life Science) with 10 % fetal bovine serum (FBS; Gibco™ Fetal Bovine Serum, Premium Plus) as nutrition and 1 % Penicillin-Streptomycin (PenStrep; Gibco™ Penicillin-Streptomycin) to inhibit bacterial growth.

2.1.2 Cell cultivation and passaging

Cultivation of the cells for proliferation was done in Nunc™ EasYFlask™ Cell Culture Flasks (Thermo Scentific™) with vented caps, which allows adequate gas exchange and keeps contamination out. The HaCaT cells are adherent and attach easily to both plastic and glass surfaces, as well as each other. Regular cell culture maintenance to ensure normal cell growth and division involved subconfluent culturing and regularly continuous addition of nutrients, preventing the cells from becoming too dense and to ensure that the level of nutrition was satisfactory for the cells. All cell cultures were monitored daily, by microscopy and by examining the colour and transparency of the medium, to ensure no contamination, good growth rates and optimal time intervals between each passage. The medium has a pH-gradient that

indicates when the nutrition level is low. By maintaining log phase growth, the number of healthy cells is maximized for use in the experiments.

Cells were passaged when the culture reached subconfluence of approximately 70-90 %. Washing and removal of dead cells were done with PBS (Phosphate-buffered Saline, Appendix A). To detach the cells from the plastic surface, and make a suspension of single cells, Trypsin (Gibco™ Trypsin-EDTA (0.05 %), phenol red) was added in an amount just enough to cover the cell sheet. Trypsin is a serine protease that cleaves protein bindings between the cells and between the cells and the plastic surface. The cell sheet was incubated with trypsin 10-15 minutes at optimal growth conditions. The detachment of the cells from the surface was observed microscopically. The cells started to round up and float around when the flask was tilted or taped by hand. Medium with FBS, natural containing trypsin inhibitors, was added to neutralize and inactivate the trypsin when the cells were completely loosened. Rigorous pipetting up and down separated adherent cell clumps into single cells and made the cell suspension homogenous. For dilution, one part of the cell suspension was left in the flask and more growth medium was added.

2.1.3 Cell count estimation

Prior to an experiment, the number of cells had to be estimated to ensure seeding of an appropriate number of cells in each well or dish. Counting of the cells was performed with Trypan Blue Stain (0.4 %, Invitrogen) and an automated cell counter (Countess™ 3 Automated Cell Counter, Invitrogen). Equal amounts of staining dye and cell suspension were mixed and added in both chambers of a disposable slide (Countess™ Cell Counting Chamber Slides, Invitrogen). The cell number per mL suspension was automatically estimated with default settings. Thereafter, the volume of suspension needed to obtain a certain number of cells was calculated based on the average number of living cells. An estimation of >95 % living cells was preferable before start of an experiment.

2.1.4 Cell starvation

In the live cell imaging experiments, cells were subjected to serum starvation for 48 hours prior to serum stimulation or treatment with other reagents. The starvation was performed by changing the growth medium to IMDM without serum, serum-free IMDM, after a confluent cell sheet was established in the wells. Serum starvation induces a quiescent cell state in the confluent keratinocyte monolayer and makes the cells more potent and responsive to further

stimulation. Cells used for IF staining and RNA isolation were also subjected to serum starvation prior to further treatment or harvest, respectively.

2.2 Live cell imaging of collective migration patterns

The aim of this part of the project was to study cell migration patterns in confluent HaCaT cell sheets that have been subjected to serum starvation initiating a quiescent cell state before stimulation with different growth factors. This was performed by live cell imaging using a previously published experimental system (Lång et al., 2018) described in section 1.3.4. The cell line HaCaT mCherry-Histone H2B was used to study cellular movements by detection of the fluorescent cell nuclei over a long period of time.

2.2.1 Preparation of cells

Cells were seeded to a confluent cell layer in 96-well glass bottom Sensoplates (Greiner Sensoplate™ plates, M4187-16EA, Merck Life Science (#655892, Greiner Bio-One)) coated with 0.02 mg/mL collagen IV (C7521, Merck Life Science). Subsequently, the cells were starved as indicated above (section 2.1.4). After starvation, the cells were stimulated with different reagents of interest. Cells stimulated with serum-free IMDM or IMDM containing 15 % FBS were used as negative and positive control, respectively. The positive control was chosen based on previous work (Lång et al., 2018) describing serum stimulation of starved cell sheets leading to activation of collective cell migration with high levels of coordination between migrating cells.

Several migration assays were performed, all including different growth factors like the lysophosphatidic acid (LPA; L7260, Merck Life Science) and the epidermal growth factor (EGF; 236-EG, R&D Systems), and inhibitors like the LPA receptor (LPAR) inhibitor Ki16425 (S1315, Selleck Chemicals), the EGF receptor (EGFR) inhibitor Gefitinib (Y0001813, Merck Life Science) and the Rho-associated kinase (ROCK) inhibitor Y-27632 (Y0503, Merck Life Sciences). Acquired data was used to analyse and compare cell migration velocity and the level of cell coordination in cell sheets treated with the specific reagents.

2.2.2 High-content microscopy of living cells

The ImageXpress Micro Confocal High-Content Imaging System (Molecular Devices) was used for the live cell imaging experiments. The microscope is equipped with an incubation chamber in which the temperature, humidity and CO_2-level are optimized for living biological

samples. Image acquisition begun one hour after the plate was inserted in the microscope, since this time is required to ensure optimized focusing during acquisition. A change in temperature between the plate material and the instrument will affect the focusing on the samples and subsequently the quality of the data and data analysis. The image acquisition is also sensitive to vibrations and mechanical disturbance in the system. An example of this is observed in one of the experiments, where the results include outliers produced due to irregular movements in the xy-stage of the instrument.

Cellular movements were monitored during a period of 30 hours and images were acquired with a time interval of 16 minutes. The microscope was run in widefield mode. Plate acquisition settings with a 4x 0.2 NA air objective, camera binning = 2, the TexasRed filter set and a 2x2 grid covering the whole well was used. The image pixel size was 3.367 µm x 3.367 µm. These experiments generated large data sets that was further analysed using *in-house* computation programmes (section 2.2.4).

2.2.3 Titration experiment of the LPAR inhibitor Ki16425

Since the LPAR inhibitor Ki16425 had never been used in the experimental system, a titration experiment was designed and performed in order to find the optimal concentration of inhibitor to be used in live cell migration assays. An optimal concentration will partly or totally inhibit the cell migration, and it is important to not use too high concentration as that will lead to unspecific inhibition. Concentrations reaching from 0.5 µM to 100 µM were tested together with FBS or LPA. The efficiency and specificity of the inhibitor could thereby be taken into consideration.

2.2.4 Processing of data acquired from migration assays

Images acquired from a single well were combined using the Create Montages and Overlays module in the MetaXpress software (Molecular Devices). This module generates a single image for each time point in all wells (tiling of images). Subsequently, this data could be further processed and analysed using the Fiji ImageJ software (imagej.net, (Schindelin et al., 2012)). The software includes different features for image adjustment, it can perform manual tracking of cell movements, visualize cell migration coordination and migration patterns, generate combined movie files and much more. However, because of the big amount of data generated by high-content imaging, it was not practical to perform the analysis manually with Fiji ImageJ.

To analyse whole data sets of acquired data, PIV (particle image velocimetry)-based scripts written in Python were used. This and further analysis, including illustration of results, were performed by *in-house* Python-based scripts run through the integrated development environment (IDE) software PyCharm (JetBrains s.r.o.). First, the datasets of single (not combined) images acquired from the MetaXpress software had to be sorted by wells instead of acquired time points during imaging, and this was done using a sorting script (Appendix B.1). The PIV analysis was performed within a selected rectangular area of each single picture. Within this area, velocity fields were generated and visualized by vectors. These analyses provided information about the migration speed and direction of migration (Appendix B.2), as well as the level of cell-to-cell coordination (Appendix B.3) in the cell layer over time.

The Plot Order Parameter (Appendix B.4) illustrates how coordinated the migration was over time, on a scale from 0 to 1. It is based on equation 1, where phi is defined by the average cosine for the angle of each vector produced by PIV with respect to the direction of the vector field. Phi describes the amount of coordination parallel to the direction of the field.

Equation 1: $$\Phi_{||} = \frac{1}{n}\sum_i \cos(\theta_i)$$ (Cohen et al., 2014)

Illustration of the migration velocity in the cell sheets is another useful feature provided by PIV analysis. The Speed plot (Appendix B.5) was used for this purpose, to visualize cell sheet velocity, presenting mean values for cell migration speed over time. The speed is presented as µm per hour (µm/h).

The script Streamline plot (Appendix B.6) visualizes migration patterns by analysing the combined images created directly of the acquired data in the MetaXpress software. A PIV-based vector field is generated and interpreted as a velocity field illustrated by curves. The curves have arrowheads showing the direction of the cell movements in a single well after a certain time of stimulation.

2.3 Visualization of actin networks by IF staining

Using immunofluorescence (IF) staining and confocal microscopy on the Leica TCS SP8 microscope (Leica Microsystems) equipped with a continuous white light laser and a 405 nm UV laser, the actin network of HaCaT wt cells, stimulated with different reagents were visualized.

2.3.1 Preparation of cells for IF staining

Cells were grown, treated with different reagents, and fixed on 12 mm round glass coverslips (VWR). Seeding of cells and serum starvation (see section 2.1.3-4) were performed in 6 cm petri dishes (Falcon® Cell Culture Dish) with the coverslips attached to the bottom of the dishes. Prior to cell treatment, the glasses were transferred to separate wells in multiwell plates. The reagents used for treatment were 12 µM LPA (L7260, Merck Life Science), 10 ng/µL EGF (236-EG, R&D Systems), 15 % FBS mixed with 10 or 20 µM Ki16425 (S1315, Selleck Chemicals), and 15 % FBS mixed with 5 µM Gefitinib (Y0001813, Merck Life Science), as well as positive and negative control of 15 % FBS and serum-free IMDM, respectively. The cell treatment was performed for 24 hours at 37 °C and 5 % CO_2.

Fixation of cells to the glass coverslips was done by exposing the cells to 4 % paraformaldehyde (PFA; 158127, Merck Life Science) for 10 minutes on ice. After fixation, 0.25 % Triton™ X-100 (T8787, Merck Life Science) was added to make the cells more permeable to fluorescent staining, using either antibodies or other fluorescent reagents, by opening pores in the cell membrane. PBS (Appendix A) was the dilution medium for both reagents and was also used in the multiple washing steps required.

2.3.2 Immunofluorescence (IF) staining

Prior to fluorescent staining, the fixed cells were treated with 0.5 % Bovine serum albumin, BSA (BSA Cohn fraction V, B2000, Saveen Werner AB). BSA works as a stabilizer and contributes to higher protein concentration without being part of the staining solutions. BSA was diluted in PBS and to remove remaining BSA, the cells were washed multiple times with PBS before the fixed cells were stained with fluorescent reagents.

The fluorescent reagent Phalloidin-iFluor 488 (ab176753, Abcam) is a so-called cyto-painter. This reagent contains Phalloidin conjugates that bind to actin filaments in the cells. The cells were incubated with this agent (1:1000 dilution) at room temperature in the dark for 30 minutes. The last step of staining was to attach the glass coverslip to a microscope slide (Thermo Scientific). This was done with Vectashield® Antifade mounting medium with DAPI (4’,6-diamidino-2-phenylindole; H-1200-10, Vector Laboratories) covering the cells on the coverslip facing downwards on the microscope slide. DAPI is a fluorescent DNA stain that colours the cell nuclei by binding to the AT regions of dsDNA.

2.3.3 Image acquisition using confocal microscopy

The Leica TCS SP8 microscope has three different lasers: a white light excitation laser, an UV laser, and a STED (Stimulated Emission Depletion) laser. The STED technology is used to achieve super-resolution and is a further development of conventional confocal microscopy.

The 405 nm UV laser was used to detect the DAPI signal, and Phalloidin was detected with the white light laser set to a wavelength of 488 nm. Acquisition of confocal images was performed sequentially for each channel using the 40x 1.3 NA oil immersion objective and hybrid detectors. Laser intensities were set for the FBS stimulated sample that showed the strongest fluorescence intensity in the 488 nm channel (Phalloidin). The instrument settings were kept constant throughout the experiment to facilitate comparison of the Phalloidin signal between samples.

Pictures were acquired in xy-direction in order to visualize the cell sheet, and in xz-direction to acquire cross sections of the cell sheet. An entire cell was imaged, either from top to bottom or side to side, by acquiring a series of images with a fixed step size of 0.75 µm. The acquired series of images is referred to as a z-stack that can be used to detect the exact position of proteins within the cell or to make projections of the whole content of a cell. The picture format used was 1024x1024 µm, which provides sufficient resolution for further image processing in Fiji ImageJ (imagej.net) or Adobe Photoshop. Multiple z-stacks were acquired randomly across each cell sheet in order to generate a representative data set for all cell treatments.

2.3.4 Image processing

The cell nuclei, imaged by DAPI staining, was used as a reference to illustrate if the actin network, stained by Phalloidin, was expressed on the basal or apical side of HaCaT cells treated with different reagents. The apical side of a cell refers to the top of the cell sheet, while the basal side is the side where the cell is attached to a surface. The intensity measurements were done using the Analyse – PlotProfile command in Fiji Images J (imagej.net), and a Python-based script (Appendix B.7) in PyCharm (JetBrains s.r.o.) was used to plot the data. Each z-stack, imaged in xz-direction, acquired from the treated cell sheet was analysed.

The fluorescence intensity measurements were performed across a selected region, a region of interest (ROI), surrounding the cell nuclei in an xz-oriented image. The ROI was positioned based on the DAPI intensity, and the Phalloidin intensity was subsequently measured across the same ROI. The intensity of DAPI was normalized giving highest expressed intensity the

value 1, which refers to the widest part of the cell nuclei, and decreasing values towards the apical and the basal sides. The intensity values measured for Phalloidin was also normalized. The same ROI was used in all images and manually positioned relative to the DAPI intensity. The plotting script used information about the normalized fluorescence intensity mean and standard deviation to compose the final figures. Due to measurement of both intensities with the same ROI positioning in each image, the plotted curve for Phalloidin intensity will show how the actin expression is positioned relative to the cell nucleus visualized by the DAPI intensity curve.

2.4 Live cell imaging monitoring actin networks

Another approach to investigate the impact of stimulating agents on actin network dynamics in HaCaT cells is by monitoring these networks by live cell imaging. The cell line used in this experiment was the HaCaT LifeAct cells, which express actin filaments labelled with a red fluorescent protein (RFP) tag. Cells were seeded to confluence in a 12 well plate (P12G-1.514-F, MatTek) coated with 0.02 mg/mL collagen IV (C7521, Merck Life Science). The cells were starved (section 2.1.4) prior to stimulation. The stimulation reagents used were 12 µM LPA (L7260, Merck Life Science) and 20 µM Ki16425 (S1315, Selleck Chemicals) mixed with 15 % FBS in addition to a positive and negative control.

Live cell imaging was performed on the Zeiss AxioObserver.Z1 microscope equipped with an Orca Flash 4.0 V3 digital CMOS camera (Hamamatsu), a 10x 0.3 NA EC Plan-Neofluar air objective, live cell incubation chamber with CO_2 and temperature control, and a Colibri 7 LED light source. This microscope is controlled by the ZEN 3.1 pro software.

Images were acquired over a period of 30 hours from the time of stimulation. The live-cell incubation chamber with CO_2 and temperature control attached to the microscope was used to ensure optimal growth conditions during microscopy. The Colibri 7 LED light source set to 555 nm was used to detect RFP labelled actin. Transmitted light and the 10x 0.3 NA EC Plan-Neofluar air objective Ph1 was used for phase contrast imaging in order to outline the cell contours. The picture format used was 1.3 µm/pixel that provides sufficient resolution for further image processing in Fiji ImageJ (imagej.net). The pictures were acquired from four sites in each well to generate a data set representative for each cell layer.

2.5 Estimating mRNA expression of LPARs in HaCaT cells

Quantitative Polymerase Chain Reaction (qPCR) was performed by the Real-Time principle, collecting data as it occurred during the amplification process, using the fluorescent dye SYBR® Green. The aim of these qPCR experiments was to estimate the expression level of messenger RNA (mRNA) for each of the six different LPA receptors (LPARs) in HaCaT wt cells.

To investigate the expression of LPARs in the general cell population, cells were harvested and RNA isolation was performed from multiple cell passages. Cell passages were selected for RNA isolation with some days interval to give the cell culture a chance to renew between each isolation.

2.5.1 RNA isolation

RNA is very sensitive for degradation. It is therefore important to keep the working environment free of RNase in order to protect the RNA samples from degrading enzymes. RNase Away™ Decontamination Reagent (Invitrogen) was used to keep equipment, lab benches and gloves clean. The water used in the following steps was Invitrogen™ UltraPure™ DNase/RNase-Free Distilled Water (Invitrogen), hereafter referred to as molecular biological water.

The HaCaT wt cells were grown to confluence on collagen IV (0.02 mg/mL) in petri dishes and starved 48 hours before harvest (section 2.1.4). Harvesting of the cells was done by trypsinization, followed by trypsin neutralization (section 2.1.2). The cell suspension was subjected to centrifugation to produce a cell pellet. The cell pellet was subsequently washed twice with PBS (Appendix A) prior to a final centrifugation step that produced the final cell pellet. The harvest was immediately followed by an RNA isolation protocol.

RNeasy Plus Mini Kit (Qiagen) was used to perform the RNA isolation. This kit includes gDNA eliminator columns that remove the genomic DNA (gDNA) from the cell lysate before the process of RNA isolation could proceed. The protocol was followed as described by the producer (Quick-Start Protocol, March 2016). After the last step, RNA elution, the RNA concentration was quantified spectrophotometrically using a NanoDrop™ One Microvolume UV-Vis Spectrophotometer (Thermo Scientific). The absorbance value, A260/A280, indicating purity and absence of proteins, should be approximately 2.0 in each sample. The RNA was stored at -80 °C.

2.5.2 Evaluation of the RNA quality

It is important to test the quality of the RNA to ensure that the fragments are intact. This was done using a 4150 TapeStation System (Agilent Technologies) and the protocol "Agilent RNA ScreenTape Guide for TapeStations". The system is an automated electrophoresis system for nucleic acids designed to analyse and evaluate the integrity and how intact the total amount of eukaryotic or prokaryotic RNA or DNA is. Each sample, in this case RNA samples, and a ladder, were mixed with a sample buffer and denatured 3 minutes at 72° C before loading into the instrument.

The software visualized the result as a digital gel with bands according to different fragment sizes compared to the ladder. It also visualized an electropherogram with peaks for the correlation between measured fluorescence and RNA amount of a given size. The RIN^e, RNA integrity number equivalent, is a software algorithm describing the RNA quality. It is based on the ratio of 28s rRNA to 18s rRNA, in eukaryotic samples, the big and small subunit of the eukaryotic ribosome, which theoretically makes up > 80 % of total RNA in a sample. The RIN^e-value range is expressed from 1 to 10, where 1 indicates totally degraded RNA and 10 indicates intact RNA of highest possible quality.

2.5.3 cDNA synthesis

RNA isolated from the HaCaT wt cells was converted to complementary DNA (cDNA) by reverse transcription (RT). This was performed with the High-Capacity cDNA Reverse Transcription Kit (Thermo Scientific) according to the manufacturer's instructions.

A 2x RT master mix was prepared and mixed 1:1 with 1 µgRNA/10 µL. The RNA amount used was calculated based on previous quantification on the NanoDrop™. The prepared samples were run on a thermal cycler (PTC-100 Programmable Thermal Cycler, MJ Research) with the following incubation steps; 25 °C in 10 minutes, 37 °C in 120 minutes, 85 °C in 5 minutes, and 4 °C on hold. Until further use, the synthesised cDNA was stored at -20 °C.

2.5.4 qPCR setup

The qPCR was ready to be set up with synthesized cDNA from RNA of good quality. In this case, all samples used had an A260/A280 value of approximately 2.0 and a RIN^e value of 10. To investigate the mRNA expression of all six LPARs, six different primer pairs were used in addition to a primer pair for the reference gene, *GAPD*, encoding GAPDH. *GAPD* was selected

as a reference gene due to its constant expression in samples from the same cell type. Detailed information about the primers is given in Table 2.1.

Table 2.1: Primers used in qPCR analysis. Summary of primers used for detection of each of the six target genes coding for LPA receptor 1-6, and the reference gene *GAPD*. All primers are designed by Eurofins. The product sizes are estimated with use of Primer-BLAST.

Target gene	Primer	Primer sequences F/R (5'-3')	Prod. size
EDG2	LPA1_F	GAATCGGGATACCATGATGAGTC	
(LPAR1)	LPA1_R	GCACACGTCTAGAAGTAACAAAACC	106 bp
EDG4	LPA2_F	CTGGTCAAGACTGTTGTCATCATCC	
(LPAR2)	LPA2_R	AGGACTCACAGCCTAAACCATCC	97 bp
EDG7	LPA3_F	TAGGGGCGTTTGTGGTATGCT	
(LPAR3)	LPA3_R	ATGGGGTTCACGACGGAGTT	139 bp
GPR23/P2RY9	LPA4_F	GCAAGCCTGCTACTCTGTCTCAA	
(LPAR4)	LPA4_R	TTGCAAATCTTTCCAAAAAGCAA	174 bp
GPR92/GPR93	LPA5_F	CGTGTCCTGACTACCGACCTACC	
(LPAR5)	LPA5_R	CAGCGAGAGGGTGAAGAGCA	185 bp
P2RY5	LPA6_F	TCATCTGCGTCCTCAAAGTCC	
(LPAR6)	LPA6_R	CCAATTCCGTGTTGTGAAGTAAAA	122 bp
GAPD	GAPD_F	TCAAGGCTGAGAACGGGAAG	
(GAPDH)	GAPD_R	GGACTCCACGACGTACTCAG	116 bp

Each sample in the qPCR reaction was set up with 2 µL diluted cDNA mixed with a reaction mix in a total reaction volume of 10 µL. The reaction mix consisted of 2x PowerUp™ SYBR® Green Master Mix (Applied Biosystems), 10 µM of forward and reverse primer, and molecular biological water. The cDNA was diluted 1:20 with molecular biological water in advance, and there two replicates of each cell passage with each primer pair were analysed. The samples used to create a standard curve, was added diluted cDNA concentrations according to section 2.5.6.

Negative controls were also included for each primer pair, where the cDNA was replaced with molecular biological water. These controls are used to check for non-specific signals from template contamination or primer dimers. No-RT controls, meaning samples that have not gone through reverse transcription (RT), thus samples with the original RNA were also prepared and included in the qPCR analysis. The no-RT controls are used to reveal the presence of any contaminating gDNA.

The qPCR experiment was performed using a StepOnePlus™ Real-Time PCR System (Applied Biosystems™) with the experimental setup for quantification based on the Relative Standard Curve method in StepOne™ Software v2.3. The program used the following thermal cycle: 10 minutes at holding stage at 95 °C for initialization, followed by 40 cycles of denaturation and polymerization at 95 °C for 15 seconds and 60 °C for 1 minute, respectively. Data was collected at hold stage of polymerization, generating C_T-values. The thermal cycle ended with a melt curve stage, running one cycle with the same temperatures and time points as previously before temperature increment of 0.3 °C ending at 95 °C for 1 minute. With data collection at the ramp and hold stage at the end, melting curves were generated by the instrument and melting temperatures (Tm) of the targets were indicated. The melting curves can be used to identify nonspecific PCR amplification.

2.5.5 Gel electrophoresis

The qPCR-products, one representative for each primer pair, were run on a 3 % agarose (UltraPure™ Invitrogen mixed with TAE) gel in order to visualize the product size and check for formation of unspecific products. 1x SYBR® Safe DNA Gel Stain 10.000x in DMSO (Invitrogen) was used as the fluorescent agent. The samples were loaded with 2µL 6x DNA Loading Dye (Thermo Scientific). Quick-Load® Purple 100 bp DNA Ladder (BioLabs) was used as DNA ladder. TAE (Tris Acetate EDTA) buffer was used to conduct electricity at the correct rate. The gel electrophoresis was run at 70 V in 50 minutes. To acquire an image of the gel, a BioRad ChemiDoc™ MP System-instrument with the software ImageLab™ (BioRad) was used with settings for UV-light.

2.5.6 The standard curve method

Standard curves of each primer pair were used to estimate the mRNA expression of the LPARs in the cDNA samples. These quantifications were based on the following equation:

$$Copy\ number_{gene(X)} = 10^{\left(\frac{CTvalue - intersect(X)}{slope(X)}\right)}$$

C_T-values were generated by the StepOnePlus instrument for each product amplificated by the primer pairs. The C_T, threshold cycle, is the PCR cycle number at which a detectable amount of product has been amplified. The standard curves were made based on C_T-values and log quantities of known concentration of DNA input. The intersect and slope were given by the trend line of the standard curve. All standard curves had a R-squared value above 0.99.

Multiple qPCR experiments were performed to optimize the standard curves before analyzing the cDNA-samples. Standard curves were made of a dilution series of pooled cDNA. The same dilution series was used for all primer pairs as all diluted concentrations of cDNA should be detected by all primer pairs. The dilution series used was in a range of 50 to 0.005 ng cDNA, corresponding to a 1:2 to 1:20000 dilution. Every cDNA-sample value had to be in the linear range of the standard curve for the primer specific to the product. The concentration of cDNA to be used for studying the mRNA expression of the LPARs was decided based on the standard curve experiments.

An additional dilution series was made with higher cDNA-concentrations in order to detect mRNA products of LPAR4. This dilution series ranged from 50 to 3.125 ng cDNA, corresponding to a 1:2 to 1:32 dilution.

2.5.7 Normalisation and statistical analysis of the qPCR results

The qPCR results were normalised to the reference gene, *GAPD*. This was done by normalisation of the mRNA expression of each LPAR relative to the mRNA expression of GAPDH in the same cDNA sample. To compare two independent qPCR experiments, the average expression of one receptor, LPAR1, was normalised relative to the average expression for each of the other receptors.

A two-sample paired t-test was performed to determine if differences observed in mRNA expression of LPARs in HaCaT wt cells are statistically significant or not. The t-test was performed in excel using a 95 % level of significance.

2.6 Knockdown of LPAR1

To further examine the function of LPAR1 in HaCaT cells, the gene encoding the protein, *EDG2*, was knocked down. This was done by using the shRNA technique, integrating a short hairpin RNA (shRNA) construct into the cell line with use of a lentiviral plasmid vector.

Two knockdown cell lines were prepared with two shRNA constructs that differed in its target sequence. The reason for generating two different cell lines was to ensure a higher chance of producing a successful knockdown cell line. Based on the nucleotide sequence for *EDG2*, the target sequences were designed manually with use of Standard Nucleotide BLAST (blastn, NCBI). The sequences were chosen based on their GC-content of 40-50 %, to ensure high specificity and stability of the constructs. The oligos composing the shRNA construct are also

designed manually, adding a 5'- and 3'-flank sequence to the forward and complementary reverse target sequence and a loop sequence between them. One forward and one reverse oligo are designed for each shRNA construct to fit the sticky ends on the chosen vector.

The knockdown cell lines are to be compared with HaCaT wt cells to study potential differences in cell phenotype. A third cell line was also produced, harbouring a shRNA construct with a target sequence not complementary to any human gene. This cell line was added to the study in order to ensure that potential phenotypic differences observed in knockdown cell lines are due to the specific shRNA. Thus, this cell line was used as a negative control and is called scrambled (scr).

Sherif Khodeer, working as a postdoc at Department of Microbiology, has performed the knockdown procedure (Khodeer & Era, 2017) (described in section 2.6.1-2.6.4) and handed over four stable cell lines as a result. The cell lines are called HaCaT wt/scr/kd1/kd2 ΔLPAR1 for wildtype, scrambled control, knockdown with shRNA1 and knockdown with shRNA2, respectively.

2.6.1 Cloning shRNA oligos to the pLKO.1 vector

There are several commercial Lentiviral vectors available. In this experiment, the pLKO.1 puro vector (Plasmid #8453, Addgene) was used. A simplified illustration of the vector with incorporated shRNA is shown in Figure 2.1.

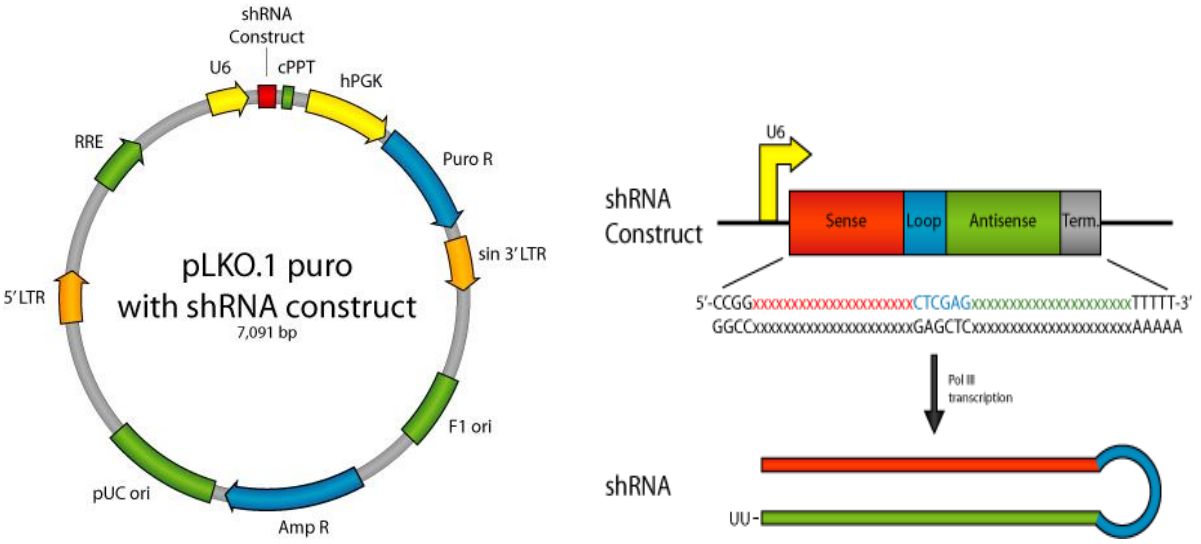

Figure 2.1: The pLKO.1 puro vector for knockdown using the shRNA technique. (A) Illustration of the pLKO.1 puro lentiviral vector with vector elements and shRNA construct. Descriptions of the elements are listed in Table 2.2. (B) Illustration of the shRNA construct inserted into the pLKO.1 puro vector to perform knockdown of a gene of interest (Addgene, 2006).

The vector has a lentiviral backbone and possesses several advantages as a gene coding for puromycin (puro) resistance used to select for positively infected cells. All the different components of the vector are presented in Table 2.2. Moreover, the vector can infect and integrate into both dividing and non-dividing cells due to the presence of long terminal repeats (LTR) and proteins within the pre-integration complex (PIC), which can mediate nuclear uptake and thereby allow infection of quiescent cells (Dimmock et al., 2017).

Table 2.2: Descriptions of the vector elements of the pLKO.1 puro vector incorporated into HaCaT cells to perform knockdown of LPAR1 (Addgene, 2006).

Vector element	Description
U6	Human U6 promoter drives RNA Polymerase III transcription for generation of shRNA transcripts.
cPPT	Central polypurine tract, cPPT, improves transduction efficiency by facilitating nuclear import of the vector's pre-integration complex in the transduced cells.
hPGK	Human phosphoglycerate kinase promoter drives expression of puromycin.
Puro R	Puromycin resistance gene for selection of pLKO.1 plasmid in mammalian cells.
sin 3'LTR	3' Self-inactivating long terminal repeat.
f1 ori	f1 bacterial origin of replication.
Amp R	Ampicillin resistance gene for selection of pLKO.1 plasmid in bacterial cells.
pUC ori	pUC bacterial origin of replication.
5'LTR	5' long terminal repeat.
RRE	Rev response element.

The first step of the knockdown procedure was to clone the designed shRNA oligos (Table 2.3) into the vector, pLKO.1 puro. By vector digestion with both EcoRI (#R3101S, NEB) and AgeI-HF (#R3552L, NEB) restriction enzymes, a linearized vector with sticky ends was produced. The two designed oligos were annealed together with the use of 10x annealing buffer (Appendix A) in a PCR reaction with gradually decreasing temperatures, generating a complementary overhang to fit the digested vectors. Then, both the linearized vector and the annealed oligos were ligated together using T4 DNA Ligase (#EL0012, Thermo Scientific).

Table 2.3: Target sequences for targeting the coding sequence of *EDG2*. These sequences were used to design shRNA oligos for knockdown of *EDG2* (LPAR1). Both target sequences for *EDG2* (LPAR1) and the oligos were designed manually and ordered from Eurofins. The sequence for the scrambled control is commonly used and is not complementary to any human gene.

Human (LPAR1) shRNA1	GTTCAACACAGGACCCAATAC
Human (LPAR1) shRNA2	TTGCAATCGAGAGGCACATTA
Scrambled shRNA	CCTAAGGTTAAGTCGCCCTCG

2.6.2 Plasmid Purification

The modified pLKO.1 puro vector was transformed into One Shot™ Stbl3™ Chemically Competent *Escherichia coli* (#C737303, Invitrogen) using a heat shock method. The bacterial cells were further plated on Ampicillin LB plates (made from BD Difco™ Dehydrated Culture Media: LB Broth, Miller (Luria-Bertani), BP Life Science and 100 µg/mL ampicillin, #0339-EU-100G, VWR) and incubated overnight at 37 °C.

The successfully transfected bacterial cells are ampicillin resistant due to a resistance gene present on the plasmid. Therefore, colonies produced on the agar plates after incubation is considered to harbour the modified vector. Subsequently, several colonies were picked and suspended in liquid LB with Ampicillin (100 µg/mL) for 16 hours at 30-37 °C with shaking. While in suspension, the *E. coli* cells were growing, dividing, and producing a lot of plasmids. Plasmids were purified using an EndoFree Plasmid Kit (#12362, Qiagen), which provides anion-exchange-based endotoxin-free plasmid DNA purification.

The same colonies selected for plasmid purification were selected for colony PCR analysis to confirm that the chosen colonies contain the pLKO.1 puro plasmid. GoTaq® Green Master Mix (M712, Promega) and two primers designed based on the plasmid sequence, U6 (GAGGGCCTATTTCCCATGATT) and PLKOR (GTATGTCTGTTGCTATTATGTC TAT), were used in the PCR analysis. The U6 and PLKOR primers were both ordered form Eurofins. Gel electrophoresis was performed to check the size of the products.

2.6.3 Production of Lentivirus

In order to introduce the shRNA-containing plasmids into HaCaT wt cells, lentiviruses were produced. This was done by using a second-generation packaging system, where the

components necessary for virus production are split across three plasmids to increase the safety of the lentivirus. The three vectors; a transfer plasmid pLKO.1 puro encoding the shRNA, a packaging plasmid psPAX2 (#12260, Addgene) and an envelope plasmid pMD2.G (#12259, Addgene), were transfected into a Lenti-X 293T cell line (#632180, Takara Bio) using FuGENE® 6 Transfection Reagent (#E2691, Promega). The viral supernatant was harvested after 48 and 72 hours and used directly for HaCaT wt infection.

2.6.4 Production of a HaCaT shLPAR1 stable cell line

The last and decisive step of the knockdown procedure was to make the stable cell lines of HaCaT with a functional knockdown of LPAR1. The viral supernatant was used to infect the target cells, HaCaT wt, for 7 hours. During infection, cells were cultured in the regular growth medium (IMDM with 10 % FBS). Subsequently, selection for the positively infected cells was begun by using the puromycin resistant trait. A killing curve for puromycin was adjusted in triplicates indicating that 0.5 µg/mL of puromycin was the optimum killing dose, where 95 % of the wt cells were killed. The selection was performed by culturing the cells in growth medium with 0.5 µg/mL Puromycin Dihydrochloride (#A1113803, Thermo Scientific/Gibco™). The selection went on for three days resulting in cell lines of HaCaT cells incorporated with a pLKO.1 puro vector expressing a shRNA construct mediating stable knockdown of *EDG2*, or the scrambled negative control.

2.7 Characterization of the LPAR1 knockdown cell lines

The stable knockdown cell lines were cultivated and passaged as previously described for the wt cells (section 2.1.2). All four cell lines included in the knockdown procedure was treated in parallel as one experiment. The cell lines were subjected to analyses on protein expression and phenotypic properties in order to examine the role of LPAR1 expression in HaCaT cells.

2.7.1 Western blot

Western blot analysis was performed in order to check the knockdown efficiency of LPAR1 in the new cell lines, HaCaT kd1 ΔLPAR1 and HaCaT kd2 ΔLPAR1. The two other cell lines generated during the knockdown process, HaCaT wt ΔLPAR1 and HaCaT scr ΔLPAR1, were included as controls.

A cell lysate of each cell line was made by lysing cells in a 1x Protein Cracking Buffer. The buffer was prepared from a 3x Protein Cracking Stock (Appendix A) by addition of β-

mercaptoethanol (Merck Life Science) and further dilution in Milli-Q-water. QIAshredder (QIAgen) columns were used to homogenize the cell lysates. The cell lysates were stored at -20 °C until use.

Step one of the Western blot procedure is protein gel electrophoresis. The cell lysates were heated up at 70 °C for 10 minutes before loading on a Bolt™ 10 % Bis-Tris Plus Mini Protein Gel (Invitrogen) installed in a Mini Gel Tank (Invitrogen). The Precision Plus Protein™ Dual Color Standards (1610374, Bio-Rad Laboratories) was used as protein ladder. Two replicates of the same sample setup were run on one gel. The electrophoresis was conducted in 1x MOPS-buffer (diluted Bolt™ MOPS SDS Running Buffer 20x, Invitrogen) and the gel was run at 200 V for 50 minutes.

Protein bands separated on the gel were transferred to a membrane, Trans-Blot® Turbo™ Mini PVDF Transfer Packs (Bio-Rad Laboratories), by blotting with the use of Trans-Blot® Turbo™ Transfer System (Bio-Rad Laboratories). The membrane was cut in two, giving one replicate of the sample setup on each part. The two half membranes were further treated in parallel but used for protein detection with different antibodies. Expression of LPAR1 was examined on one membrane, and the other part was used as a protein loading control of α-tubulin. In the protein loading control, equal protein expression is expected for each sample. It is very important not to touch the membrane at any point, since it is very sensitive to protein contaminations that result in background noise during membrane development. It is also important to keep the membrane soaked at all times. A rocking platform facilitates uniform soaking of the membranes during antibody incubation and use of very large volumes are thereby avoided.

To prepare the proteins on the membranes for binding to antibodies, the membranes were incubated 1 hour with 5 % skim milk (Skim milk powder, 70166, Merck Life Science, in PBS-Tween) to block the proteins. Thereafter the membranes were incubated with a primary antibody at 4 °C overnight. The primary antibodies were diluted in 5 % skim milk. Two different primary antibodies detecting LPAR1 were tested. Information about the antibodies used for Western blot analysis is provided in Table 2.4.

The membranes were washed with PBS-Tween (Appendix A) before incubation with a secondary antibody targeting the primary antibody. The secondary antibodies were diluted in PBS-Tween. Incubation was performed for 1 hour at room temperature.

The secondary antibodies are conjugated with a HRP (Horseradish peroxidase) tag, and the SuperSignal™ West Pico Plus Chemiluminescent Substrate (Thermo Scientific) is used to detect the presence of antibodies bounded to proteins on the membrane. The substrate, a luminol-based chemiluminescent substrate, is composed of a luminol solution and a peroxide solution. Antigen is detected by the reaction where luminol is oxidized in the presence of HRP and peroxide, producing a prolonged chemiluminescence. The membranes were incubated with the chemiluminescent substrate solution just before detection and imaging on a BioRad ChemiDoc™ MP System-instrument using the software ImageLab™ (BioRad).

Table 2.4: Antibodies used for Western blot analysis. Two, a polyclonal and a monoclonal, primary antibodies targeting LPAR1 and one antibody targeting the protein loading control, α-tubulin, were used for detection of proteins by Western blot. One secondary antibody conjugated with HRP was used for each protein. Detection size of the protein band and the dilution factor are given.

Target protein	Antibody	Detection size	Dilution
LPAR1	Primary antibody nr. 1: Anti-EDG2 /LPA-1 antibody. Rabbit polyclonal. ab23698, Abcam.	43 kDa	1:250
	Primary antibody nr. 2: Recombinant Anti-EDG2 / LPA-1 antibody [EPR9710]. Rabbit monoclonal. ab166903, Abcam.	39 kDa	1:2000
	Secondary antibody: Donkey Anti-Rabbit IgG H&L (HRP). ab6802, Abcam.		1:5000
α-tubulin	Primary antibody: Monoclonal anti-α-tubulin antibody produced in mouse. T5168, Merck Life Science.	50 kDa	1:5000
	Secondary antibody: Donkey Anti-Mouse IgG H&L (HRP). ab6820, Abcam.		1:5000

2.7.2 Studying cell morphology

By using an Olympus CKX53 Cell Culture Microscope with 4x objective and the CellSens imaging software, images of the cell cultures were acquired. Imaging was performed at different levels of cell sheet confluence to compare cell morphologies of the four cell lines.

2.7.3 Live cell imaging of knockdown cell lines

A live cell migration experiment was set up to investigate cell movements and migration patterns in the cell lines with knockdown of LPAR1. All four cell lines were included in the same experiment. The experiment was performed on the Zeiss AxioObserver.Z1 microscope with settings for phase contrast imaging with transmitted light, as previously described in section 2.4.

Cells were seeded to confluence in a 12-well glass-bottom plate (P12G-1.514-F, MatTek) coated with 0.02 mg/mL collagen IV (C7521, Merck Life Science). Three wells were seeded with each cell line, and the cells were starved for 48 hours (section 2.1.4). Subsequently, cells were treated with either 12 µM of LPA (L7260, Merck Life Science), 15 % FBS (positive control) or serum-free IMDM (negative control).

2.7.4 Analysis of acquired data from live cell imaging

The data acquired from the Zeiss microscope was analysed in order to investigate the impact of LPAR1 expression according to activation and coordination in migrating cell sheets. The TrackMate function in Fiji ImageJ (imagej.net/TrackMate; (Tinevez et al., 2017)) was used to manually track the migrating cells in the cell sheets, and a Python-based script (Appendix B.8) in PyCharm (JetBrains s.r.o) was used to plot the data. Figures showing the velocities generated in the migrating cell sheets were produced.

2.8 Data analysis and Image processing

Image processing and data analysis are performed using the software Fiji ImageJ (imagej.net, (Schindelin et al., 2012)), Microsoft® Excel® and PyCharm (JetBrains s.r.o.). Figures and illustrations are made in Adobe Photoshop CS6. Detailed information about the procedures used for each experiment can be found in the specific method sections described above.

3 Results

3.1 Cell migration patterns

Live cell imaging was used for investigation of cell migration patterns by monitoring the fluorescent nuclei expressed in HaCaT mCherry-Histone H2B cells. The cells were stimulated after a quiescent cell state was established in the cell sheet, and the cell movements were subsequently monitored for 30 hours. The results are shown as figures where cell sheet coordination or cell sheet velocities are compared between different cell stimuli. Cell migration patterns are also visualized using streamline plots.

3.1.1 Cell migration patterns of stimulated HaCaT cells

Different stimulating reagents are used to gather insight on how specific cell receptors regulate cell migration. In Figure 3.1 and 3.2, cells stimulated with LPA or EGF are compared with a positive control, FBS. A diagram showing data acquired from the positive control together with starved cells as negative control is also included (Figure 3.1.A/3.2.A). As a control to EGF stimulated cells, the EGF receptor (EGFR) inhibitor Gefitinib was included in the experiments. This result is presented in Appendix C including visualization of cell sheet coordination (Figure C.1) and speed (Figure C.2). Figure 3.1 is produced using the Plot Order Parameter script that provides plots showing the level of coordination between the migrating cells.

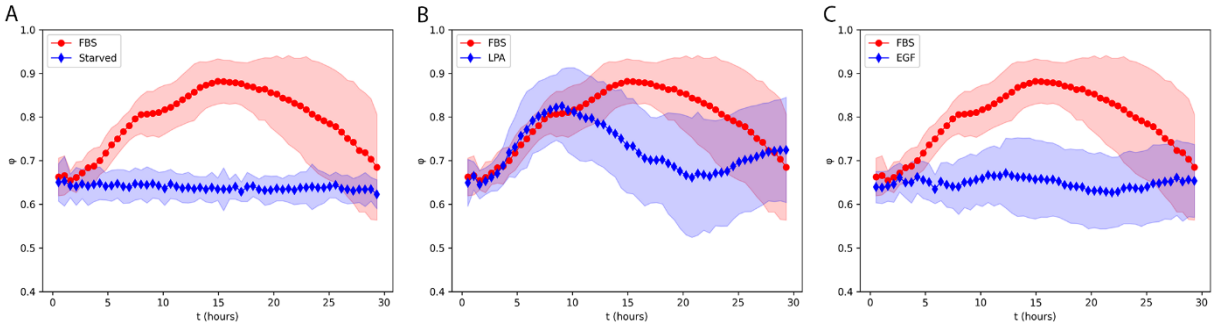

Figure 3.1: Coordination of migrating cells stimulated with different reagents. The factor φ describes the amount of coordination parallel to the direction of migration in the cell layer of positive, FBS, and negative, starved, control cells (A), FBS and LPA stimulated cells (B) and FBS and EGF stimulated cells (C). The plots are showing mean values with standard deviation.

The positive control, in this case FBS stimulated cells, is shown as the red graph in each of the three plots in Figure 3.1. FBS stimulated cells show a gradually increasing coordination in the cell layer, and the highest level of coordination is achieved about 15 hours after stimulation. When comparing FBS with LPA stimulated cell sheets (Figure 3.1.B), the same level of coordination is observed by the maximum values of the standard deviation. Interestingly, LPA

stimulated cells coordinate their cell movements faster than FBS stimulated cells. However, this high degree of coordination is observed during a shorter time period than with FBS stimulation.

The graph with EGF stimulated cells (Figure 3.1.C) shows a low level of coordinated migration. The mean values are similar to the graph for the negative control cells (Figure 3.1.A), where the cells do not migrate, but the standard deviation is showing larger variations. The reason explanation of this observation is further commented when presenting the streamline plot (Figure 3.3). Even if the coordination is defined between zero and one, the PIV data generates vector fields of vectors with angels of zero to 180 degrees, giving minimum mean φ-factor values above 0.5, as seen for the negative control cells.

In Figure 3.2, three plots of cell sheet velocity are shown for the stimulating agents LPA and EGF, together with positive and negative control, FBS and starved cells, respectively.

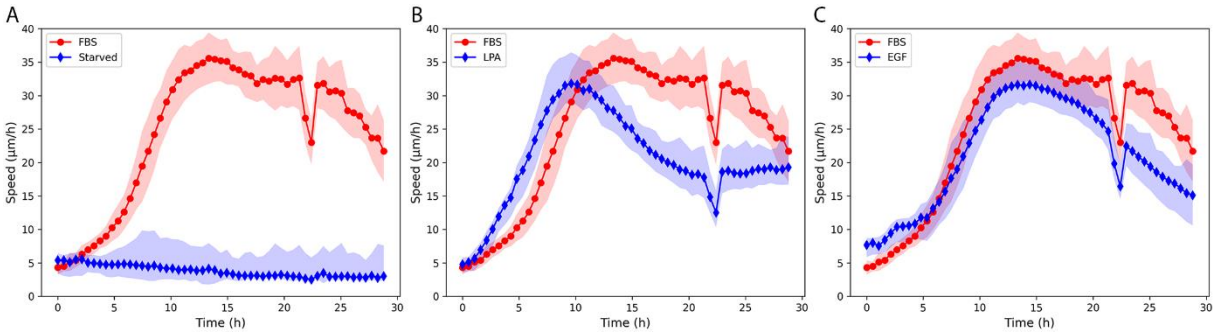

Figure 3.2: Cell sheet velocities generated after stimulation with different reagents. The speed in the migrating cell sheet is expressed as µm/h. The three plots are comparing positive, FBS, and negative, starved, control cells (A), FBS and LPA stimulated cells (B) and FBS and EGF stimulated cells (C). Mean values with standard deviation are shown. The outliers are due to irregular movements in the xy-stage of the ImageXpress microscope.

The red graph in each plot in Figure 3.2 is showing a maximum migration speed for the FBS stimulated cells between 35 and 40 µm/h. The time point for maximum cell sheet velocity corresponds to the time point of highest cell sheet coordination (Figure 3.1). For the LPA stimulated cells (Figure 3.2.B), maximum speed is reached at an earlier time point after stimulation, but the velocities generated are lower than with FBS, and these cells reach a plateau speed after approximately 20 hours. The EGF stimulated cells (Figure 3.2.C) have a speed curve, which closely follows that of FBS stimulated cells although the mean values are about 5 µm/h lower at the time point of maximum speed. Together, the results presented in Figure 3.1 and 3.2 show a clear difference in the ability of these three reagents (FBS, LPA and EGF) to

regulate cell sheet coordination, while all three reagents are able to activate similar cell sheet velocities.

Figure 3.3 illustrates the migration patterns in wells of stimulated HaCaT cells by streamline plots. Streamline plots were generated over time and the figure shows representative images after 16 hours of stimulation. The cells are stimulated with FBS, LPA or EGF.

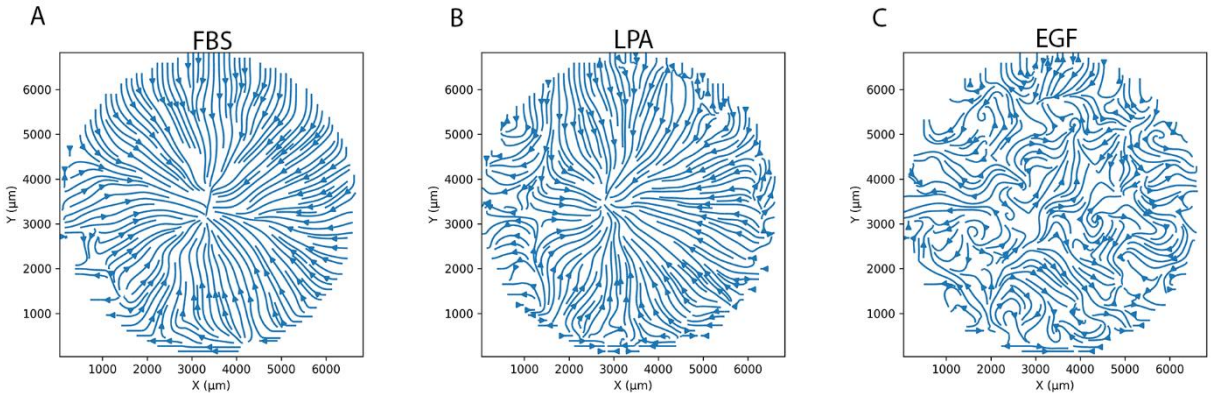

Figure 3.3: Streamline plots of migrating cells. Each arrow in the vector fields illustrate the direction of the cell movements in a single well of cells stimulated with FBS (A), LPA (B) and EGF (C). The x- and y-axis are presenting the size of the well in µm.

The streamline plots (Figure 3.3) show that FBS and LPA stimulated cells move in the same direction as one coordinated unit, in this case towards the centre of the well. Cells stimulated with EGF, on the other hand, show a different migration pattern with cells migrating in all directions. Here, the cell sheet shows local regions of highly coordinated cells, while other regions show no coordination. This corresponds to the result presented in Figure 3.1.C. EGF stimulated cells showed large variations in cell sheet coordination as shown by the standard deviation, at the same time as the mean values was similar to the coordination level of the negative control cells. The difference occurs due to the presence of local regions with high coordination or no coordination in the cell sheets that gives us a broad range of coordinated values (standard deviation), while the mean values add the different coordination values together, resulting in a total level of coordination with low φ-values and a graph similar to that shown for the starved cells.

3.1.2 The effect of the LPA receptor inhibitor Ki16425 on cell migration

In order to examine the role of LPA receptor signalling in HaCaT cells, the inhibitor Ki16425 was used. According to the producer, Ki16425 inhibits LPAR1 and partly LPAR3. Titration experiments were performed to test the effect of the Ki16425 inhibitor on the experimental system. The cells were stimulated with different concentrations of the inhibitor mixed with FBS

or LPA. This is done to examine differences in inhibition efficiency when different mixes of signalling proteins are present in the reactions. In Figure 3.4, coordination of cells stimulated with FBS and 10 or 20 µM Ki16425 are shown, in addition to control cells.

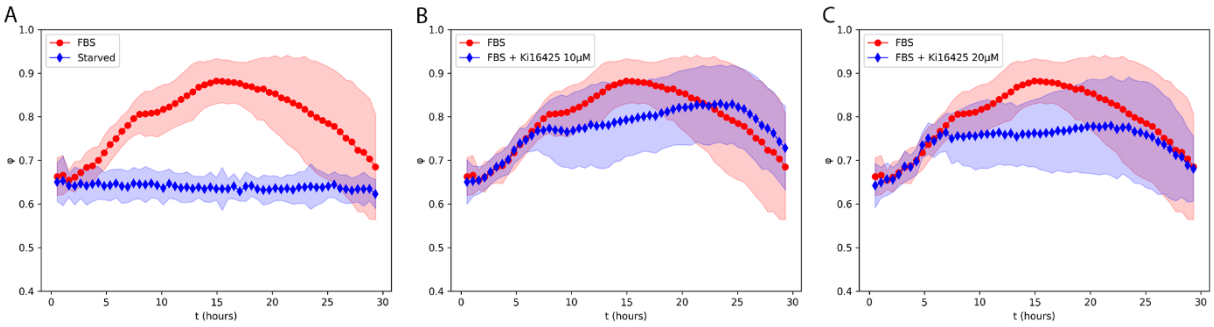

Figure 3.4: Coordination plot for titration of Ki16425 mixed with FBS. The amount of coordination in the cell sheet is described by the factor φ in the plots. The plots illustrate the positive control, FBS, as the red graph and starved cells, negative control (A), cells stimulated with 10 µM Ki16425 (B) and 20 µM Ki16425 (C) as blue graphs. The plots are showing mean values with standard deviation.

Figure 3.4 illustrates that treatment of cells with the LPA receptor inhibitor Ki16425 reduces the level of cell sheet coordination compared to cells stimulated with FBS alone. The mean values indicate lower levels of maximum coordination both with 10 and 20 µM Ki16425, all though the large variations shown by the standard deviation does not indicate a significant difference.

To check if the inhibitor has an effect on the migration speed for cells treated with FBS and Ki16425, plots showing cell sheet velocity were produced. These are shown in Figure 3.5.

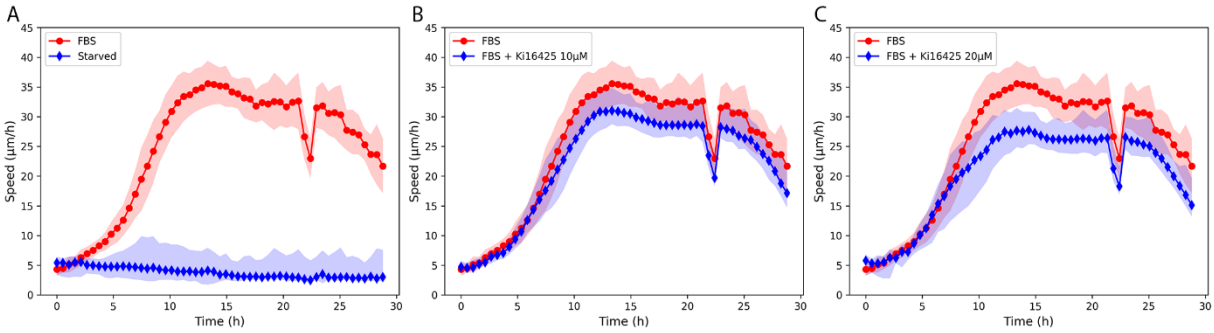

Figure 3.5: Migration velocity for titration of Ki16425 mixed with FBS. Illustration of cell sheet velocities (µm/h) produced after stimulation with 10 µM (B) and 20 µM (C) Ki16425. The positive control, FBS, are included as the red graph in each plot, and starved cell sheets, the negative control is also included (A). The plots are showing mean values with standard deviation. The outliers are caused by irregular movements in the xy-stage of the ImageXpress microscope.

The plots in Figure 3.5 show a reduction in cell migration velocities produced when the cells are treated with Ki16425. However, the curves of Ki16425-treated cells follow the curve of FBS stimulated cells until around 7 hours of stimulation when a reduction of approximately 5 and 10 µm/h for 10 and 20 µM Ki16425 is observed.

Subsequently, the titration experiment of Ki16425 was performed with LPA in the same way as with FBS to examine differences due to signalling proteins present in the reactions. In Figure 3.6 and 3.7 cells stimulated with three different concentrations of the inhibitor, 5, 10 and 20 µM, are plotted. Figure 3.6 illustrates the level of coordination in the cell sheets.

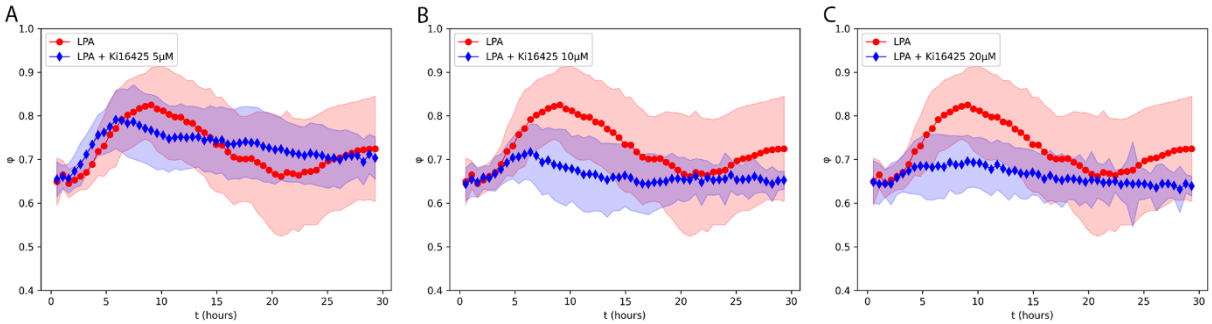

Figure 3.6: Cell coordination for titration of Ki16425 mixed with LPA. The factor φ describes the amount of coordination in the migrating cell sheets. The red graphs show the level of coordination between cells stimulated with LPA. The titration of Ki15425 with LPA is shown in blue with 5 (A), 10 (B) and 20 (C) µM Ki16425. The plots are showing mean values with standard deviation.

Figure 3.6 shows that Ki16425 affects the migration pattern in the cell sheet, leading to reduced levels of coordination compared with LPA stimulated cell sheets. Notably, the level of coordination is more reduced in the cell sheets treated with higher concentrations of Ki16425. This is observed with both FBS and LPA (Figure 3.4 and 3.6). Compared with Figure 3.4, the inhibitor has a more pronounced effect on cell coordination when it is mixed with LPA compared to FBS.

In Figure 3.7 the cell sheet velocity is illustrated for cells stimulated with LPA and different concentrations of Ki16425.

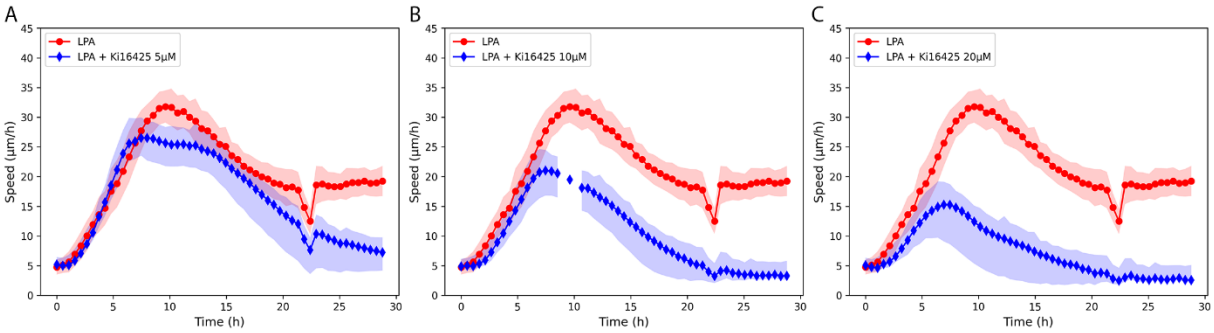

Figure 3.7: Cell sheet velocity for titration of Ki16425 with LPA. The speed (µm/h) of the migrating cells is illustrated for 5 (A), 10 (B) and 20 (C) µM Ki16425 mixed with LPA. Migration speed of cells stimulated with only LPA is presented as the red graph in each plot. The plots are showing mean values with standard deviation. The outliers at 22 hours are due to irregular movements in the xy-stage of the ImageXpress microscope. The missing data points in the blue graph in plot B is due to unknown errors during data processing.

Figure 3.7 is showing reduced migration speed for cells stimulated with increasing concentrations of inhibitor. Compared to Figure 3.5, the inhibitor has a bigger effect on cell sheet velocity when the cells are stimulated with only LPA compared to FBS. With 10 µM Ki16425 the average maximum speed is lowered by approximately 10 µm/h and 5 µm/h for LPA and FBS stimulated cells, respectively. Based on these four figures, Figure 3.4-3.7, the effect of the inhibitor is clearly concentration dependent.

3.1.3 The effect of the ROCK inhibitor, Y-27632, on cell migration

Another inhibitor included in the experiments was Y-27632. This inhibitor affects both Rho-associated kinase 1 and 2, and it thereby regulates many important cell functions like actin organization and cell migration (see section 1.4.4). In this experiment, Y-27632 was included to examine its effect on activation of cell migration in HaCaT cells, and to investigate the importance of actin organization for cell migration. Figure 3.8 and 3.9 are presenting results on the coordination and the velocity of migrating cells when they were treated with this inhibitor. The inhibitor is mixed with FBS or LPA. In Figure 3.8 the coordination is shown.

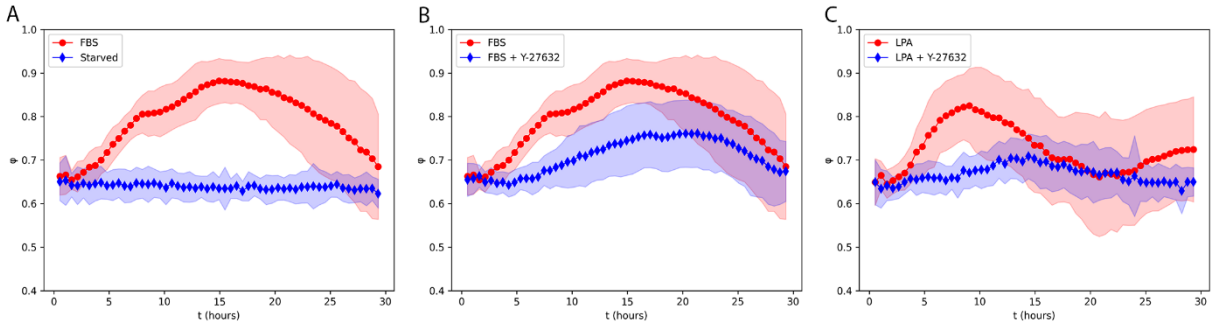

Figure 3.8: Coordination affected by Y-27632. The factor φ describes how coordinated the migration in the cell layer was when cells were stimulated as positive, FBS, or negative, starved, control (A), with FBS and FBS mixed with Y-27632 (B), and LPA and LPA mixed with Y-27632. The plots are showing mean values with standard deviation.

The Figure 3.8 is showing reduced levels of coordination after treatment with the Y-27632 inhibitor, both in FBS and LPA stimulated cell sheets. With LPA, the effect is more pronounced with mean values at its maximum after about 15 hours of stimulation and otherwise coordination levels resembling the negative control cells.

In Figure 3.9 the migration speed of the cells treated with Y-27632 is illustrated in plots showing cell sheet velocity.

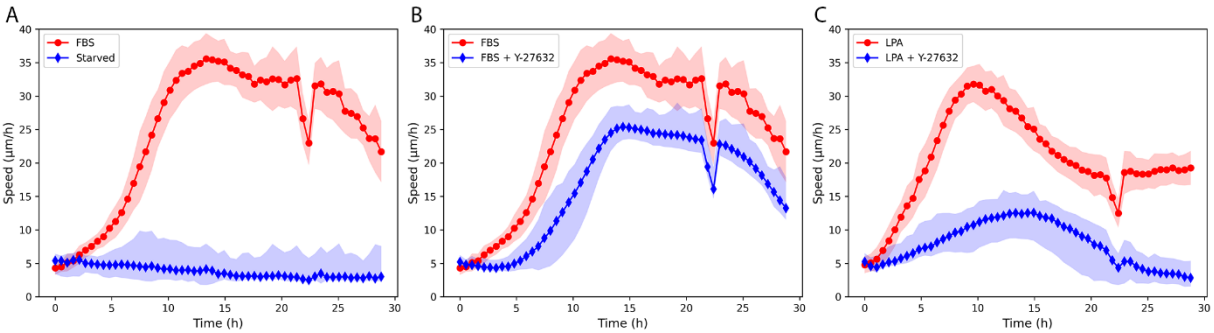

Figure 3.9: Migration speed generated after Y-27632 treatment. The migration speed (µm/h) of the stimulated cell sheets is illustrated for cells stimulated as positive, FBS, and negative, starved, controls (A), cells stimulated with FBS and FBS mixed with Y-27632 (B) and LPA and LPA mixed with Y-27632 (C). Mean values with standard deviation are shown. The outliers are due to irregular movements in the xy-stage of the ImageXpress microscope.

Both cells stimulated with FBS and LPA show reduced migration speed due to inhibition using Y-27632, according to Figure 3.9. The effect is, here as well as for the coordination, more pronounced in LPA stimulated cells than the cells stimulated with FBS. The maximum speed is approximately reduced twofold with LPA compared to stimulation with FBS.

Due to ROCKs regulatory functions in activation and stabilisation of the actin network, and these results presenting changes in cell sheet velocity and coordination upon ROCK inhibition,

it is interesting to further investigate the expression of actin in cell sheets treated with different reagents.

3.2 Visualization of actin networks

Experiments were performed in order to examine if actomyosin networks are involved in the regulation of cell sheet coordination. This is done by visualization of the actin networks in HaCaT cells, and by investigating changes in the expression of actin filaments after stimulation with different reagents. These experiments were performed using immunofluorescent (IF) staining of HaCaT wt cells and live cell imaging of HaCaT LifeAct cells.

3.2.1 Immunofluorescently stained actin networks

IF stained actin networks in HaCaT wt cells were imaged using a confocal microscope. Images were acquired in both xz- and xy-orientation (see section 2.3.3). The images were analysed based on the location of actin filaments in the cell layer and visible phenotypic variations. The results are presented in Figure 3.10 and 3.11. Cross section images, xz-orientation, were used to produce the intensity plots shown in Figure 3.10. The figure illustrates actin expression in the cells, which is shown by the distribution of the Phalloidin intensity. The intensity of DAPI, colouring the cell nuclei, is included as a reference that show the positioning of the cell during analysis. The apical side of a cell refers to the top of the cell sheet, while the basal side is the side where the cell is attached to a surface. Cells treated with the LPAR inhibitor Ki16425 are presented as well as cells stimulated with FBS, LPA, EGF and starved cells for comparison.

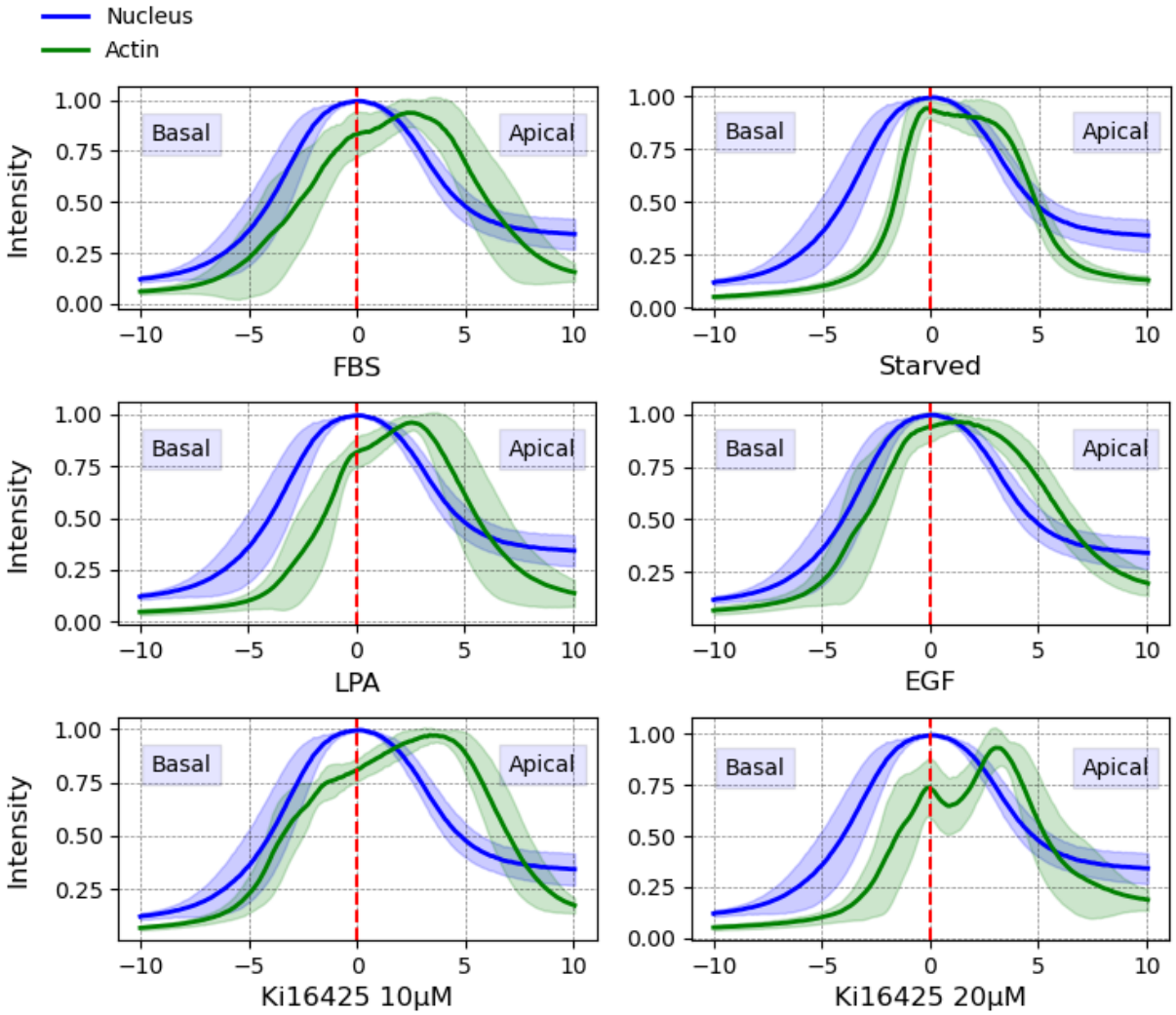

Figure 3.10: Apical and basal actin expression in HaCaT cells. DAPI has coloured the cell nuclei and Phalloidin has coloured the actin filaments. The distribution of the Phallioidin intensity is plotted relative to the distribution of the DAPI intensity. The basal and apical expression of actin are illustrated for FBS stimulated and starved cells (upper panels), cells stimulated with LPA and EGF (middle panels), and cells treated with 10µM and 20µM Ki16425 mixed with FBS (lower panels). Mean values of normalized data is shown with standard deviation.

Figure 3.10 shows that DAPI is expressed more or less evenly in the cell nuclei and is therefore a good reference marker. The same reference values of DAPI intensity are shown in all plots, and used as a reference to show where the basal and apical side of the cell is situated in the diagram, and how actin is expressed relative to this. For most of the cell treatments, actin expression is observed mainly towards the apical side of the cell. For FBS and LPA stimulated cells, actin is expressed quite similar, but with LPA the curve is a bit lower at the centre with a higher maximum intensity apically. For the starved cells and the EGF stimulated cells, the figure shows that actin is expressed more evenly across the cell. The plots representing cells treated with Ki16425 are showing mainly apical actin expression.

To visualize actin networks across a cell sheet after stimulation, representative images for each cell treatment are presented in Figure 3.11.

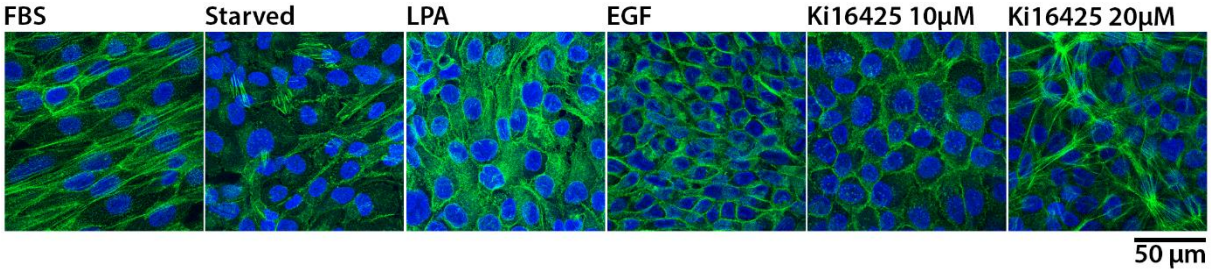

Figure 3.11: IF stained HaCaT cells. Pictures of cell sheets stained with the immunofluorescent dyes DAPI (blue), colouring the cell nuclei, and Phalloidin (green), colouring actin filaments. The cell layers constitute of FBS stimulated cells, starved cells, cells stimulated with LPA and EGF, and cells treated with 10 and 20 µM Ki16425 mixed with FBS.

The pictures in Figure 3.11 show that cell sheets stimulated with FBS and LPA are expressing actin filaments that form a network on top of the cells. Starved cells and EGF stimulated cells do not show the same phenotype. Cell sheets treated with the LPAR inhibitor Ki16425 express actin networks, and especially the cell sheet stimulated with 20 µM Ki16425 shows the presence of large actin networks with long actin filaments crossing apically along the entire cell sheet.

3.2.2 Expression of actin visualized in HaCaT LifeAct cells

Live cell imaging was performed on HaCaT LifeAct cells. Cell sheets of starved cells, FBS stimulated cells, LPA stimulated cells and cells treated with 20 µM Ki16425 mixed with FBS were included in the experiment that aimed to investigate changes in actin expression due to the different cell treatments. The cell contours were detected by phase contrast imaging and fluorescent actin was imaged by using a LED light source set to 555 nm. Figure 3.12 is presenting the cell contours (A), fluorescent actin (B) and a merged image (C) of the same FBS stimulated LifeAct cell sheet.

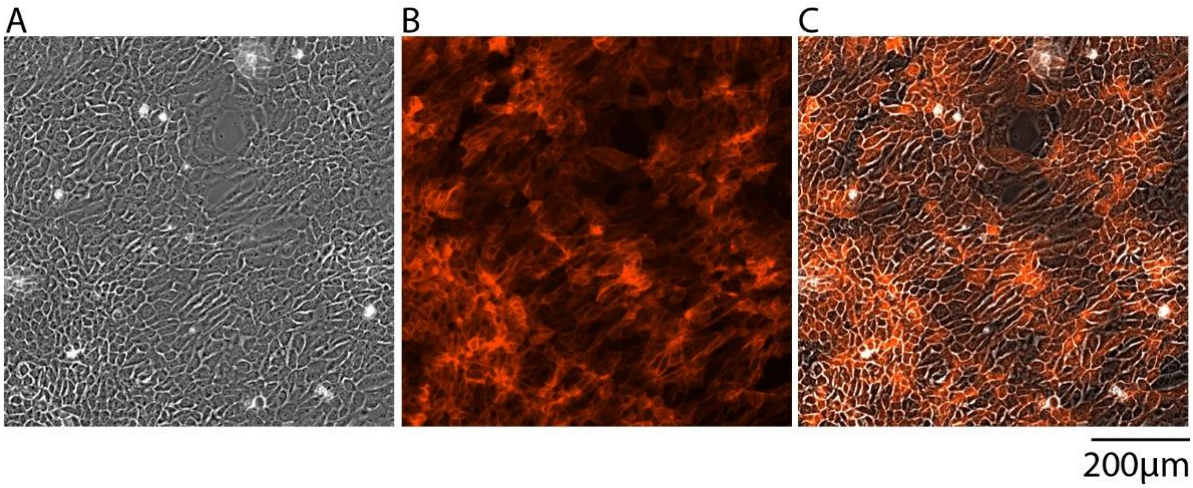

Figure 3.12: Cell contours and actin expression of FBS stimulated HaCaT LifeAct cells. The same cell sheet image acquired by live cell imaging is presented in three ways by showing cell contours (A), fluorescent actin (B) and both channels merged together (C).

Figure 3.12 shows that both cell contours and actin networks are successfully detected by the instrument during cell migration. In the middle of the figure, in the image showing the actin network (Figure 3.12.B), variations in actin expression are observed. There are regions with less expressed actin where the actin filaments appear to be more stretched out, and surrounding regions with higher expression of actin that are more densely packed. This corresponds to the cell contours (Figure 3.1.A) showing cells that are stretched out compared with cells nearby that have a rounder shape. A higher expression of actin is also observed in the areas where multiple cells gather during migration. In the merged image, where both cell contours and actin filaments are shown (Figure 3.1.C), the same features are observed, however, the observations mentioned are more distinct when the cell shape and actin network is shown separately.

Due to difficulties of showing the cell contours and actin networks clearly at the same time, only the actin filaments will be shown in the next figure. Representative images of cell sheets with fluorescent actin filaments for each of the treatments are shown in Figure 3.13.

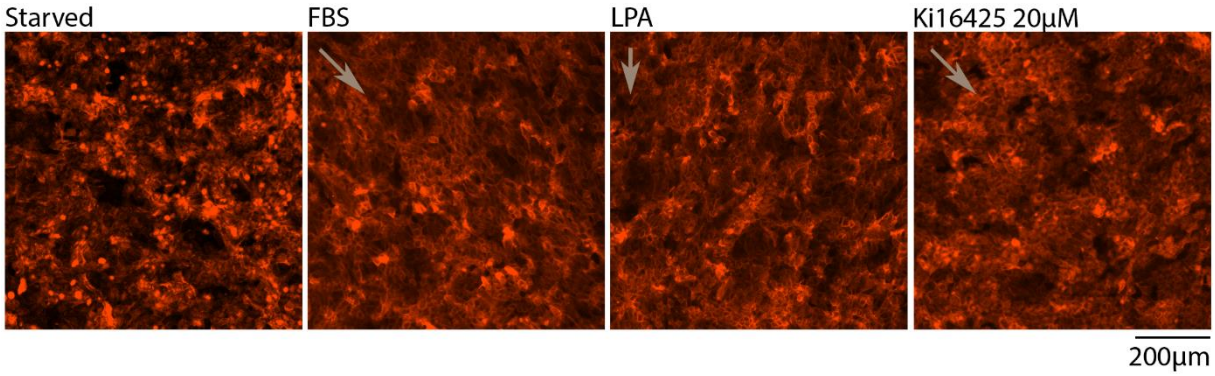

Figure 3.13: Expression of actin in treated HaCaT LifeAct cells. Cell sheets of starved cells, cells stimulated with FBS, LPA stimulated cells and cells treated with 20 µM Ki16425 are presented in the figure. The images are acquired during live cell imaging approximately 20 hours after stimulation. The direction of migration is illustrated with grey arrows.

Figure 3.13 shows generally high levels of expressed actin in the cell sheets, except for the starved cell sheet where the expression is lower and uneven. In the image of LPA stimulated cells, the cells are migrating downwards (grey arrow). Here, several lines with high actin expression are observed in the upper part of the picture, and these are positioned parallel to the direction of migration. These line features of highly expressed actin in the direction of the cell movements are also observed in the other cell sheets, both FBS stimulated and after treatment with the LPAR inhibitor Ki16425.

3.3 Expression levels of LPARs in HaCaT cells

To estimate the expression level of mRNA for the six different LPARs in HaCaT wt cells, qPCR experiments were performed. The results are based on investigating the expression of LPARs in three cell passages (n=3), the qPCR analyses of the same samples were repeated twice. Figure 3.14 presents the results as a diagram, where the mRNA expression for the LPARs in each experiment are normalized relative to LPAR1 set to 1. In Appendix D, a diagram of normalized values to GAPDH, the mRNA expression of the reference gene *GAPD*, is presented for each experiment. The colours in the diagrams (Figure D.1 and D.2) are matching the representative values in Figure 3.14. Standard deviation is included to the relative normalized values in Figure 3.14.

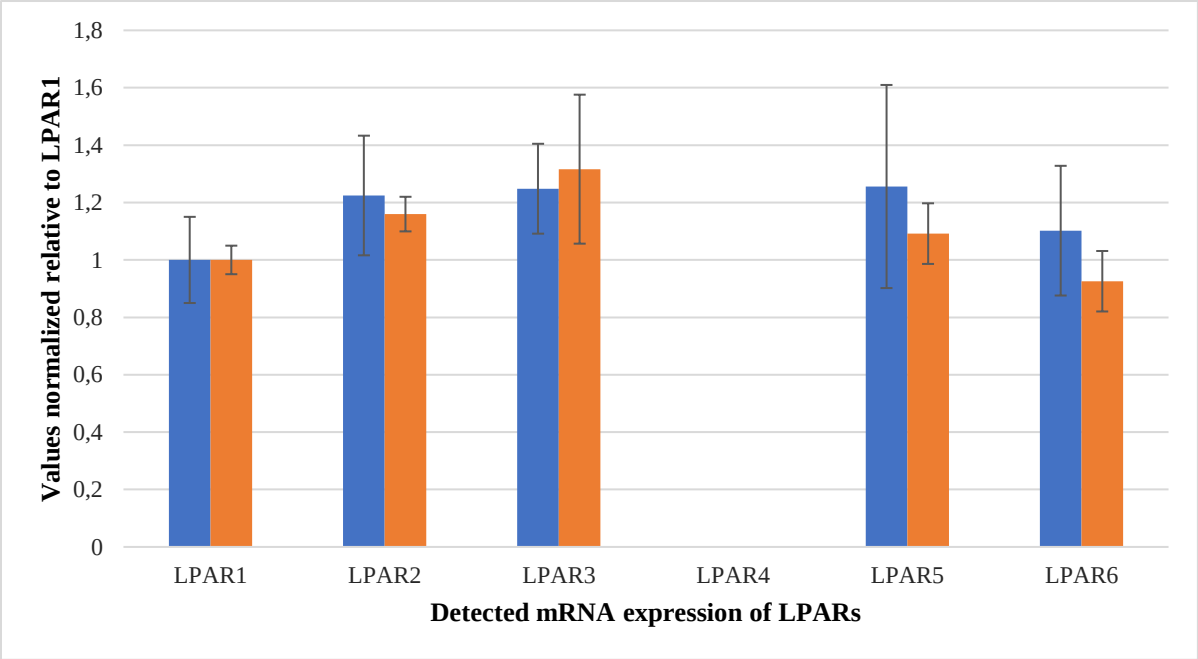

Figure 3.14: mRNA expression of LPAR1-6 in HaCaT wt cells. The diagram shows data from two independent qPCR experiments normalized relative to the representative LPAR1 expression set to 1. Mean expression of three cell passages with standard deviation is shown. Expression of LPAR4 was not detectable.

The diagram in Figure 3.14 is showing expression levels for the LPA receptors between 0.9 and 1.3. The standard deviations show the variance between the three cell passages analysed. Expression of LPAR4 was not detectable. The two-sample paired t-test performed with 95 % level of significance resulted in a significant difference in expression between LPAR4 and the other receptors.

Additional qPCR experiments were done with dilution series containing higher cDNA concentrations in order to detect mRNA expression of LPAR4. Still, the StepOnePlus™ Real-Time PCR System in combination with SYBR® Green were not able to detect amplified product to estimate the mRNA expression of this receptor. Gel electrophoresis with positive and negative samples from these experiments is presented in Figure 3.15. Samples for detection of GAPDH and LPAR1 were included as controls.

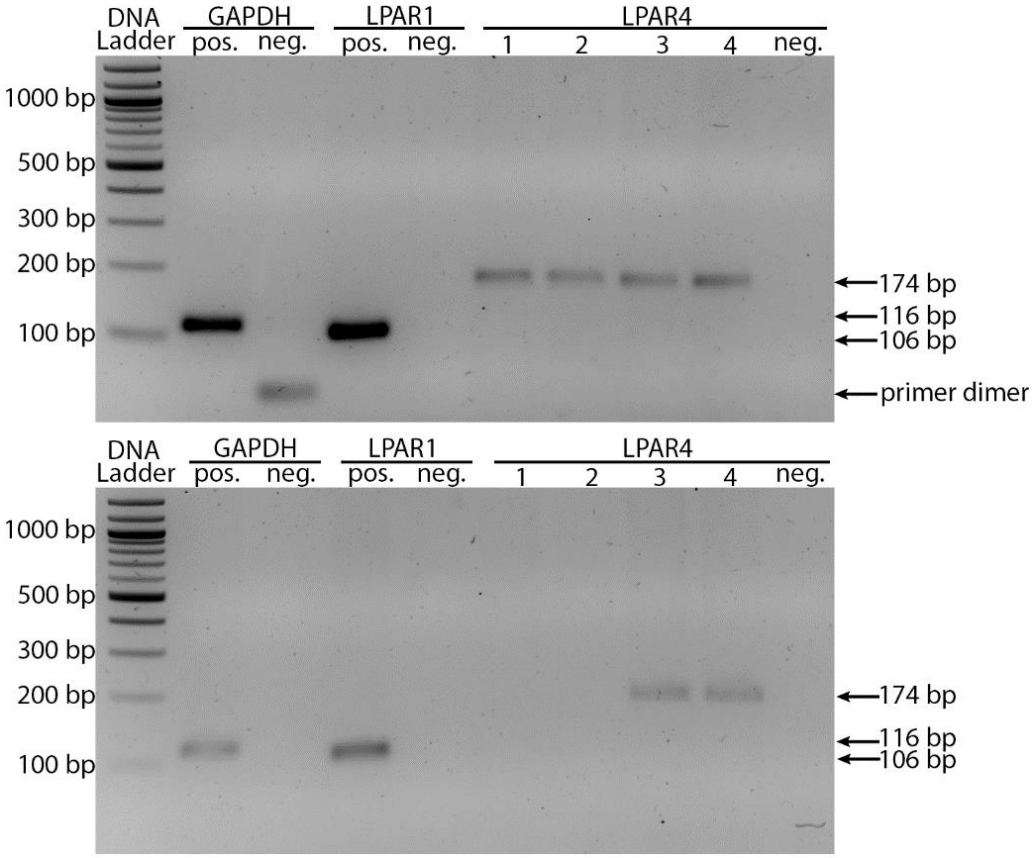

Figure 3.15: Gel electrophoresis of qPCR products to detect LPAR4. Results from two independent experiments are shown. Four positive samples of LPAR4 are included as well as one positive sample for GADH and LPAR1 used as controls, in addition to negative control samples. The product sizes correlate with Table 2.1.

The gel electrophoresis presented in Figure 3.15 shows the presence of amplificated product of mRNA corresponding to LPAR4 in six of eight samples chosen from these two experiments. However, amplification of mRNAs corresponding to GAPDH and LPAR1 is much higher based on the stronger bands visible on the gel. The negative controls indicated no contamination of cDNA, but amplification of primer dimers was visible in one of the samples for GAPDH.

In Appendix D an image of gel electrophoresis with qPCR products from the experiments presented in Figure 3.14 is included (Figure D.3). Results from an experiment with no-RT controls are presented in Table D.1 and indicate that the samples do not contain gDNA that potentially could affect the qPCR-results.

3.4 Characterization of LPAR1 knockdown cell lines

The shRNA technique was used to produce two HaCaT cell lines with a target sequence each knocking down expression of the LPAR1 receptor, by knocking down the *EDG2* gene. These

cell lines are characterized together with the scrambled control and wt cell line following the knockdown procedure. Western blot was performed to investigate the protein expression of LPAR1 in the cell lines, and thereby evaluate the effect of the knockdown. Changes in phenotype were examined microscopically, both by comparing cell morphology and monitoring migration patterns by live cell imaging.

3.4.1 Analysis of the knockdown efficiency

Western blot analysis was performed to investigate if the knockdown cell lines expressed less LPAR1 protein after the knockdown procedure was completed. By comparing the level of expressed LPAR1 protein in the knockdown cell lines to the control cell lines, the knockdown efficiency can be evaluated. Each experiment was performed with one antibody targeting LPAR1 and one antibody targeting alpha-tubulin. Detection of alpha-tubulin was used as a control to check that the same amount of protein was loaded onto the gel for each sample of cell lysate. Figure 3.16 illustrates the Western blot of the HaCaT ΔLPAR1 cell lines with the polyclonal LPAR1 antibody.

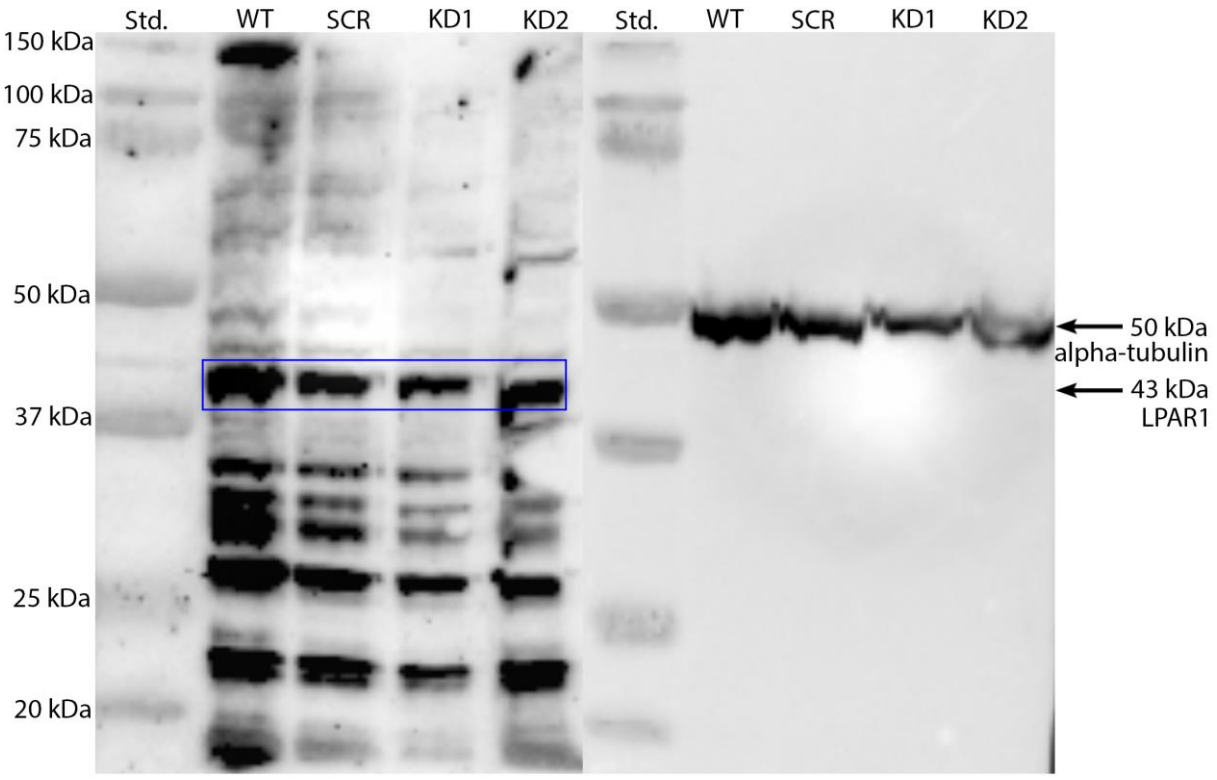

Figure 3.16: Western blot of HaCaT ΔLPAR1 cell lines with polyclonal LPAR1 antibody. The image combines results from two Western blots, detection of LPAR1 expression (left) and expression of the loading control alpha-tubulin (right). The blue frame indicates the band corresponding to the LPAR1 product size according to the antibody producer.

The left Western blot in Figure 3.16 shows a high degree of unspecific antibody binding to proteins present in the cell lysate. This background noise makes it difficult to evaluate if LPAR1 is less expressed, thereby knocked down, in the HaCaT kd1 ΔLPAR1 and HaCaT kd2 ΔLPAR1 cell lines. The blue frame outlines the protein band with the correct size, according to the antibody producer. However, since these bands show some variation in thickness, as is also observed for other bands further down on the blot, it is difficult to determine the knockdown efficiency.

After repeating the Western blot experiment using the polyclonal LPAR1 antibody (primary antibody nr. 1 in Table 2.4) without better results, a new LPAR1-specific antibody was bought. Results from the Western blot experiment with this antibody, a monoclonal antibody (primary antibody nr. 2 in Table 2.4), are shown in Figure 3.17.

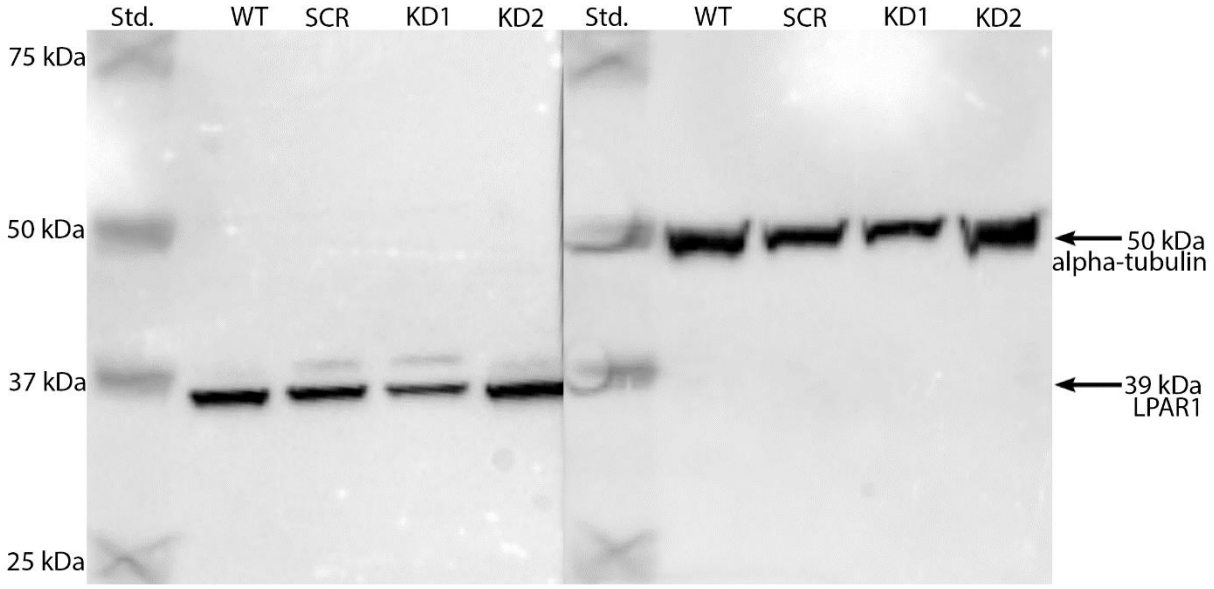

Figure 3.17: Western blot of HaCaT ΔLPAR1 cell lines with monoclonal LPAR1 antibody. The image combines results from two Western blots, detection of LPAR1 expression (left) and expression of the loading control alpha-tubulin (right).

Figure 3.17 shows Western blot detection of LPAR1 using a monoclonal LPAR1 antibody. This antibody shows a much higher specificity than the first one tested, resulting in detection of one protein band in each cell line. The size of the band is estimated to be 39 kDa, according to the antibody producer. However, the detected band is somewhat smaller than estimated, approximately 37 kDa. For the HaCaT kd1 ΔLPAR1 the figure shows a band that is thinner than bands visualized for the three other cell lines. This indicates that the *EDG2* gene, and thus

expression of the LPAR1 receptor, is partly knocked down in the HaCaT kd1 ΔLPAR1 cell line.

3.4.2 Phenotypic changes in knockdown cells

Changes in phenotype for the knockdown cell lines are examined by studying cell morphology and by live cell imaging experiments. The morphology of the cell lines was observed microscopically. Representative images are presented in Figure 3.18, where the cells are in a subconfluent cell sheet state.

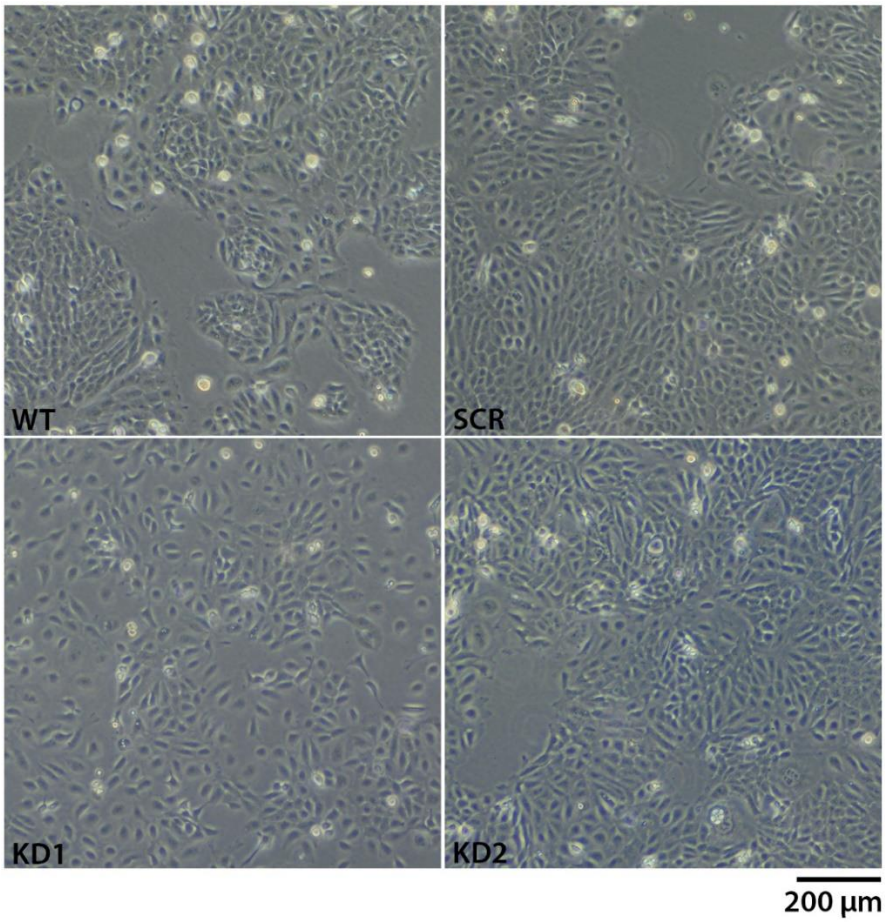

Figure 3.18: Morphology of HaCaT ΔLPAR1 cell lines. Images of subconfluent cell sheets of wt, scr, kd1 and kd2 cells acquired with a light microscope.

Figure 3.18 shows that the cell morphology of HaCaT kd1 ΔLPAR1, especially, is different from the other three cell lines. It seems like these cells do not stretch out and form colonies with a defined border like in particular the wt cells do. It appears like the kd1 cells prefer not to bind to each other, as there is space between the cells and the cells has a more rounded shape. Even if they are positioned next to each other, it looks more like a group of single cells than a

connected cell sheet. The kd2 cells seems more like colony forming cells, but they have less defined colony edges compared to the wt and scr cells.

Using live cell imaging with settings for phase contrast imaging by transmitted light, cell movements and migration patterns were investigated. Samples of each cell line were stimulated with FBS or LPA. A starved cell control was also included for each cell line. For obvious reasons, the results are best visualized by video, however, still images from each video has been selected to show the general features of each cell line. Figure 3.19 and Figure 3.20 shows representative images of the cell sheets during live cell imaging after 20 hours of stimulation. Figure 3.19 is showing FBS stimulated cell sheets.

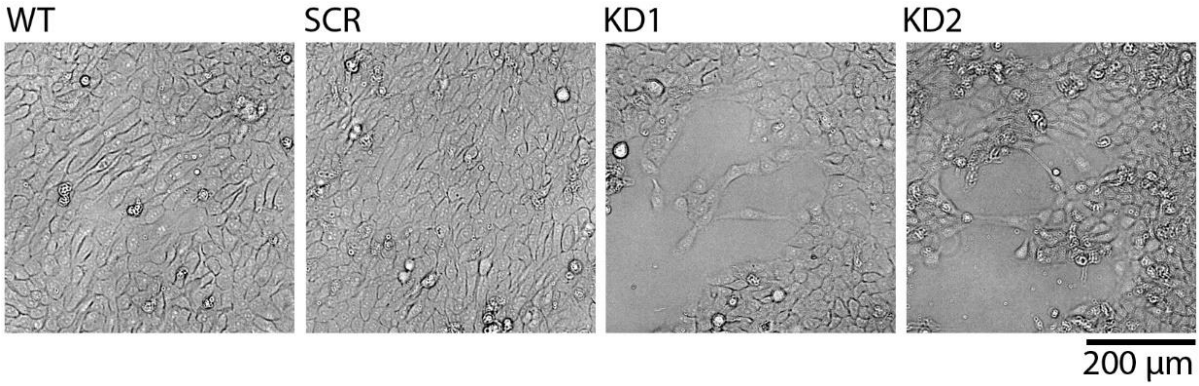

Figure 3.19: Cell sheet integrity and coordination in FBS stimulated HaCaT ΔLPAR1. The images represent cell sheets of the four cell lines (wt, scr, kd1 and kd2) after 20 hours of stimulation with FBS. The images are acquired during live cell imaging.

A different migration pattern was observed for the knockdown (kd) cell sheets than the wt and scr cell sheets. The most distinct difference was that the kd cells tend to lose contact with each other during migration, as opposed to the wt and scr cells. During migration, the kd cell sheets were torn apart, while the wt and scr cells were able to keep their integrity and migrate as an intact unit. This is shown in Figure 3.19.

Figure 3.20 is showing representative images of cell sheets during live cell imaging after 20 hours of stimulation with LPA.

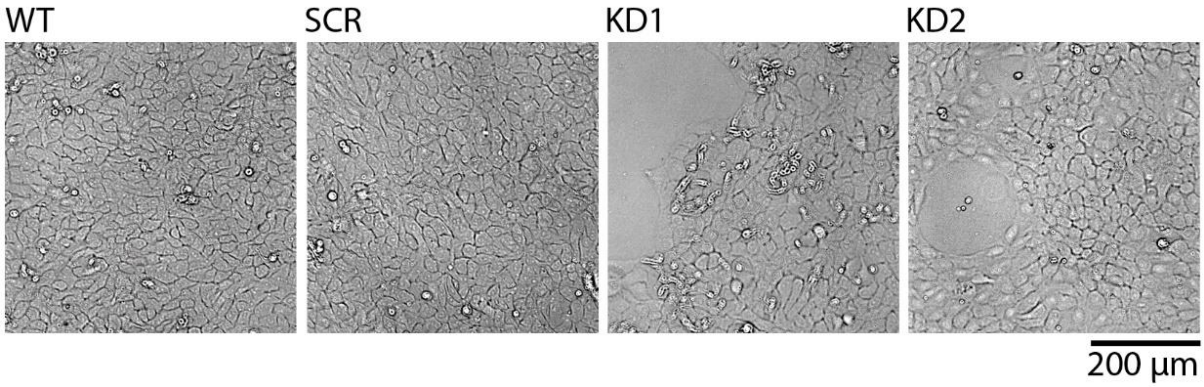

Figure 3.20: Cell sheet integrity and coordination in LPA stimulated HaCaT ΔLPAR1. The images represent cell sheets of the four cell lines (wt, scr, kd1 and kd2) after 20 hours of stimulation with LPA. The images are acquired during live cell imaging.

In Figure 3.20, results acquired from LPA stimulated cell sheets show the same feature as Figure 3.19 of FBS stimulated cell sheets. In addition, the confluent cell sheets of knockdown cells (kd1 and kd2) are torn apart during LPA stimulated migration.

Using data acquired from live cell imaging, the migration velocity in the migrating cell sheets was analysed. This was performed using the TrackMate function in the Fiji ImageJ software (imagej.net/TrackMate; (Tinevez et al., 2017)). Figure 3.21 is showing the results from this analysis. One panel of each cell line with the three different treatments are presented.

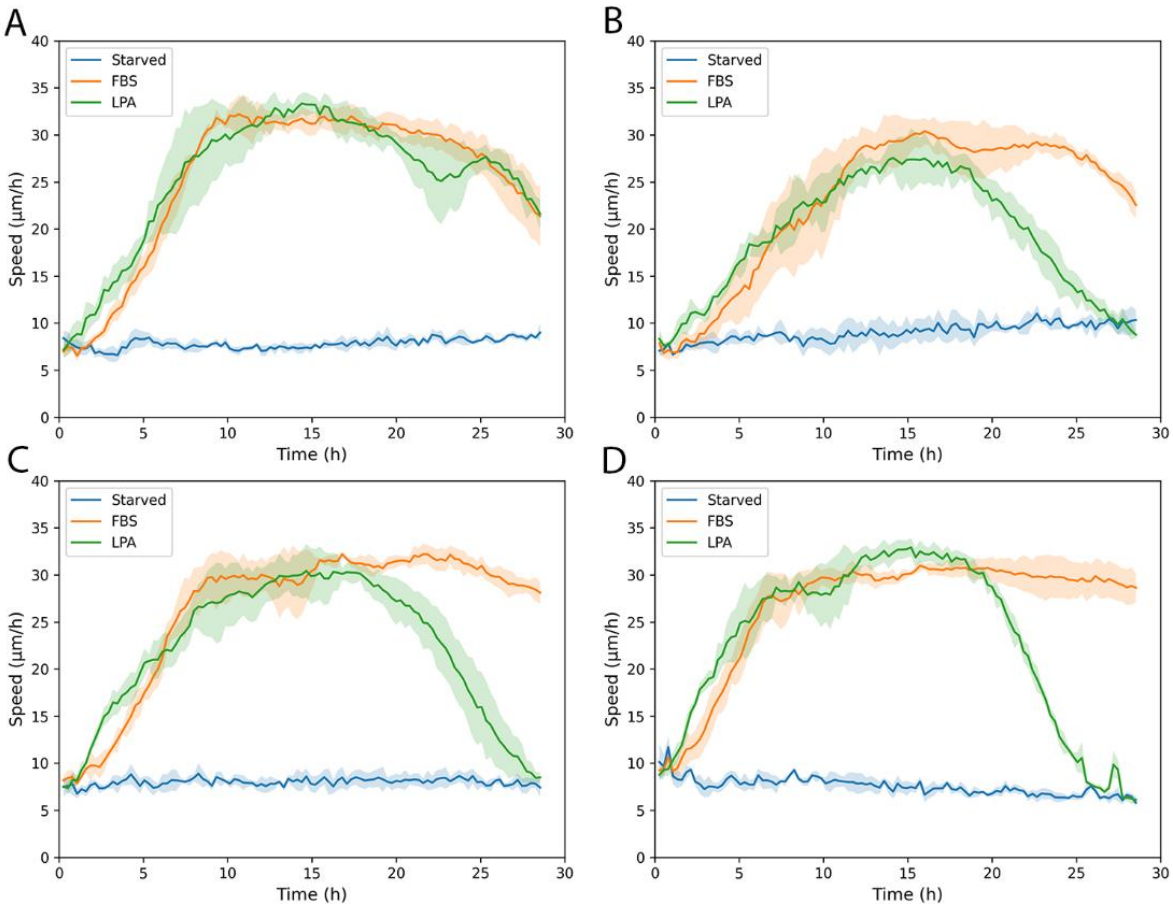

Figure 3.21: Cell sheet velocities for HaCaT ΔLPAR1 cell lines. These panels present the speed (µm/h) in the cell sheets during the time of live cell imaging. Panel A is the wt cell line, B is the scr cell line while the lower panels, C and D, represents the knockdown cell lines of kd1 and kd2, respectively. In each panel, the blue lines represent starved cells, the orange line is cells stimulated with FBS and the green line is of LPA stimulated cells.

Figure 3.21 shows some differences in migration velocities generated after FBS and LPA stimulation between the four cell lines, even if the maximum speed of approximately 30 µm/h is the same for them all. With FBS stimulation, the knockdown cells (Figure 3.21.C and D) have a longer plateau phase of maximum speed than the two other cell lines, in which the migration speed is decreasing after 20-25 hours of stimulation. For LPA stimulated cell sheets, the wt cell line (Figure 3.21.A) differs from the three others. The scr cell line, in addition to the knockdown cell lines shows a decreasing migration velocity before 20 hours of stimulation and reaches the same velocity as the starved cells before imaging is completed. The wt cells is also showing decreasing migration velocities at the same time point, but still show an average migration speed of 20 µm/h at the end of imaging. Interestingly, a more clear difference in cell sheet coordination compared to migration speed was observed (according to Figure 3.19 and 3.20) between these four cell lines.

4 Discussion

4.1 The ability of LPA to regulate cell migration

Live cell imaging studies on cell migration patterns in confluent keratinocyte cell sheets generated useful information of how different growth factors affect cell migration behaviours. The results showed a clear difference in the ability of FBS, EGF and LPA to activate and regulate cell sheet coordination, while all three reagents had the ability to activate cell movements with similar cell sheet velocities.

Cell sheets stimulated with FBS or LPA showed high levels of cell sheet coordination (Figure 3.1.B), with cells migrating as a coordinated unit directed towards a common centre (Figure 3.3.A and 3.3.B). Furthermore, the results indicate that LPA has the ability to coordinate the cell movements faster (Figure 3.2), however, FBS stimulation mediates cell coordination over a longer time period. Cell sheets stimulated by EGF, on the other hand, resulted in a more chaotic cell migration pattern with local regions of high levels of coordination and other regions with no cell sheet coordination (Figure 3.3.C). Notably, EGF stimulation activated cell movements with high cell sheet velocities similar to FBS stimulated cell sheets (Figure 3.2).

These results correspond well with a previous published study (Lång et al., 2018) showing that EGF alone can active migration but is not sufficient to induce collective migration, as observed with stimulation by regular blood serum or FBS. LPA was previously shown to be involved in a variety of biological processes, among them the ability to promote migration of keratinocytes (Lei et al., 2019; Mazereeuw-Hautier et al., 2005). These results are supporting those previous findings.

Confirming that LPA is involved in activation and regulation of collective cell sheet migration leads to the next point of investigation, including studies on LPA receptors and signalling pathways. In these experiments, the LPA receptor 1 (LPAR1) was chosen for further investigation. One way to start the examination is to use inhibitors with known inhibitory effects and observe changes in cellular behaviour after inhibition. The inhibitor Ki16425 is, according to the producer, able to specifically inhibit LPAR1 and partly LPAR3.

The Ki16425 inhibitor had never been used in this experimental system of live cell migration, and therefore a titration experiment was performed in order to determine the optimal concentration of inhibitor. The results showed that Ki16425 had an inhibitory effect both on the level of coordination in cell sheets (Figure 3.4 and 3.6) and the cell sheet velocities (Figure 3.5

and 3.7), and that the effect of Ki16425 was concentration dependent. It was also shown that the inhibitory effect on cell sheets stimulated with LPA was higher than the effect on cell sheets stimulated with FBS. This is an expected result due to the fact that FBS contains more growth factors that can activate cell migration responses through other receptors than LPAR1. The optimal concentration is regarded as 10-20 μM, producing an inhibitory effect on collective cell migration in cell sheets stimulated with LPA and FBS, respectively, without a complete impairment of cell motility.

However, results obtained using the Ki16425 inhibitor indicate that it is not LPAR1 alone that is activating and regulating collective cell sheet migration. The difference between the inhibitory effects on FBS stimulated cell sheets compared with the LPA stimulated cell sheets, is validated by the fact that FBS contains more factors that mediate activation of migration. Furthermore, it cannot be confirmed that the function of LPAR1 is totally inhibited. Even if the inhibitor is shown to be specific towards the receptors binding LPA, unspecific binding to other cell membrane receptors may occur. Due to the results showing that the inhibitory effect is concentration dependent, and that a higher concentration resulted in a stronger inhibition of collective cell sheet migration, it is not unthinkable that Ki16425 inhibits other receptors as well.

The signalling pathways for LPA (Figure 1.2) are complex, and the six G-coupled receptors are all able to signal through several subfamilies. It is an intricate network, and LPA can also regulate functions though other pathways. Based on the results obtained from these studies of cell migration patterns, and due to a potentially unspecific inhibition by the inhibitor, it is not possible to conclude that LPAR1 is alone involved in LPA mediated cell migration responses.

4.2 Actomyosin as a potential influence on collective cell migration

Actomyosin networks and its structure visualized by actin filaments was examined due to the hypothesis that LPA contributes to cell sheet coordination by regulating the formation and maintenance of apical actomyosin networks. Formation of such apical actomyosin networks couple cells together and thus could be of importance for cell sheet coordination during collective cell migration. Live cell imaging performed on HaCaT cell sheets treated with the ROCK inhibitor Y-27632 showed an inhibitory effect on both the level of cell sheet coordination (Figure 3.8) and the cell sheet velocities (Figure 3.9) produced in FBS and LPA stimulated cell sheets. The inhibitory effect was more pronounced in the LPA stimulated cell

sheets, which strengthen the hypothesis that there is a potential correlation between LPA signalling and regulation of actomyosin by changes in actin dynamics.

Visualization of apical actomyosin networks by immunofluorescence staining of actin filaments with Phalloidin, showed actin expression mainly towards the apical side of cells after FBS and LPA stimulation (Figure 3.10). However, formation of apical actin filaments was also observed in cell sheets treated with the LPAR inhibitor Ki16425 (Figure 3.10). Starved cell sheets and cell sheets stimulated with EGF showed a more even actin expression throughout the cells. To summarize, stimulation of confluent quiescent keratinocyte cell sheets with FBS, LPA or the LPAR1 inhibitor stimulated formation of apical actin networks across the cell sheet (also shown in Figure 3.11).

These results were somewhat unexpected, since inhibition of LPA resulted in reduced cell sheet coordination and migration speed in contrast to FBS and LPA stimulation. Thus, it was assumed that inhibition of LPAR1 would lead to less apical actin expression based on the hypothesis that LPA stimulation results in formation of apical actin networks that mediate cell sheet coordination. The fact that Ki16425 treatment does not lead to a reduced expression of actin networks may be due to lack of specificity for the receptor, leading to incomplete binding to the LPAR1 causing incomplete inhibition of the LPA signal. Another explanation is that actin dynamic regulation and formation of actomyosin networks is regulated by additional signalling pathways that exist due to the great importance of actin in the cells.

Experiments for live cell imaging of HaCaT LifeAct cells that express fluorescently labelled actin displayed how the actomyosin networks are expressed during cell sheet migration. Regions with high expression and density of actin filaments and regions with less actin expression and lower density of actin filaments was shown to correspond to the cells contour that is rounder or more stretched out, respectively (Figure 3.12). This indicates that there is a connection between the cells' behaviour in the cell sheet and the formation and maintenance of actomyosin networks.

Cell sheets treated with different reagents previously shown to influence coordination of cell sheet migration and cell sheet velocities differently (Figure 3.1-3.7), gave results showing generally high expression of actin (Figure 3.13). Most interestingly while monitoring the migrating cell sheets, specific lines of particular high density of actin filaments was detected. These lines were positioned parallel to the direction of the cell migration in the stimulated collectively migrating cell sheets. This was observed in cell sheets stimulated with FBS and

LPA, and is strengthening the hypothesis of LPAs ability to contribute to formation and maintenance of the actomyosin networks, and that actin filaments and actomyosin is important for coupling cells together and thus mediate coordination in the cell layer during collective cell migration.

On the other hand, the correlation between highly expressed actin filaments and parallel cell sheet migration was also observed when the cell sheets were treated with the LPAR inhibitor Ki16425, in addition to FBS. This result weakens the hypothesis that LPA alone is important for formation and maintenance of actomyosin networks. The results obtained with Ki16425 discussed above are valid in this context.

4.3 LPARs expressed in HaCaT cells

Studies of mRNA expression of the six LPARs by performing qPCR experiments, indicated small differences in the expression level of five of six receptors expressed in HaCaT cells. For one of the receptors, LPAR4, the mRNA expression was significantly lower than the others (shown in Figure 3.14 and validated by two-sample paired t-test performed with 95 % level of significance). At the same time, results from gel electrophoresis (Figure 3.15) indicate that LPAR4 is expressed in the cells. The conclusion is that all six LPARs are expressed in HaCaT cells, but LPAR4 is expressed in lower amount and that the qPCR method used is not sensitive enough to detect this level of expression. Based on these findings, the question of which of the six LPA receptors that mediates activation and regulation of collective cell migration still remains open.

Previous studies have investigated the mRNA expression of LPARs in different experimental systems, including studies on obesity among others. Brown et al., 2017 studied mRNA expression of LPARs in murine and human myocardium and adipose tissue in order to investigate regulation of LPA in response to obesity. By use of qPCR and a SYBR Green dye for detection, they found that the expression levels of LPARs were different in non-obese humans compared to obese individuals, except for expression of LPAR3, which was not detected, and LPAR1. Moreover, the results showed that expression levels of LPAR4, 5 and 6 were downregulated in obese tissue samples. The authors concluded thereby that LPAR4-6 are negatively associated with human obesity and suggest that excessive weight gain may alter LPA receptor signalling (Brown et al., 2017). This study is interesting due to the coherence of obesity, diabetes and chronic wounds.

The purpose of estimating the mRNA expression levels of the six LPARs, was to investigate if the HaCaT cells express higher levels of one of the LPARs compared to the others. The interest was especially directed towards examining if one specific receptor could be directly coupled to activation of the collective cell migration observed in the experimental system. If one receptor had been estimated with a significantly higher mRNA expression level than the other receptors, this may be coupled to the functions they are able to stimulate through signalling pathways in keratinocytes. Cells from three separate cell passages were included in these qPCR experiments and the cells were harvested in a dormant cell state. In future experiments it would be interesting to harvest cells after stimulation with different reagents, and investigate if this leads to a difference in the mRNA expression levels of the LPARs as the cells are migrating.

These qPCR experiments were performed with the real-time technique and SYBR® Green as fluorescent agent emitting increased fluorescence signal intensity proportional to the amount of PCR product produced. This method was not sensitive enough to detect the low mRNA expression levels of LPAR4. Since there are other techniques available that are more specific than dsDNA binding dyes, the experiments should be repeated using TaqMan® reagents or the ddPCR technique. The TaqMan® probe has the advantage of specific hybridization between the designed probe and the target sequence, which thereby is more specific than using a dsDNA binding dye when performing real-time qPCR. The experiment can also be performed by using ddPCR especially for estimation of very low mRNA expression levels. With performance of thousands of amplification reactions in a sample, this technique is proven to be suitable for extremely low-target quantification where preparation requirements as sample dilution and other treatments for real-time qPCR will lead to undetectable target levels (Taylor et al., 2017).

4.4 Effect and altered behaviour of LPAR1 knockdown in HaCaT cells

Gene knockdown was performed using the shRNA technique in order to investigate phenotypic changes like changes in morphology and altered migration behaviour in HaCaT cells with reduced expression of LPAR1. Potential changes could give an indication of the functional role of LPAR1 in activation and regulation of collective cell migration. Western blot analysis was performed in order to examine the effect of the knockdown procedure. First, a polyclonal antibody was used, resulting in high degree of non-specific binding (Figure 3.16) and difficulties of determining whether the protein expression was reduced or not. It was therefore bought another LPAR1-specific primary antibody, this time a monoclonal antibody.

Overall, the result (Figure 3.17) indicates that the knockdown procedure resulted in a successful reduction of LPAR1 expression, shown by detection of a thinner protein band on the membrane, in one of the knockdown cell lines, HaCaT kd1 ΔLPAR1. The other knockdown cell line, HaCaT kd2 ΔLPAR1, expresses the target protein in the same levels as the control cell lines. The Western blot methodology used is regarded as adequate for protein detection, however, optimization of some steps could potentially give an even more precise result with possibilities of protein quantification.

Even if just one of the knockdown cell lines showed reduced expression of LPAR1, both cell lines displayed changes in cell morphology (Figure 3.18). Microscopy images of subconfluent cell layers of the HaCaT kd1 ΔLPAR1 cell line show cells with a more rounded shape that prefer to spread as individual cells instead of binding together. The other knockdown cell line, HaCaT kd2 ΔLPAR1, expresses a cell morphology that differs from wt cells especially in the way they do not display a defined cell colony edge. These changes can indicate that the cells have been affected by the less expressed LPAR1, but the changes can also occur due to the knockdown procedure itself, even though the scr cell line seems to be unaffected based on the cell morphology.

Due to changes in cell morphology, it was interesting to further monitor the cell migration patterns using live cell imaging. The results showed cell sheets of the knockdown cell lines that were torn apart during cell migration. This happened independently of stimulation with FBS (Figure 3.19) or LPA (Figure 3.20). The results indicate that the integrity of the cell sheet was altered, and that LPAR1 is important to maintain strong interactions between the cells. The results also showed that cell sheet velocities obtained were similar in all four cell lines (Figure 3.21). A further hypothesis is that this can have something to do with altered actin expression in the cells, and that changes in signalling pathways due to less LPA binding is involved.

The shRNA technique was used to perform the knockdown. This was considered as the best choice due to available time to perform the experiment and the need of a cell line with a stable knockdown expressed over time. The siRNA technique was not chosen due to impossible generation of a long-time knockdown cell line, and the CRISPR-Cas system was considered as too time-consuming. In addition to knockdown effects caused by CRISPR-Cas, this system can also be used to create cell lines with gene knockouts (Joung et al., 2017). This would had been the best choice to ensure absolutely no expression of the LPAR1 receptor and it could thereby have given the most accurate observation in a loss-of-function study.

5 Conclusion and Further research

Studies of cell migration patterns in quiescent epithelial cell sheets of HaCaT mCherry-Histone H2B cells showed that LPA has the ability to activate and regulate collective cell migration. However, based on the results obtained from these studies, and due to a potentially unspecific inhibition by the Ki16425 inhibitor, it is not possible to conclude that LPAR1 is alone involved in LPA mediated cell migration responses.

The role of actomyosin as a potential influence on collective cell migration and the correlation between actomyosin networks and cell sheet coordination is strengthened based on the results obtained during the project period. Expression of actin filaments that build up actomyosin networks were successfully visualized. In which way LPA contributes to this collaboration is on the other hand still something that has to be further investigated.

Based on estimation of mRNA expression levels of LPARs in HaCaT wt cells, the conclusion is that all six LPARs are expressed, but LPAR4 is expressed in lower amount that the qPCR method used is not sensitive enough to detect. The experiment should be repeated by using another fluorescent reagent or a more sensitive technique. A significantly higher expression level of one of the LPARs was not detected, thus the question of which of the six LPA receptors that mediates collective cell migration still remains open.

Established LPAR1 knockdown cell lines showed changes in cell morphology and migration behaviour. Further examination of the knockdown cell lines will be to incorporate a fluorescent reagent as mCherry into the cells, forming stable cell lines that express mCherry-Histone H2B proteins in the nuclei. Subsequently, these cell lines can be used in live cell imaging experiments in order to monitor cell movements and run the same PIV analyses used to study cell migration patterns in HaCaT mCherry-Histone H2B cells. These studies will provide useful information of the regulatory role of LPAR1 in activation of cell sheet motility and coordination. Combining gene knockdown with the CRISPR-Cas system with fluorescent labelling of cell nuclei in order to study LPAR1 regulation in relation to collective cell migration could also be an interesting possibility for further research.

The overall aim of this thesis was to contribute to a better understanding of how LPA activates and regulates collective cell migration in human skin. This was successfully examined through five aspects of LPA and how it influences the keratinocyte cell line, HaCaT. Further research

is needed to obtain more knowledge about how LPA can contribute to improve skin repair in chronic wounds.

References

Abudayyeh, O. O., Gootenberg, J. S., Essletzbichler, P., Han, S., Joung, J., Belanto, J. J., Verdine, V., Cox, D. B. T., Kellner, M. J., Regev, A., et al. (2017). RNA targeting with CRISPR-Cas13. *Nature*, 550 (7675): 280-284. doi: 10.1038/nature24049.

Addgene. (2006). *pLKO.1 - TRC Cloning Vector* Available at: http://www.addgene.org/protocols/plko/ (accessed: 2.3.21).

Adrian, R. J. (2005). Twenty years of particle image velocimetry. *Experiments in Fluids*, 39 (2): 159-169. doi: 10.1007/s00348-005-0991-7.

Afonso, O., Figueiredo, A. C. & Maiato, H. (2017). Late mitotic functions of Aurora kinases. *Chromosoma*, 126 (1): 93-103. doi: 10.1007/s00412-016-0594-5.

Alberts, B., Johnson, A., Lewis, J., Morgan, D., Raff, M., Roberts, K. & Walter, P. (2015a). Analyzing Cells, Molecules, and Systems - Analyzing and Manipulating DNA In *Molecular Biology of The Cell*, pp. 463-484. New York: Garland Science, Taylor & Francis Group.

Alberts, B., Johnson, A., Lewis, J., Morgan, D., Raff, M., Roberts, K. & Walter, P. (2015b). Analyzing Cells, Molecules, and Systems - Studying Gene Expression and Function. In *Molecular Biology of The Cell*, pp. 485-508. New York: Garland Science, Taylor & Francis Group.

Alberts, B., Johnson, A., Lewis, J., Morgan, D., Raff, M., Roberts, K. & Walter, P. (2015c). The Cell Cycle - Control of Cell Division and Cell Growth. In *Molecular Biology of The Cell*, pp. 1010-1018. New York: Garland Science, Taylor & Francis Group.

Alberts, B., Johnson, A., Lewis, J., Morgan, D., Raff, M., Roberts, K. & Walter, P. (2015d). Cell Junctions and the Extracellular Matrix - Cell-Matrix Junctions. In *Molecular Biology of The Cell*, pp. 1074-1081. New York: Garland Science, Taylor & Francis Group.

Alberts, B., Johnson, A., Lewis, J., Morgan, D., Raff, M., Roberts, K. & Walter, P. (2015e). Cell Juntions and the Extracellular Matrix - The Extracellular Matrix of Animals. In *Molecular Biology of the Cell*, pp. 1057-1074. New York: Garland Science, Taylor & Francis Group.

Alberts, B., Johnson, A., Lewis, J., Morgan, D., Raff, M., Roberts, K. & Walter, P. (2015f). The Cytoskeleton - Cell Polarization and Migration. In *Molecular Biology of the Cell*, pp. 951-960. New York: Garland Science, Taylor & Francis Group.

Boukamp, P., Petrussevska, R. T., Breitkreutz, D., Hornung, J., Markham, A. & Fusenig, N. E. (1988). Normal keratinization in a spontaneously immortalized aneuploid human keratinocyte cell line. *J Cell Biol*, 106 (3): 761-71. doi: 10.1083/jcb.106.3.761.

Brown, A., Hossain, I., Perez, L. J., Nzirorera, C., Tozer, K., D'Souza, K., Trivedi, P. C., Aguiar, C., Yip, A. M., Shea, J., et al. (2017). Lysophosphatidic acid receptor mRNA levels in heart and white adipose tissue are associated with obesity in mice and humans. *PloS one*, 12 (12): e0189402-e0189402. doi: 10.1371/journal.pone.0189402.

Bustin, S. A., Benes, V., Garson, J. A., Hellemans, J., Huggett, J., Kubista, M., Mueller, R., Nolan, T., Pfaffl, M. W., Shipley, G. L., et al. (2009). The MIQE Guidelines: Minimum Information for Publication of Quantitative Real-Time PCR Experiments. *Clinical Chemistry*, 55 (4): 611-622. doi: 10.1373/clinchem.2008.112797.

Cohen, D. J., James Nelson, W. & Maharbiz, M. M. (2014). Galvanotactic control of collective cell migration in epithelial monolayers. *Nature Materials*, 13 (4): 409-417. doi: 10.1038/nmat3891.

Dimmock, N. J., Easton, A. J. & Leppard, K. N. (2017). The process of infection: IIC. The replication of RNA viruses with a DNA intermediate and vise versa. In *Introduction to Modern Virology*, pp. 121-135. School of Life Sciences, university of Warwick, Coventry: Wiley Blacwell.

Dreifke, M. B., Jayasuriya, A. A. & Jayasuriya, A. C. (2015). Current wound healing procedures and potential care. *Materials Science and Engineering: C*, 48: 651-662. doi: 10.1016/j.msec.2014.12.068.

Guerra, A., Belinha, J. & Jorge, R. N. (2018). Modelling skin wound healing angiogenesis: A review. *Journal of Theoretical Biology*, 459: 1-17. doi: 10.1016/j.jtbi.2018.09.020.

Haeger, A., Wolf, K., Zegers, M. M. & Friedl, P. (2015). Collective cell migration: guidance principles and hierarchies. *Trends Cell Biol*, 25 (9): 556-66. doi: 10.1016/j.tcb.2015.06.003.

Han, H. (2018). RNA Interference to Knock Down Gene Expression. *Methods in molecular biology (Clifton, N.J.)*, 1706: 293-302. doi: 10.1007/978-1-4939-7471-9_16.

Hernández-Araiza, I., Morales-Lázaro, S. L., Canul-Sánchez, J. A., Islas, L. D. & Rosenbaum, T. (2018). Role of lysophosphatidic acid in ion channel function and disease. *Journal of Neurophysiology*, 120 (3): 1198-1211. doi: 10.1152/jn.00226.2018.

Huang, R.-P. (2001). Detection of multiple proteins in an antibody-based protein microarray system. *Journal of Immunological Methods*, 255 (1): 1-13. doi: 10.1016/S0022-1759(01)00394-5.

Im, K., Mareninov, S., Diaz, M. F. P. & Yong, W. H. (2019). An Introduction to Performing Immunofluorescence Staining. *Methods in molecular biology (Clifton, N.J.)*, 1897: 299-311. doi: 10.1007/978-1-4939-8935-5_26.

Joung, J., Konermann, S., Gootenberg, J. S., Abudayyeh, O. O., Platt, R. J., Brigham, M. D., Sanjana, N. E. & Zhang, F. (2017). Genome-scale CRISPR-Cas9 knockout and transcriptional activation screening. *Nature protocols*, 12 (4): 828-863. doi: 10.1038/nprot.2017.016.

Khodeer, S. & Era, T. (2017). Identifying the Biphasic Role of Calcineurin/NFAT Signaling Enables Replacement of Sox2 in Somatic Cell Reprogramming. *STEM CELLS*, 35 (5): 1162-1175. doi: 10.1002/stem.2572.

Kita-Matsuo, H., Barcova, M., Prigozhina, N., Salomonis, N., Wei, K., Jacot, J. G., Nelson, B., Spiering, S., Haverslag, R., Kim, C., et al. (2009). Lentiviral vectors and protocols for creation of stable hESC lines for fluorescent tracking and drug resistance selection of cardiomyocytes. *PloS one*, 4 (4): e5046-e5046. doi: 10.1371/journal.pone.0005046.

Koenderink, G. H. & Paluch, E. K. (2018). Architecture shapes contractility in actomyosin networks. *Current Opinion in Cell Biology*, 50: 79-85. doi: 10.1016/j.ceb.2018.01.015.

Koivisto, L., Jiang, G., Häkkinen, L., Chan, B. & Larjava, H. (2006). HaCaT keratinocyte migration is dependent on epidermal growth factor receptor signaling and glycogen synthase kinase-3α. *Experimental Cell Research*, 312 (15): 2791-2805. doi: 10.1016/j.yexcr.2006.05.009.

Kümper, S., Mardakheh, F. K., McCarthy, A., Yeo, M., Stamp, G. W., Paul, A., Worboys, J., Sadok, A., Jørgensen, C., Guichard, S., et al. (2016). Rho-associated kinase (ROCK) function is essential for cell cycle progression, senescence and tumorigenesis. *eLife*, 5: e12994-e12994. doi: 10.7554/eLife.12203.

Lei, L., Su, J., Chen, J., Chen, W., Chen, X. & Peng, C. (2019). The role of lysophosphatidic acid in the physiology and pathology of the skin. *Life Sci*, 220: 194-200. doi: 10.1016/j.lfs.2018.12.040.

Lo, C.-M., Wang, H.-B., Dembo, M. & Wang, Y.-l. (2000). Cell Movement Is Guided by the Rigidity of the Substrate. *Biophysical Journal*, 79 (1): 144-152. doi: 10.1016/S0006-3495(00)76279-5.

Lång, E., Grudic, A., Pankiv, S., Bruserud, Ø., Simonsen, A., Bjerkvig, R., Bjørås, M. & Bøe, S. O. (2012). The arsenic-based cure of acute promyelocytic leukemia promotes cytoplasmic sequestration of PML and PML/RARA through inhibition of PML body recycling. *Blood*, 120 (4): 847-857. doi: 10.1182/blood-2011-10-388496.

Lång, E., Połeć, A., Lång, A., Valk, M., Blicher, P., Rowe, A. D., Tønseth, K. A., Jackson, C. J., Utheim, T. P., Janssen, L. M. C., et al. (2018). Coordinated collective migration and

asymmetric cell division in confluent human keratinocytes without wounding. *Nat Commun*, 9 (1): 3665. doi: 10.1038/s41467-018-05578-7.

Mahmood, T. & Yang, P.-C. (2012). Western blot: technique, theory, and trouble shooting. *North American journal of medical sciences*, 4 (9): 429-434. doi: 10.4103/1947-2714.100998.

Makarova, K. S. & Koonin, E. V. (2015). Annotation and Classification of CRISPR-Cas Systems. *Methods in molecular biology (Clifton, N.J.)*, 1311: 47-75. doi: 10.1007/978-1-4939-2687-9_4.

Mann, M., Hendrickson, R. C. & Pandey, A. (2001). Analysis of Proteins and Proteomes by Mass Spectrometry. *Annual Review of Biochemistry*, 70 (1): 437-473. doi: 10.1146/annurev.biochem.70.1.437.

Mao, W., Kang, M. K., Shin, J. U., Son, Y. J., Kim, H. S. & Yoo, H. S. (2018). Coaxial Hydro-Nanofibrils for Self-Assembly of Cell Sheets Producing Skin Bilayers. *ACS Applied Materials & Interfaces*, 10 (50): 43503-43511. doi: 10.1021/acsami.8b17740.

Mazereeuw-Hautier, J., Gres, S., Fanguin, M., Cariven, C., Fauvel, J., Perret, B., Chap, H., Salles, J.-P. & Saulnier-Blache, J.-S. (2005). Production of Lysophosphatidic Acid in Blister Fluid: Involvement of a Lysophospholipase D Activity. *Journal of Investigative Dermatology*, 125 (3): 421-427. doi: 10.1111/j.0022-202X.2005.23855.x.

Mishra, M., Tiwari, S. & Gomes, A. V. (2017). Protein purification and analysis: next generation Western blotting techniques. *Expert review of proteomics*, 14 (11): 1037-1053. doi: 10.1080/14789450.2017.1388167.

Moore, C. B., Guthrie, E. H., Huang, M. T.-H. & Taxman, D. J. (2010). Short hairpin RNA (shRNA): design, delivery, and assessment of gene knockdown. *Methods in molecular biology (Clifton, N.J.)*, 629: 141-158. doi: 10.1007/978-1-60761-657-3_10.

Murphy, Z. (2017). *Hematology | Hemostasis: Coagulation Cascade*: Ninja Nerd Lectures. Available at: https://www.youtube.com/watch?v=SGzp9wqeu84 (accessed: 10.5.21).

NCBI. (n.a.). *BLAST: Basic Loacl Alignment Search Tool*. Bethesda MD, USA. Available at: https://blast.ncbi.nlm.nih.gov/Blast.cgi (accessed: 15.10.2020).

Pandya, P., Orgaz, J. L. & Sanz-Moreno, V. (2017). Actomyosin contractility and collective migration: may the force be with you. *Curr Opin Cell Biol*, 48: 87-96. doi: 10.1016/j.ceb.2017.06.006.

Parham, P. (2015). Elements of the Immune System and their Roles in Defense. In *The Immune System*, pp. 1-26. New York: Garland Science, Taylor & Francis Group.

Psychogios, N., Hau, D. D., Peng, J., Guo, A. C., Mandal, R., Bouatra, S., Sinelnikov, I., Krishnamurthy, R., Eisner, R., Gautam, B., et al. (2011). The human serum metabolome. *PloS one*, 6 (2): e16957-e16957. doi: 10.1371/journal.pone.0016957.

Rhim, J. H., Jang, I.-S., Kwon, S. T., Song, K. Y., Yeo, E.-J. & Park, S. C. (2010). Activation of Wound Healing in Aged Rats by Altering the Cellular Mitogenic Potential. *The Journals of Gerontology: Series A*, 65A (7): 704-711. doi: 10.1093/gerona/glq065.

Riaz, A., Huang, Y. & Johansson, S. (2016). G-Protein-Coupled Lysophosphatidic Acid Receptors and Their Regulation of AKT Signaling. *International Journal of Molecular Sciences*, 17: 215. doi: 10.3390/ijms17020215.

Rodrigues, M., Kosaric, N., Bonham, C. A. & Gurtner, G. C. (2019). Wound Healing: A Cellular Perspective. *Physiological reviews*, 99 (1): 665-706. doi: 10.1152/physrev.00067.2017.

Schaks, M., Giannone, G. & Rottner, K. (2019). Actin dynamics in cell migration. *Essays Biochem*, 63 (5): 483-495. doi: 10.1042/ebc20190015.

Schindelin, J., Arganda-Carreras, I., Frise, E., Kaynig, V., Longair, M., Pietzsch, T., Preibisch, S., Rueden, C., Saalfeld, S., Schmid, B., et al. (2012). Fiji: an open-source platform for biological-image analysis. *Nature methods*, 9 (7): 676-682. doi: 10.1038/nmeth.2019.

Schroeder, A., Mueller, O., Stocker, S., Salowsky, R., Leiber, M., Gassmann, M., Lightfoot, S., Menzel, W., Granzow, M. & Ragg, T. (2006). The RIN: an RNA integrity number for assigning integrity values to RNA measurements. *BMC molecular biology*, 7: 3-3. doi: 10.1186/1471-2199-7-3.

Selbach, M. & Mann, M. (2006). Protein interaction screening by quantitative immunoprecipitation combined with knockdown (QUICK). *Nature Methods*, 3 (12): 981-983. doi: 10.1038/nmeth972.

Sjaastad, Ø. V., Sand, O. & Hove, K. (2016). The Skin. In *Physiology of Domestic Animals*, pp. 749-754. Oslo: Scandinavian Veterinary Press.

Taylor, S. C., Laperriere, G. & Germain, H. (2017). Droplet Digital PCR versus qPCR for gene expression analysis with low abundant targets: from variable nonsense to publication quality data. *Scientific Reports*, 7 (1): 2409. doi: 10.1038/s41598-017-02217-x.

Thermo Fisher Scientific. (s.a.-a). *Protein Biology Learning Center*. Pierce Protein Methods, Fluorescent Probes. Available at: https://www.thermofisher.com/no/en/home/life-science/protein-biology/protein-biology-learning-center/protein-biology-resource-library/pierce-protein-methods/fluorescent-probes.html#2 (accessed: 3.5.21).

Thermo Fisher Scientific. (s.a.-b). *Real-Time PCR Learning Center*. TaqMan vs. SYBR Chemistry for Real-Time PCR: Thermo Fisher Scientific. Available at: https://www.thermofisher.com/no/en/home/life-science/pcr/real-time-pcr/real-time-pcr-learning-center/real-time-pcr-basics/taqman-vs-sybr-chemistry-real-time-pcr.html#top (accessed: 29.1.21).

Thorlakson, H. H., Engen, S. A., Schreurs, O., Schenck, K. & Blix, I. J. S. (2017). Lysophosphatidic acid induces expression of genes in human oral keratinocytes involved in wound healing. *Arch Oral Biol*, 80: 153-159. doi: 10.1016/j.archoralbio.2017.04.008.

Tinevez, J.-Y., Perry, N., Schindelin, J., Hoopes, G. M., Reynolds, G. D., Laplantine, E., Bednarek, S. Y., Shorte, S. L. & Eliceiri, K. W. (2017). TrackMate: An open and extensible platform for single-particle tracking. *Methods*, 115: 80-90. doi: 10.1016/j.ymeth.2016.09.016.

Van Roy, F. & Berx, G. (2008). The cell-cell adhesion molecule E-cadherin. *Cellular and Molecular Life Sciences*, 65 (23): 3756-3788. doi: 10.1007/s00018-008-8281-1.

Vandesompele, J. (2019). *qPCR guide*: Eurogentec. Available at: https://www.gene-quantification.de/eurogentec-qPCR-guide.pdf (accessed: 29.1.21).

Ye, J., Coulouris, G., Zaretskaya, I., Cutcutache, I., Rozen, S. & Madden, T. L. (2012). Primer-BLAST: a tool to design target-specific primers for polymerase chain reaction. *BMC bioinformatics*, 13: 134-134. doi: 10.1186/1471-2105-13-134.

Zhao, M., Song, B., Pu, J., Wada, T., Reid, B., Tai, G., Wang, F., Guo, A., Walczysko, P., Gu, Y., et al. (2006). Electrical signals control wound healing through phosphatidylinositol-3-OH kinase-γ and PTEN. *Nature*, 442 (7101): 457-460. doi: 10.1038/nature04925.

Appendix

Appendix A: Recipes for buffers and solutions

Annealing buffer, 10x

400 mM Tris-HCl, pH 7.9

500 mM NaCl

100 mM $MgCl_2$

PBS/PBS-Tween

NaCl: 137 mM

KCl: 2.7 mM

Na_2HPO_4: 10 mM

KH_2PO_4: 1.8 mM

To make PBS-Tween, add 0.1% Tween® 20 detergent.

Protein Cracking Stock, 3x

6 % SDS (sodium dodecyl sulphate)

30 % Glycerol

10 mM Tris, pH 8

Bromophenol blue

Appendix B: Python-based scripts

B.1: Sorting script

```
import os
import shutil
import sys

Wells = "D:\\IXMC data\\180121 MigrationAssay-newKi Sofie_Plate_5666\\Wells\\"
os.makedirs(Wells)

#make new folder names
folder_name = ["A01", "A02", "A03", "A04", "A05", "A06", "A07", "A08", "A09", "A10", "A11",
"A12", "B01", "B02", "B03", "B04", "B05", "B06", "B07", "B08", "B09", "B10", "B11", "B12",
"C01", "C02", "C03", "C04", "C05", "C06", "C07", "C08", "C09", "C10", "C11", "C12", "D01",
"D02", "D03", "D04", "D05", "D06", "D07", "D08", "D09", "D10", "D11", "D12", "E01", "E02",
"E03", "E04", "E05", "E06", "E07", "E08", "E09", "E10", "E11", "E12", "F01", "F02", "F03",
"F04", "F05", "F06", "F07", "F08", "F09", "F10", "F11", "F12", "G01", "G02", "G03", "G04",
"G05", "G06", "G07", "G08", "G09", "G10", "G11", "G12", "H01", "H02", "H03", "H04", "H05",
"H06", "H07", "H08", "H09", "H10", "H11", "H12"]

#Iterate through the files in your directory
for x in range(0,len(folder_name)):
    if not os.path.exists(Wells+folder_name[x]):
        os.makedirs(Wells+folder_name[x])

for Timepoints in range(0, 113): #number of timepoints (must be exact)
    path = "D:\\IXMC data\\180121 MigrationAssay-newKi
Sofie_Plate_5666\\TimePoint_"+str(Timepoints+1)+"\\"
#Dont change \\TimePoint_"+str(Timepoints+1)+"\\
    time = "Timepoint_"+"%.3d" % (Timepoints + 1)

#make a list of all the files in a directory and store it in the variable names #Note that the
command os.listdi does not work since the items will not be iterable
    names = []
    for subdir, dirs, files in os.walk(path):
        for file in files:
           names.append(os.path.join(file))

    for files in names:
        if "A01" in files and not os.path.exists(Wells+"A01/"+time+"_"+files):
shutil.move(path+files, Wells+"A01/"+time+"_"+files)
#repeate this command for A02-A12, B01-B12,…,H01-H12

        print("...done with " + files)
#to follow the process. All files are sorted when it writes the filename of the last well.
```

B.2: PIV-analysis for migration speed and direction, 4XPIV_4

```
import numpy as np
from openpiv import tools, validation, process, filters, scaling, pyprocess
from scipy.ndimage import rotate
import os
import openpyxl
import time
import matplotlib.pyplot as plt

def Vector_Magnitude(u, v):
    "Calculates vector magnitude from component vectors u and v"
    return np.sqrt((u**2) + (v**2))

#scaling_factor: µm/px
def scale(u, v, scaling_factor):
    scaled_u = np.multiply(u, scaling_factor)
    scaled_u = np.divide(scaled_u, 0.26)
    scaled_v = np.multiply(v, scaling_factor)
    scaled_v = np.divide(scaled_v, 0.26)
    return scaled_u, scaled_v

def frame_rotation(frame_1, rotation):
    frame_1 = tools.imread(frame_1)
    rotate_1 = rotate(frame_1, rotation)#rotate image 45° counter clockwise
    middel_Y = rotate_1.shape[0] / 2 #finds the middle of the image y-axis
    average_1 = np.average(rotate_1[int(middel_Y)][0:200])
```

```
    low_1 = average_1 / 3
    high_points_1 = []
    low_points_1 = []
    for i in rotate 1[int(middel Y)]:
        if i > low_1:
            high_points_1.append(i)
        else:
            low_points_1.append(i)
            if len(low_points_1) > 10:
                break
    x_length = len(high_points_1)
    return middel_Y, x_length

def find_rectangle(frame_1):
    if "s1" in frame_1:
        return frame_rotation(frame_1=frame_1, rotation=225)
    elif "s2" in frame_1:
        return frame_rotation(frame_1=frame_1, rotation=315)
    elif "s3" in frame_1:
        return frame_rotation(frame_1=frame_1, rotation=135)
    elif "s4" in frame_1:
        return frame_rotation(frame_1=frame_1, rotation=45)
    else: pass

def reject_outliers(data, m):
    "algorithm for removal of outliers from a list"
    return data[abs(data - np.mean(data)) < m * np.std(data)]

def remove_outliers(array, k):
    "takes in an array, flips the array 90 degrees, removes outlier values from each row"
    # Returns a 1-dimensional list of cleaned averaged values

    array_90 = np.rot90(array, k=3)
    clean_list = []
    for dirt in array_90:
        clean = reject_outliers(dirt, m=k)
        clean_nr = np.average(clean)
        clean_list.append(clean_nr)
    return clean_list

def pick_angle(tag):
    if "s1" in tag:
        return 225
    elif "s2" in tag:
        return 315
    elif "s3" in tag:
        return 135
    elif "s4" in tag:
        return 45
    else:
        print("wrong tag")

def PIV(frame_a, frame_b, middel_Y, x_length, tag):
    angle = pick_angle(tag=tag)

    frame_a = tools.imread(frame_a)
    rotate_a = rotate(frame_a, angle) #rotate image 45° counter clockwise
    cropped_a = rotate_a[int(middel_Y - 100):int(middel_Y + 100), x_length - 900:x_length - 5]

    frame b = tools.imread(frame b)
    rotate_b = rotate(frame_b, angle)  # rotate image 45° counter clockwise
    cropped_b = rotate_b[int(middel_Y - 100):int(middel_Y + 100), x_length - 900:x_length - 5]

    u, v, sig2noise = process.extended_search_area_piv(cropped_a.astype(np.int32),
cropped_b.astype(np.int32),
        window size=24, overlap=12, search area size=48, sig2noise method='peak2peak' )
    x, y = process.get_coordinates( image_size=frame_a.shape, window_size=24, overlap=12)
    u, v, mask = validation.sig2noise_val( u, v, sig2noise, threshold = 2)
    u, v, mask = validation.global_val( u, v, (-1000, 2000),(-1000, 1000) )
    u, v = filters.replace_outliers( u, v, method='localmean', max_iter=10, kernel_size=2)
    u, v = scale(u, v, scaling_factor = 3.367)
#scaling factor 1.68 (binning 1); scaling factor 3.367 (binning 2)

    return u, v

def single_well(path, path_out):
```

```
    list_of_lists = [names_s1, names_s2, names_s3, names_s4]=[[],[],[],[]]
    for subdir, dirs, files in os.walk(path):
        for file in files:
            if "s1" in file:
                names_s1.append(os.path.join(file))
            elif "s2" in file:
                names_s2.append(os.path.join(file))
            elif "s3" in file:
                names_s3.append(os.path.join(file))
            elif "s4" in file:
                names_s4.append(os.path.join(file))
            else:
                pass

    for list, tag in zip(list_of_lists, ["s1", "s2", "s3", "s4"]):
        list u mean = []
        list_V_mean = []
        middel_Y, x_length = find_rectangle(path + list[0])
        print(x_length)
        if x_length < 900:
            print("rectangle smaller than 1000 pixels")
            pass
        elif x_length is None:
            pass
        else:
            for frame_a, frame_b in zip(*[iter(list)]*2):
                u, v = PIV(frame_a=path + frame_a, frame_b=path + frame_b, middel_Y=middel_Y,
x_length=x_length, tag = tag)
                V = Vector_Magnitude(u, v)
                direction = remove_outliers(array=u, k=2)
                speed = remove_outliers(array=V, k=2)
                list_u_mean.append(direction)
                list_V_mean.append(speed)

            book = openpyxl.Workbook()
            sheet = book.active

            c = 1
            for list in list_u_mean:
                sheet.cell(row=1, column=c).value = "u"
                for i in range(0, len(list)):
                    sheet.cell(row = i + 2, column = c).value = list[i]
                c = c + 2

            c2 = 2
            for list2 in list_V_mean:
                sheet.cell(row=1, column=c2).value = "V"
                for i in range(0, len(list2)):
                    sheet.cell(row = i + 2, column = c2).value = list2[i]
                c2 = c2 + 2

            book.save(path_out + path[-4:-1] + tag + ".xlsx")
            print(tag + " done")

all_wells = ["A01", "A02", "A03", "A04", "A05", "A06", "A07", "A08", "A09", "A10", "A11",
"A12", "B01", "B02", "B03", "B04", "B05", "B06", "B07", "B08", "B09", "B10", "B11", "B12",
"C01", "C02", "C03", "C04", "C05", "C06", "C07", "C08", "C09", "C10", "C11", "C12", "D01",
"D02", "D03", "D04", "D05", "D06", "D07", "D08", "D09", "D10", "D11", "D12", "E01", "E02",
"E03", "E04", "E05", "E06", "E07", "E08", "E09", "E10", "E11", "E12", "F01", "F02", "F03",
"F04", "F05", "F06", "F07", "F08", "F09", "F10", "F11", "F12", "G01", "G02", "G03", "G04",
"G05", "G06", "G07", "G08", "G09", "G10", "G11", "G12", "H01", "H02", "H03", "H04", "H05",
"H06", "H07", "H08", "H09", "H10", "H11", "H12"]

list_of_wells = [#put in the relevant files from "all wells"]

Folder in = "E:\\IMexp. MigrationAssay newKi 180121\\Wells\\"
Folder_out = "E:\\IMexp. MigrationAssay newKi 180121\\4xPIV_4_180121-2\\"

start = time.time()

um_per_pixel = 3.367
hours = 0.53
scaling_factor = um_per_pixel/hours

for well in list_of_wells:
    print("working on " + well)
```

```
    single_well(path = Folder_in + well + "\\", path_out = Folder_out)

end = time.time()
print("The entire analysis took " + str(end - start) + " seconds")
```

B.3: PIV-analysis for cell coordination, 4XPIV_5

```
import numpy as np
from openpiv import tools, validation, process, filters, scaling, pyprocess
from scipy.ndimage import rotate
import os
import openpyxl
import time
import math
import matplotlib.pyplot as plt

def Vector_Magnitude(u, v):
    "Calculates vector magnitude from component vectors u and v"
    return np.sqrt((u**2) + (v**2))

#scaling_factor: µm/px

def scale(u, v, scaling_factor):
    scaled_u = np.multiply(u, scaling_factor)
    scaled_u = np.divide(scaled_u, 0.26)
    scaled_v = np.multiply(v, scaling_factor)
    scaled_v = np.divide(scaled_v, 0.26)
    return scaled_u, scaled_v

#for The Plot Order Parameter

def order(u, v):
    angle = math.atan(v/u)
    number = math.cos(angle)
    return number

def frame_rotation(frame_1, rotation):
    frame_1 = tools.imread(frame_1)
    rotate_1 = rotate(frame_1, rotation)#rotate image 45° counter clockwise
    middel_Y = rotate_1.shape[0] / 2  #finds th middle of the image y-axis
    average_1 = np.average(rotate_1[int(middel_Y)][0:200])
    low_1 = average_1 / 3
    high_points_1 = []
    low_points_1 = []
    for i in rotate_1[int(middel_Y)]:
        if i > low_1:
            high_points_1.append(i)
        else:
            low_points_1.append(i)
            if len(low_points_1) > 10:
                break
    x_length = len(high_points_1)
    return middel_Y, x_length

def find_rectangle(frame_1):
    if "s1" in frame_1:
        return frame_rotation(frame_1=frame_1, rotation=225)
    elif "s2" in frame_1:
        return frame_rotation(frame_1=frame_1, rotation=315)
    elif "s3" in frame_1:
        return frame_rotation(frame_1=frame_1, rotation=135)
    elif "s4" in frame_1:
        return frame_rotation(frame_1=frame_1, rotation=45)
    else: pass

def reject_outliers(data, m):
    "algorithm for removal of outliers from a list"
    return data[abs(data - np.mean(data)) < m * np.std(data)]

def remove_outliers(array, k):
    "takes in an array, flips the array 90 degrees, removes outlier values from each row"
    # Returns a 1-dimensional list of cleaned averaged values

    array_90 = np.rot90(array, k=3)
    clean_list = []
```

```
    for dirt in array_90:
        clean = reject_outliers(dirt, m=k)
        clean_nr = np.average(clean)
        clean list.append(clean nr)
    return clean_list

def pick_angle(tag):
    if "s1" in tag:
        return 225
    elif "s2" in tag:
        return 315
    elif "s3" in tag:
        return 135
    elif "s4" in tag:
        return 45
    else:
        print("wrong tag")

def PIV(frame_a, frame_b, middel_Y, x_length, tag):
    angle = pick_angle(tag=tag)

    frame_a = tools.imread(frame_a)
    rotate_a = rotate(frame_a, angle)  # rotate image 45° counter clockwise
    cropped_a = rotate_a[int(middel_Y - 100):int(middel_Y + 100), x_length - 900:x_length - 5]

    frame_b = tools.imread(frame_b)
    rotate_b = rotate(frame_b, angle)  # rotate image 45° counter clockwise
    cropped_b = rotate_b[int(middel_Y - 100):int(middel_Y + 100), x_length - 900:x_length - 5]

    u, v, sig2noise = process.extended_search_area_piv(cropped_a.astype(np.int32),
cropped_b.astype(np.int32),
        window_size=24, overlap=12, search_area_size=48, sig2noise_method='peak2peak' )
    x, y = process.get_coordinates( image_size=cropped_a.shape, window_size=24, overlap=12)
    u, v, mask = validation.sig2noise_val( u, v, sig2noise, threshold = 2)
    u, v, mask = validation.global_val( u, v, (-50, 50), (-50, 50) )
    u, v = filters.replace_outliers( u, v, method='localmean', max_iter=10, kernel_size=2)
#u, v = scale(u, v, scaling_factor = 1.68) #scaling factor 1.68(binning 1); scaling factor
3.367 (binning 2)

    return u, v

def single_well(path, path_out):

    list_of_lists = [names_s1, names_s2, names_s3, names_s4]=[[],[],[],[]]

    for subdir, dirs, files in os.walk(path):
        for file in files:
            if "s1" in file:
                names_s1.append(os.path.join(file))
            elif "s2" in file:
                names_s2.append(os.path.join(file))
            elif "s3" in file:
                names_s3.append(os.path.join(file))
            elif "s4" in file:
                names_s4.append(os.path.join(file))
            else:
                pass

    for list, tag in zip(list_of_lists, ["s1", "s2", "s3", "s4"]):
        list u mean = []
        list_V_mean = []
        list_order = []
        middel_Y, x_length = find_rectangle(path + list[0])
        print(x_length)
        if x_length < 900:
            print("rectangle smaller than 1000 pixels")
            pass
        elif x_length is None:
            pass
        else:
            for frame_a, frame_b in zip(*[iter(list)]*2):
                u, v = PIV(frame a=path + frame a, frame b=path + frame b, middel Y=middel Y,
x_length=x_length, tag = tag)
                flat_u = u.flatten()
                flat_v = v.flatten()
                box = []
```

```
                for cu, cv in zip(flat_u, flat_v):
                    number = order(cu, cv)
                    box.append(number)
                list order.append(box)

            book = openpyxl.Workbook()
            sheet = book.active

            c = 1
            for list in list order:
                sheet.cell(row=1, column=c).value = "order"
                for i in range(0, len(list)):
                    sheet.cell(row = i + 2, column = c).value = list[i]
                c = c + 1

            book.save(path out + path[-4:-1] + tag + ".xlsx")
            print(tag + " done")

all_wells = ["A01", "A02", "A03", "A04", "A05", "A06", "A07", "A08", "A09", "A10", "A11",
"A12", "B01", "B02", "B03", "B04", "B05", "B06", "B07", "B08", "B09", "B10", "B11", "B12",
"C01", "C02", "C03", "C04", "C05", "C06", "C07", "C08", "C09", "C10", "C11", "C12", "D01",
"D02", "D03", "D04", "D05", "D06", "D07", "D08", "D09", "D10", "D11", "D12", "E01", "E02",
"E03", "E04", "E05", "E06", "E07", "E08", "E09", "E10", "E11", "E12", "F01", "F02", "F03",
"F04", "F05", "F06", "F07", "F08", "F09", "F10", "F11", "F12", "G01", "G02", "G03", "G04",
"G05", "G06", "G07", "G08", "G09", "G10", "G11", "G12", "H01", "H02", "H03", "H04", "H05",
"H06", "H07", "H08", "H09", "H10", "H11", "H12"]

list_of_wells = [#put in the relevant/all files from "all wells"]

Folder_in = "D:\\IXMC data\\030920 MigrationAssay Sofie_Plate_4319\\Wells\\"
Folder_out = "D:\\Sofie\\Pycharm_projects\\project1\\4xPIV_5_030920\\"

for well in list_of_wells:
    print("working on " + well)
    single_well(path = Folder_in + well + "\\", path_out = Folder_out)
```

B.4: The Plot Order Parameter

```
import pandas as pd
import numpy as np
import matplotlib.pyplot as plt
import os

def extract_file_names_from_directory(directory):
    file_names = []
    for subdir, dirs, files in os.walk(directory):
        for file in files:
            file_names.append(os.path.join(file))
    return file_names

def one_sample(file_list):
    list_of_list = []
    for file in file_list:
        if file[0:5] in file_list:
            df_data = pd.read_excel(path + file + ".xlsx")
            data = df_data.to_numpy()
            data = np.rot90(data)
            data = np.flipud(data)
            data[np.isnan(data)] = 0
            numbers = []
            for i in data:
                average = np.average(i)
                numbers.append(average)
            list of list.append(numbers)
        else:
            print(file)
    return list_of_list

def plot_one_sample(sample):
    sample array = np.array(sample)
    sample_average = np.average(sample_array, 0)
    sample_std = np.std(sample_array, 0)
    return sample_average, sample_std

path = "E:\\Pycharm_projects\\project1\\4xPIV_5_030920\\"
```

```
#fill in Dataset1 and 2 with data for the graphs wanted in the plot. All sites per well should
be included if it contains data.
Dataset1 =    ["A03s1","A03s2","A03s3","A03s4","B03s1","B03s2","B03s3","B03s4",
"C03s1","C03s2","C03s3","C03s4","D03s1","D03s2","D03s3","D03s4",
 "E03s1","E03s2","E03s3","E03s4","F03s1","F03s2","F03s3","F03s4",
 "G03s1","G03s2","G03s3","G03s4","H03s1","H03s2","H03s3","H03s4"]
Dataset2 = ["A06s1","A06s2","A06s3","A06s4","B06s1","B06s2","B06s3","B06s4",
 "C06s1","C06s2","C06s3","C06s4","D06s1","D06s2","D06s3","D06s4",
 "E06s1","E06s2","E06s3","E06s4","F06s1","F06s2","F06s3","F06s4",
 "G06s1","G06s2","G06s3","G06s4","H06s1","H06s2","H06s3","H06s4"]

file_names = extract_file_names_from_directory(directory = path)
print(file_names)

sample1 = one sample(Dataset1)
sample2 = one_sample(Dataset2)

# Generate average and standard deviation
sample1_a, sample1_s = plot_one_sample(sample1)
sample2_a, sample2_s = plot_one_sample(sample2)

# Generate X-axis
x = np.arange(len(sample1_a))
x = np.multiply(x, 32)
x = np.divide(x, 60)

fig, ax = plt.subplots()

ax.plot(x[1:], sample1_a[1:], linewidth = 1, color="red", marker='o')
ax.fill_between(x[1:], sample1_a[1:] - sample1_s[1:], sample1_a[1:] + sample1_s[1:],
alpha=0.2, color="red")
ax.plot(x[1:], sample2_a[1:], linewidth = 1, color="blue", marker='d')
ax.fill_between(x[1:], sample2_a[1:] - sample2_s[1:], sample2_a[1:] + sample2_s[1:],
alpha=0.2, color="blue")

labels = ["EGF", "LPA"]
plt.legend(labels, fontsize=10)

ax.set_ylim(0.4 ,1)
ax.set_xlabel("t (hours)")
ax.set_ylabel("φ")
plt.savefig("Order_plot_EGFandLPA_0309", dpi = 300)
```

B.5: The Speed plot

```
import pandas as pd
import numpy as np
import matplotlib.pyplot as plt

def single_site(path, file):
    df = pd.read_excel (path + file)
    line = []
    for i in range(1, len(df.columns), 2):
        t = df.iloc[:, i]
        t = np.average(t)
        line.append(t)
    return(line)

def group_average_std(group):
    list_of_lists = []
    for file in group:
        t = single_site(path, file)
        list of lists.append(t)
    average = np.average(list_of_lists, axis=0)
    std = np.std(list_of_lists, axis=0)
    return average[1:], std[1:]

# Extracting data from  xlsx-files
path = "E:\\IMexp. MigrationAssay newKi 180121\\4xPIV_4_180121-2\\"

#fill in group1 and 2 with data for the graphs wanted in the plot. All sites per well should
be included if it contains data.
group1 = ["A03s1.xlsx", "A03s2.xlsx", "A03s3.xlsx", "A03s4.xlsx", "B03s1.xlsx", "B03s2.xlsx",
"B03s3.xlsx", "B03s4.xlsx", "C03s1.xlsx", "C03s2.xlsx", "C03s3.xlsx", "C03s4.xlsx",
```

```
"D03s1.xlsx", "D03s2.xlsx", "D03s3.xlsx", "D03s4.xlsx", "E03s1.xlsx", "E03s2.xlsx",
"E03s3.xlsx", "E03s4.xlsx", "F03s1.xlsx", "F03s2.xlsx", "F03s3.xlsx", "F03s4.xlsx",
"G03s1.xlsx", "G03s2.xlsx", "G03s3.xlsx", "G03s4.xlsx", "H03s1.xlsx", "H03s2.xlsx",
"H03s3.xlsx", "H03s4.xlsx"]
group2 = ["A07s1.xlsx", "A07s2.xlsx", "A07s3.xlsx", "A07s4.xlsx", "B07s1.xlsx", "B07s2.xlsx",
"B07s3.xlsx", "B07s4.xlsx", "C07s1.xlsx", "C07s2.xlsx", "C07s3.xlsx", "C07s4.xlsx",
"D07s1.xlsx", "D07s2.xlsx", "D07s3.xlsx", "D07s4.xlsx", "E07s1.xlsx", "E07s2.xlsx",
"E07s3.xlsx", "E07s4.xlsx", "F07s1.xlsx", "F07s2.xlsx", "F07s3.xlsx", "F07s4.xlsx",
"G07s1.xlsx", "G07s2.xlsx", "G07s3.xlsx", "G07s4.xlsx", "H07s1.xlsx", "H07s2.xlsx",
"H07s3.xlsx", "H07s4.xlsx"]

average1, std1 = group_average_std(group1)
average2, std2 = group_average_std(group2)

# creating values along the x_axix
x = range(0, len(average1))
x = (np.multiply(x,32))/60

# plotting the data
fig, ax = plt.subplots(1,1)

ax.plot(x, average1, label="LPA", color="red", marker='o')
ax.fill_between(x, average1 + std1, average1 - std1, facecolor='red', alpha=0.2)

ax.plot(x, average2, label="LPA + Ki16425 5µM", color="blue", marker='d')
ax.fill_between(x, average2 + std1, average2 - std2, facecolor='blue', alpha = 0.2)

ax.set_ylabel("Speed (µm/h)", fontsize=12)
ax.set_xlabel("Time (h)", fontsize=12)

plt.ylim(0,40)

plt.legend(loc= 'upper left')
plt.show()

fig.savefig("E:\\IMexp. MigrationAssay newKi 180121\\Speed_plot_180121\\Fig_LPAandKi5",
dpi=300, bbox_inches='tight')
```

B.6: The Streamline plot

```
import numpy as np
from openpiv import tools, validation, process, filters, scaling, pyprocess
from scipy.ndimage import rotate
import os
import openpyxl
import time
import matplotlib.pyplot as plt
import scipy.ndimage

def extract_file_names_from_directory(directory):
    file_names = []
    for subdir, dirs, files in os.walk(directory):
        for file in files:
            file_names.append(os.path.join(file))
    return file_names

def scale2(u, v, M, factor):
    u2 = np.multiply(u, factor)
    v2 = np.multiply(v, factor)
    M2 = np.multiply(M, factor)
    return u2, v2, M2

def PIV(frame_a, frame_b, window_size, overlap, search_area_size):
    frame a = tools.imread(frame a)
    frame_b = tools.imread(frame_b)
    u, v, sig2noise = process.extended_search_area_piv(frame_a.astype(np.int32),
frame_b.astype(np.int32),
        window_size=window_size, overlap=overlap, search_area_size=search_area_size,
sig2noise_method='peak2peak' )
    x, y = process.get coordinates( image size=frame a.shape, window size=window size,
overlap=overlap)
    u, v, mask = validation.sig2noise_val( u, v, sig2noise, threshold = 3)
    u, v, mask = validation.global_val( u, v, (-10, 10), (-10, 10) )
    u, v = filters.replace_outliers( u, v, method='localmean', max_iter=10, kernel_size=4)
    M = np.hypot(u, v)
```

```
    print(M.min(), M.max())
    return x, y, u, v, M

path = "E:\\IMexp. MigrationAssay newKi 180121\\180121 MigrationAssay-newKi Sofie_5666\\F08\\"
path_out = "E:\\IMexp. MigrationAssay newKi 180121\\Streamline_plot_180121\\F08\\"

names = extract_file_names_from_directory(path)
print(names)

k= 0
for frame_a, frame_b in zip(names, names[1:]):
    x, y, u, v, M = PIV(path + frame_a, path + frame_b,
                        window_size=24,
                        overlap=12,
                        search_area_size=48)

    u, v, M =  scale2(u = u, v = v, M = M, factor = 12.63)
    x = np.multiply(x, 3.367)
    y = np.multiply(y, 3.367)

# Flipping v-components 180 degrees is required to obtain the correct vector orientation:
    v = np.flipud(v)
# These operations reduce the number of arrows in the plot through averaging:
    resized_x = scipy.ndimage.zoom(x, 24. / 169)
    resized_y = scipy.ndimage.zoom(y, 24. / 169)
    resized_u = scipy.ndimage.zoom(u, 24. / 169)
    resized_v = scipy.ndimage.zoom(v, 24. / 169)
    resized_M = scipy.ndimage.zoom(M, 24. / 169)

 # Make the plot:
    fig, ax = plt.subplots(ncols=1, nrows=1)
    im = ax.streamplot(x, y, u, v, density=2)
    ax.set_xlabel("X (µm)")
    ax.set_ylabel("Y (µm)")
    plt.gca().set_aspect('equal', adjustable='box')
    plt.savefig(path_out + "image" + str(k), dpi = 300)
    print("Done with Image " + str(k))
    k = k + 1
```

B.7: Intensity plot for actin

```
import matplotlib.pyplot as plt
import numpy as np
import openpyxl

wb = openpyxl.load_workbook('Data til plott.xlsx',data_only=True)
ark1 = wb.get_sheet_by_name('Ark1')

lengde = 175-3 # the length of data
X_axis = np.zeros(lengde)
DAPI = np.zeros(lengde)
stdDAPI = np.zeros(lengde)
FBS = np.zeros(lengde)
stdFBS = np.zeros(lengde)
no_FBS = np.zeros(lengde)
stdno_FBS = np.zeros(lengde)
EGF = np.zeros(lengde)
stdEGF = np.zeros(lengde)
LPA = np.zeros(lengde)
stdLPA = np.zeros(lengde)
FBS_Ki16425_10 = np.zeros(lengde)
stdFBS_Ki16425_10 = np.zeros(lengde)
FBS_Ki16425_20 = np.zeros(lengde)
stdFBS Ki16425 20 = np.zeros(lengde)

for i in range(0,lengde):
    X_axis[i] = (ark1.cell(column=2, row=i + 4).value)
    DAPI[i] = (ark1.cell(column=4, row=i + 4).value)
    stdDAPI[i] = (ark1.cell(column=5, row=i + 4).value)
    FBS[i] = (ark1.cell(column=7, row=i + 4).value)
    stdFBS[i] = (ark1.cell(column=8, row=i + 4).value)
    no_FBS[i] = (ark1.cell(column=22, row=i + 4).value)
    stdno_FBS[i] = (ark1.cell(column=23, row=i + 4).value)
    EGF[i] = (ark1.cell(column=13, row=i + 4).value)
    stdEGF[i] = (ark1.cell(column=14, row=i + 4).value)
```

```
    LPA[i] = (ark1.cell(column=10, row=i + 4).value)
    stdLPA[i] = (ark1.cell(column=11, row=i + 4).value)
    FBS_Ki16425_10[i] = (ark1.cell(column=16, row=i +4).value)
    stdFBS_Ki16425_10[i] = (ark1.cell(column=17, row=i +4).value)
    FBS_Ki16425_20[i] = (ark1.cell(column=25, row=i +4).value)
    stdFBS_Ki16425_20[i] = (ark1.cell(column=26, row=i +4).value)

#Plotting
fig, ((ax1, ax2), (ax3, ax4)) = plt.subplots(nrows=2, ncols=2, figsize=(8, 5))
ax1.plot(X_axis, DAPI, linewidth = 2, label="Nucleus")
ax1.fill_between(X_axis, DAPI - stdDAPI, DAPI + stdDAPI, color ='blue', alpha  = 0.2)
ax1.plot(X_axis, FBS, linewidth = 2,label = "Actin")
ax1.fill_between(X_axis, FBS - stdFBS, FBS + stdFBS, color ='green', alpha = 0.2)
ax1.grid(color='k', linestyle='--', linewidth=0.5, alpha=0.5)
ax1.legend(bbox_to_anchor=(0., 1.02, 0., .102), loc=8, frameon=False)
ax1.set_title('FBS', fontsize=12)
ax1.text(-9.5, 0.5, 'Basal',  bbox=['facecolor':'b', 'alpha':0.1])
ax1.text(7, 0.5, 'Apical',  bbox=['facecolor':'b', 'alpha':0.1])
ax1.set_ylabel('Intensity', rotation=90, labelpad=10, fontsize=12)
ax1.axvline(x=0, linestyle="--", color="r")

ax2.plot(X_axis, DAPI, linewidth = 2, label="Nucleus")
ax2.fill_between(X_axis, DAPI - stdDAPI, DAPI + stdDAPI, color ='blue', alpha  = 0.2)
ax2.plot(X_axis, EGF, linewidth = 2, label = "Actin")
ax2.fill_between(X_axis, EGF - stdEGF, EGF + stdEGF, color ='green', alpha = 0.2)
ax2.grid(color='k', linestyle='--', linewidth=0.5, alpha=0.5)
ax2.set_title('EGF', fontsize=12)
ax2.text(-9.5, 0.5, 'Basal',  bbox=['facecolor':'b', 'alpha':0.1])
ax2.text(7, 0.5, 'Apical',  bbox=['facecolor':'b', 'alpha':0.1])
ax2.axvline(x=0, linestyle="--", color="r")

ax3.plot(X_axis, DAPI, linewidth = 2, label="Nucleus")
ax3.fill_between(X_axis, DAPI - stdDAPI, DAPI + stdDAPI, color ='blue', alpha  = 0.2)
ax3.plot(X_axis, LPA, linewidth = 2, label = "Actin")
ax3.fill_between(X_axis, LPA - stdLPA, LPA + stdLPA, color ='green', alpha = 0.2)
ax3.grid(color='k', linestyle='--', linewidth=0.5, alpha=0.5)
ax3.set_xlabel('LPA', fontsize=12)
ax3.text(-9.5, 0.5, 'Basal',  bbox=['facecolor':'b', 'alpha':0.1])
ax3.text(7, 0.5, 'Apical',  bbox=['facecolor':'b', 'alpha':0.1])
ax3.set_ylabel('Intensity', rotation=90, labelpad=10, fontsize=12)
ax3.axvline(x=0, linestyle="--", color="r")

ax4.plot(X_axis, DAPI, linewidth = 2, label="Nucleus")
ax4.fill_between(X_axis, DAPI - stdDAPI, DAPI + stdDAPI, color ='blue', alpha  = 0.2)
ax4.plot(X_axis, FBS_Ki16425_10, linewidth = 2, label = "Actin")
ax4.fill_between(X_axis, FBS_Ki16425_10 - stdFBS_Ki16425_10, FBS_Ki16425_10 +
stdFBS_Ki16425_10, color ='green', alpha = 0.2)
ax4.grid(color='k', linestyle='--', linewidth=0.5, alpha=0.5)
ax4.set_xlabel('Ki16425 10µM', fontsize=12)
ax4.text(-9.5, 0.5, 'Basal',  bbox=['facecolor':'b', 'alpha':0.1])
ax4.text(7, 0.5, 'Apical',  bbox=['facecolor':'b', 'alpha':0.1])
ax4.axvline(x=0, linestyle="--", color="r")

plt.tight_layout(pad=3, w_pad=2, h_pad=1.0)
fig.savefig('C:\\Users\\huygens\\Desktop\\Sofie\\Fig 1.png', dpi=300)
plt.show()
plt.close()
```

B.8: Plot for TrackMate

```
import numpy as np
import matplotlib.pyplot as plt
import openpyxl as openpyxl

def get_column_list(list, ark):
    column_list = []
    for name in list:
        for i in range(0, ark.max_column):
            if name in str(ark.cell(row = 1, column = i + 1).value):
                column list.append(i+1)
    return(column_list)

def get_colun(column_number, ark):
    column=np.zeros(ark.max_row)
    for i in range(0, ark.max_row-2):
```

```
        column[i] = ark.cell(column = column_number, row = i +2).value
    return(column)

def get row average(column list, ark, row number):
    row_numbers  = []
    for i in column_list:
        row_numbers.append(ark.cell(column = i, row = row_number).value)
    average = np.average((row_numbers))
    return(average)

def get_X(ark):
    X = np.zeros(ark.max_row)
    for i in range(0, ark.max_row-2):
        X[i] = ark.cell(column = 1, row = i +2).value
    return(X)

# The data to be plotted is in this file
wb = openpyxl.load_workbook("Average_std_Sofie_100221.xlsx", data_only=True)
ark = wb.active

# Put names of columns to be plotted, here three graphs per plot
plot_list =    [["Mean-Speed_A04_s1","Mean-Speed_A04_s2","Mean-Speed_A04_s3","Mean-
Speed_A04_s4"],
                ["Mean-Speed_B04_s1","Mean-Speed_B04_s2","Mean-Speed_B04_s3","Mean-
Speed_B04_s4"],
                ["Mean-Speed_C04_s1","Mean-Speed_C04_s2","Mean-Speed_C04_s3","Mean-
Speed_C04_s4"]]

# For each line in the graph put a label here
label_list = ["Starved", "FBS", "LPA"]

# Create the correct X(time) axis
X = get_X(ark)

average_list = []
std_list = []

for group in plot_list:
    column_list=get_column_list(list=group, ark=ark)
    columns=[]
    for i in column_list:
        column=get_colun(column_number=i, ark=ark)
        columns.append(column)
    average=np.average(columns, axis=0)
    std=np.std(columns, axis=0)
    average_list.append(average)
    std_list.append(std)

#Plotting the data
fig, ax = plt.subplots(1,1)

for average, std, label in zip(average_list, std_list, label_list):
    plt.plot(X[1:-2], average[1:-2], alpha = 1, label=label)
    plt.fill_between(X[1:-2], average[1:-2]-std[1:-2], average[1:-2]+std[1:-2], alpha=0.2)

plt.legend(loc='upper left')
plt.ylim(0, 40)
plt.xlim(0, 30)
plt.xlabel("Time (h)", fontsize=12)
plt.ylabel("Speed (µm/h)", fontsize=12)
plt.savefig("KD2_Knockdexp_2_100221_Sofie", dpi=300)
```

Appendix C: Complementary results of cell migration patterns

These figures are cited to in section 3.1.1. Gefitinib is an inhibitor of the EGF receptor, EGFR, and cells treated with Gefitinib are thereby used as a control to EGF stimulated cells. Gefitinib is diluted in medium containing FBS prior to treatment of the cells. The plots are showing mean values with standard deviation.

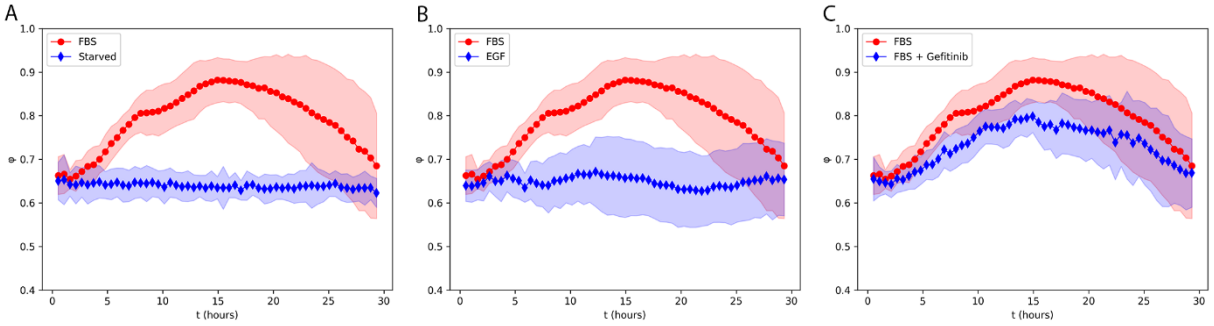

Figure C.1: Control samples to EGF stimulated cells in live cell imaging. The level of coordination in the cell sheets is given by the factor φ. The red graph in each plot is a positive control of FBS stimulated cells. The blue graphs illustrate coordination in starved cell sheets as a negative control (A), EGF stimulated cell sheets (B) and cell sheets treated with the EGFR-inhibitor Gefitinib (C). The cell sheets treated with Gefitinib shows a lower level of coordination than the positive control. Compared to the graph of cells stimulated with EGF, the coordination is shown to be higher after treatment with Gefitinib. This is unexpected graphics due to the migration behaviour observed in the video of these acquired data, where no particular migration is observed. EGF is important for activation of migration and inhibiting the EGFR should then lead to inhibited cell migration. The coordination shown in the plot can be explained in context to Figure C.2, where the cells treated with Gefitinib show generation of low cell sheet velocities, and thereby some migration that could be coordinated even if it is a general low level of migration.

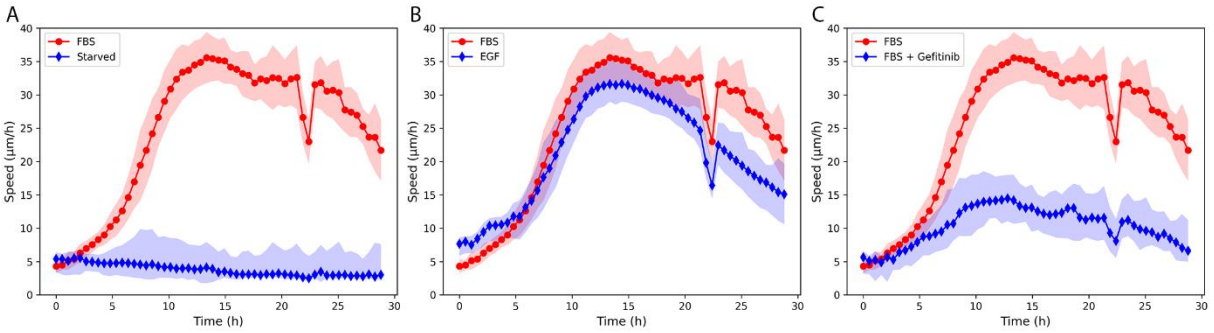

Figure C.2: Control samples to EGF stimulated cells in live cell imaging, illustrated by cell sheet velocities (μm/h). The red graph in each plot is a positive control of FBS stimulated cells. The blue graphs show cell sheet velocities in starved cell sheets as a negative control (A), EGF stimulated cell sheets (B) and cell sheets treated with the EGFR-inhibitor Gefitinib (C). The graph of cell sheets treated with Gefitinib shows lower cell sheet velocities than cells stimulated with EGF, indicating successful inhibition of the EGFR in the HaCaT cells. The outliers are due to irregular movements in the xy-stage of the ImageXpress microscope.

Appendix D: Complementary qPCR results

This appendix contains complementary results to the qPCR analysis of mRNA expression levels of LPARs in HaCaT wt cells, presented in section 3.3. Figure D.1 and D.2 present values for mRNA expression of LPAR1-6 normalized to GAPDH, the mRNA expression of the reference gene *GAPD*, for the two independently performed experiments. Figure D.3 presents images of a gel electrophoresis performed as a control to the qPCR experiment. One positive and one negative sample representative for each LPAR are included from each of the two experiments. To reveal the potential presence of contaminating genomic DNA (gDNA), a qPCR experiment including no-RT controls was performed. Table D.1 presents the result from this experiment, showing the differences between mRNA expression of the LPARs and GAPDH in the no-RT control samples compared with cDNA samples.

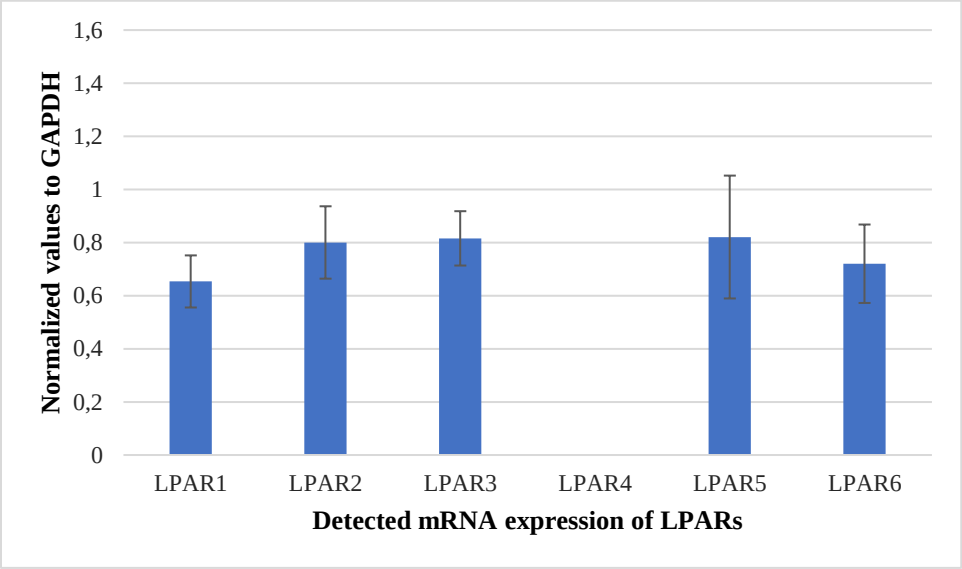

Figure D.1: The first independent qPCR experiment. The detected values for mRNA expression of the LPARs are normalized to the mRNA expression of GAPDH. Values for LPAR4 were not detected.

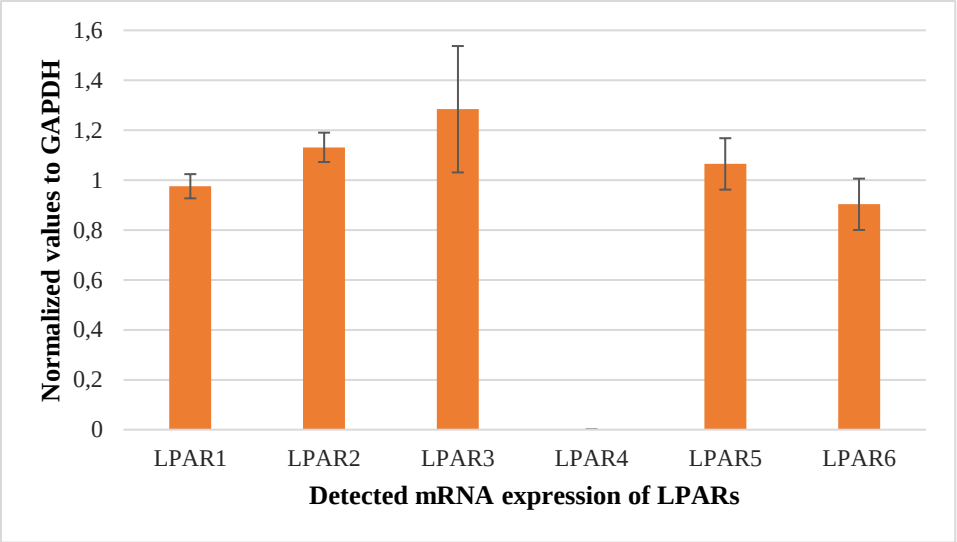

Figure D.2: The second independent qPCR experiment. The detected values for mRNA expression of the LPARs are normalized to the mRNA expression of GAPDH. Values for LPAR4 were not detected.

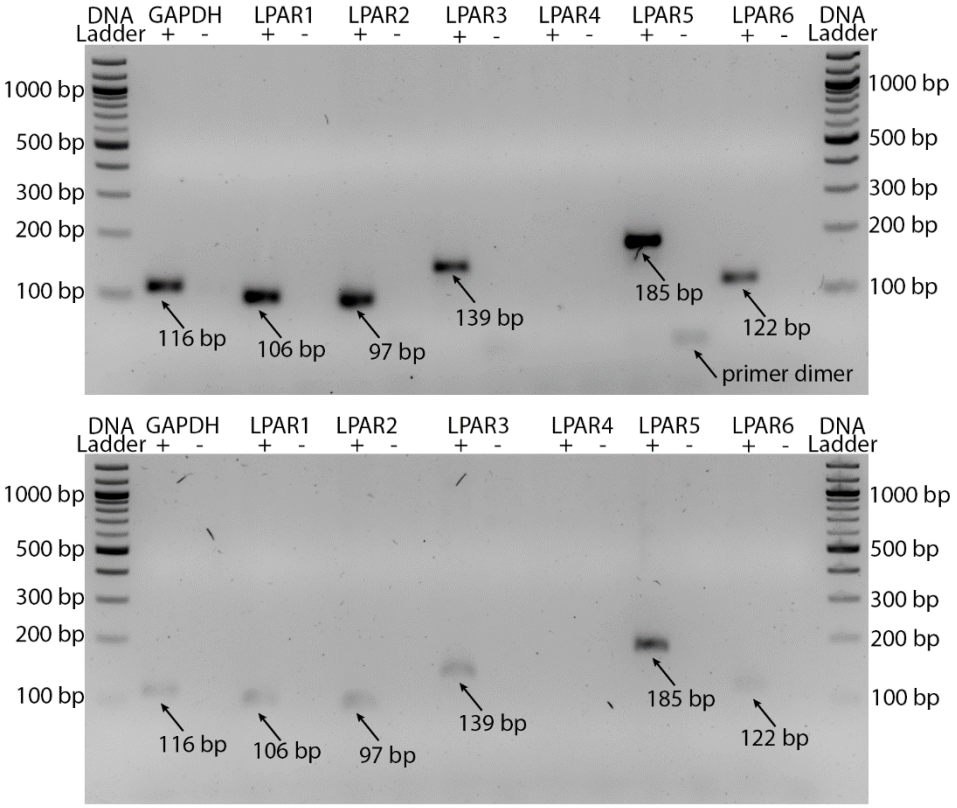

Figure D.3: Gel electrophoresis of one representative sample for each of the six receptors, LPAR1-6, and negative controls, from the two qPCR experiments performed. This shows the presence, and successfull amplification, of the mRNA product of interest for each LPAR, except LPAR4, and no product amplification in the negative control samples. The product sizes match the given sizes in Table 2.1.

Table D.1: C_T-values (A) and Copy numbers (B) for comparison of cDNA and respective no-RT controls (RNA). Some of the values were non-detectable (ND). The values are indicating that the RNA does not include gDNA that could potentially affect the qPCR-results.

A: C_T-values of cDNA and respective no-RT (RNA) controls

	cDNA2	RNA2	cDNA3	RNA3	cDNA4	RNA4	cDNA5	RNA5
GAPDH	16,87	37,02	18,17	32,62	17,43	29,65	16,94	36,81
LPAR1	26,46	ND	27,42	ND	26,52	ND	25,95	ND
LPAR2	21,94	37,14	22,62	34,35	22,11	30,80	21,77	35,25
LPAR3	24,90	39,56	25,24	36,92	25,24	36,83	24,27	37,12
LPAR4	ND	ND	ND	ND	ND	ND	ND	ND
LPAR5	27,49	ND	28,15	ND	27,11	ND	26,95	ND
LPAR6	27,80	ND	28,67	ND	27,86	36,91	27,80	ND

B: Copy numbers of cDNA and respective no-RT (RNA) controls

	cDNA2	RNA2	cDNA3	RNA3	cDNA4	RNA4	cDNA5	RNA5
GAPDH	$6.03*10^{2}$	$2.23*10^{-7}$	$1.47*10^{2}$	$2.55*10^{-5}$	$3.30*10^{2}$	$6.29*10^{-4}$	$5.60*10^{2}$	$2.78*10^{-7}$
LPAR1	$2.10*10^{3}$	ND	$7.90*10^{2}$	ND	$1.97*10^{3}$	ND	$3.55*10^{3}$	ND
LPAR2	$3.93*10^{3}$	$4.59*10^{-4}$	$1.91*10^{3}$	$8.60*10^{-3}$	$3.30*10^{3}$	$3.55*10^{-1}$	$4.71*10^{3}$	$3.32*10^{-3}$
LPAR3	$1.23*10^{4}$	$5.80*10^{-3}$	$8.72*10^{3}$	$8.02*10^{-2}$	$8.70*10^{3}$	$8.71*10^{-2}$	$2.29*10^{4}$	$6.55*10^{-2}$
LPAR4	ND	ND	ND	ND	ND	ND	ND	ND
LPAR5	$3.45*10^{2}$	ND	$1.76*10^{2}$	ND	$5.02*10^{2}$	ND	$5.93*10^{2}$	ND
LPAR6	$2.27*10^{3}$	ND	$1.04*10^{3}$	ND	$2.14*10^{3}$	$6.56*10^{-1}$	$2.26*10^{3}$	ND

Norges miljø- og biovitenskapelige universitet
Noregs miljø- og biovitskapelege universitet
Norwegian University of Life Sciences

Postboks 5003
NO-1432 Ås
Norway